1-1-2015

The Adsorption of Polyatomic Molecules on Carbon Surfaces

Jared T. Burde
University of Denver

The Adsorption of Polyatomic Molecules on Carbon Surfaces

A Dissertation

Presented to

the Faculty of Natural Sciences and Mathematics

University of Denver

In Partial Fulfillment

of the Requirements for the Degree

Doctor of Philosophy

By

Jared T. Burde

August 2015

Advisor: Dr. M. Mercedes Calbi

Author: Jared T. Burde
Title: The Adsorption of Polyatomics on Carbon Surfaces
Advisor: Dr. M. Mercedes Calbi
Degree Date: August 2015

ABSTRACT

Carbon nanotubes exhibit the structure and chemical properties that make them apt substrates for many adsorption applications. Of particular interest are carbon nanotube bundles, whose unique geometry is conducive to the formation of pseudo-one-dimensional phases of matter, and graphite, whose simple planar structure allows ordered phases to form in the absence of surface effects. Although both of these structures have been the focus of many research studies, knowledge gaps still remain. Much of the work with carbon nanotubes has used simple adsorbates[1-43], and there is little kinetic data available. On the other hand, there are many studies of complex molecules adsorbing on graphite; however, there is almost no kinetic data reported for this substrate. We seek to close these knowledge gaps by performing a kinetic study of linear molecules of increasing length adsorbing on carbon nanotube bundles and on graphite. We elucidated the process of adsorption of complex admolecules on carbon nanotube bundles, while at the same time producing some of the first equilibrium results of the films formed by large adsorbates on these structures. We also extended the current knowledge of adsorption on graphite to include the kinetics of adsorption. The kinetic data that we have produced enables a more complete understanding of the process of adsorption of large admolecules on carbon nanotube bundles and graphite.

We studied the adsorption of particles on carbon nanotube bundles and graphite using analytical and computational techniques. By employing these methods separately but in parallel, we were able to constantly compare and verify our results. We calculated and simulated the behavior of a given system throughout its evolution and then analyzed our results to determine which system parameters have the greatest effect on the kinetics of adsorption. Our analytical and computational results show good agreement with each other and with the experimental isotherm data provided by our collaborators.

As a result of this project, we have gained a better understanding of the kinetics of adsorption. We have learned about the equilibration process of dimers on carbon nanotube bundles, identifying the “filling effect”, which increases the rate of total uptake, and explaining the cause of the transient “overshoot” in the coverage of the surface. We also measured the kinetic effect of particle-particle interactions between neighboring adsorbates on the lattice. For our simulations of monomers adsorbing on graphite, we succeeded in developing an analytical equation to predict the characteristic time as a function of chemical potential and of the adsorption and interaction energies of the system. We were able to further explore the processes of adsorption of dimers and trimers on graphite (again observing the filling effect and the overshoot). Finally, we were able to show that the kinetic behaviors of monomers, dimers, and trimers that have been reported in experimental results also arise organically from our model and simulations.

TABLE OF CONTENTS

LIST OF TABLES

LIST OF FIGURES

CHAPTER ONE
INTRODUCTION

One of the most abundant elements on Earth, carbon has chemical characteristics that make it one of the most broadly utile materials known to mankind. Carbon atoms combine with each other, and sometimes with other atomic species, to form a wide range of chemically-inert nanostructures that are uniquely-suited for adsorption applications. Indeed, the sorptive properties of carbon have been known for thousands of years; the ancient Egyptians used primitive forms of carbon nanostructures, like charcoal and carbon black, to absorb poisons in the body[38,44]. More recently, the discovery of new carbon nanostructures, especially carbon nanotubes[2], has opened the door to finely tuned, focused adsorbents. When grown, carbon nanotubes are drawn together by the Van Der Waals forces between them to spontaneously to form bundles containing anywhere between three and several thousand nanotubes[43]. Parts of the bundle are inaccessible to adsorbates; it has been widely shown that particles do not adsorb in the interstitial channels between neighboring nanotubes in the interior of the bundle[23] (there is simply not enough space) and the interiors of the nanotubes themselves are only available if the nanotubes have been opened through chemical or mechanical means[1]. However, the exterior surface of a nanotube bundle still offers adsorption sites with different binding energies, as well as the possibility for the development of quasi-one-dimensional phases of matter. It has been the goal of several research studies[1-67], including those advanced by the Calbi group[3,4,10] at the University of Denver, to better understand the process of adsorption of gases onto carbon nanotube bundles, focusing both on the equilibrium characteristics of the system (that is, the arrangement of the adsorbates on the surface) and the kinetic behavior of the system (how the system reaches equilibrium).

With as much potential as carbon nanostructures have as substrates for adsorption, of equal importance is the choice of adsorbate. Our group is interested in the adsorption of hydrocarbon molecules. These admolecules are inert at low temperatures (like those used in isotherm experiments) and are chemically similar to each other, with the main difference being in the number of "links" in the molecular chain. They are also widely used in industrial applications, and in energy applications in particular, so our increased understanding of their behavior will be useful in a variety of fields. We are further driven by our continued collaboration with the Migone group at SIUC, experts in isotherm experiments, who have performed many isotherm measurements of hydrocarbons adsorbing on CNTBs. In our first work in conjunction with Dr. Migone[3], we considered the adsorption of monomers on carbon nanotube bundles and found that the characteristic time needed for the system to reach equilibrium actually decreases as the fractional coverage of the adsorbent goes up, meaning one must wait far longer for a low-coverage system to equilibrate than a high-coverage system. However, we modeled methane as a quasi-spherical adsorbate, so the behavior we found is not necessarily isolated to hydrocarbons but could instead be found in other systems of monomers as well.

As the Migone group continued their work, they found that this decrease in characteristic time with increased equilibrium coverage continues for dimers (ethane), but that this kinetic behavior reverses for trimers (propane) and longer hydrocarbons[65]. We wish to explain this change in kinetics of hydrocarbons as the molecular length increases. Part of this understanding is being able to determine if the change in kinetics is inherent to the increasing molecular chain length, or whether it stems from the heterogeneity of the binding sites available in CNTBs, or some combination thereof. Then, the focus of this work is to understand the kinetics of adsorption of linear chain molecules on carbon surfaces, with an eye toward the specific case of hydrocarbon molecules adsorbing on carbon nanotube bundles.

In order to identify the parameters that play the greatest role in controlling the kinetics of adsorption, we developed the simplest models possible that still recreate the characteristic behavior of the system. Complexity was added in order to determine the effect of secondary parameters on the overall behavior of the system. We began with a one-dimensional,

homogeneous lattice, which represents the groove between two adjacent nanotubes on the exterior of the bundle. We later included two additional lines of adsorption sites in order to better model this groove and the parallel lines of particles that form as the adsorbates begin to spread across the external surface of the bundle. Finally, we consider a two-dimensional, homogeneous surface, representing a planar sheet of graphene, in order to observe the adsorption of chain molecules in the absence of surface effects.

Each of the surfaces we discussed above are represented by lattices of discrete adsorption sites. We allow only single-site occupation, meaning only one particle can reside in a given site at a given time, and we model our adsorbates so that a dimer is two connected monomers, and a trimer, three. These longer molecules are allowed to lay flat on the surface (occupying as many sites as their length indicates) or may stand upright on the surface. With the lattice-gas model thusly implemented, we apply the Kinetic Monte Carlo (KMC) algorithm to our system and allow it to evolve from an empty lattice to its equilibrium configuration. The KMC algorithm gives us the number of particles on the lattice as a function of time, allowing us to extract information both regarding the equilibrium configuration of the system (the orientation of the particles relative to each other and to the surface, for example) and, more importantly, the kinetic behavior of the system, as we can directly measure the speed with which the system progresses towards its equilibrium.

Through the course of this project, we were able to make significant gains in our understanding of the kinetics of adsorption of linear molecules on carbon surfaces. More realistic simulations allowed us to observe an increase in characteristic time with coverage even for monomers, given sufficiently high nearest-neighbor interactions. Using improved analytical techniques, we were also able to explain and predict this increasing characteristic time with coverage, even for systems that include particle-particle interactions. We also observed an “overshoot” in the coverage of dimers adsorbing on carbon surfaces and were able to explain the cause of this overshoot. We found that dimers, like monomers, can also exhibit an increase in characteristic time with increased equilibrium coverage in systems with very high nearest-neighbor interactions, and again we were able to gain insight into the causes of this behavior.

Finally, we showed that longer characteristic times follow directly from the inherent complexity of a system of adsorbing trimers. Thus, we showed that our model predicted the same behavior that has been observed in experiments, and our simulation results provide us with a greater understanding of why this change in behavior occurs.

In Chapter 1 we have offered a statement of purpose for this project, detailing the intellectual merit of our study and the knowledge gaps we hoped to close through our work. We survey the available literature in Chapter 2, discussing the recent findings that have influenced and may be influenced by our project. Chapter 3 includes a description of our methods and procedures. Our results are found in Chapters 4 through 6, in which we discuss the output of our simulations from each type of model. We conclude the report of our findings in Chapter 7, followed by the appendices, in which we given full details of our calculations and simulations.

CHAPTER TWO
REVIEW OF LITERATURE

Polyatomic molecules are the byproduct of reactions between individual atoms, which form bonds in order to complete their outermost electron orbitals. Sharing electrons between atoms (either of the same or differing species) increases the overall stability for the system. The resulting molecules are usually electrically neutral. However, even neutral molecules have a nonzero, time-dependent dipole moment. When averaged over time, these fluctuating dipole moments create an attraction between two neutral particles; the force felt by each particle is called a dispersion force or a van der Waals force[1]. Under the influence of these forces, interacting particles can gain potential energy via proximity, without a permanent physical change to either unit. This process is called adsorption[1].

We have spoken of the process of adsorption in terms of the interaction between two simple, solitary molecules. A much more realistic (and useful) example, however, is a gas of small molecules adsorbing on a substrate. In such a system, the particles in the gas (called adsorbates or admolecules) feel an attraction to the surface of the substrate (called an adsorbent) due to interactions with the many atoms composing that surface. The adsorbed particles can form films that exhibit a wide-range of chemical properties, depending on the interplay between the binding energy a given particle feels toward the substrate and the interaction energy it receives from its neighboring adsorbates.

Section 2.1: Carbon nanostructures

Carbon is an excellent adsorbent due to its natural stability and the many structures it can form. Many of these carbon substrates are porous, providing the added benefit of stronger binding energies and increased surface area for adsorption. The films and other adsorbed phases

that can be observed in carbon nanostructures are of great academic and practical interest and have been the focus of vigorous research for many years[1-43].

The use of carbon for adsorption dates back millennia. Early civilizations burned wood and other plant material, like coconut husks[38,44], to produce charcoal and activated carbon. These nanostructures are highly porous structures with a wide pore-size distribution, making them well-suited for a variety of "catchall" applications but inapt for targeting particles of a specific size. The structures of graphite and graphene were discovered in far more recently. These forms continue to be an important focus of adsorption research; their simple planar geometry makes them very easy model and investigate. For many years, these were all the allotropes of carbon known to the scientific community (excluding diamond, which is not generally used as an adsorption substrate). In the final decade of the 20th century, however, a flurry of discoveries almost doubled the number of nanostructures that carbon had been observed. The C-60 fullerene, also called a "Bucky ball" was discovered in the mid-1980s[1]. This nanostructure looks like a soccer ball because of the hexagonal and pentagonal rings of carbon atoms that combine to form its spherical shape. Carbon nanotubes were then discovered in 1991[2]. Carbon nanotubes are long cylindrical tubes, one carbon atom thick, that terminate at either end in a semispherical cap[1]. Figure 2.01 shows the cap and part of the body of a typical carbon nanotube. When grown, carbon nanotubes tend to form bundles containing anywhere between three and several thousand nanotubes[1]. Most recently, researchers have begun studying carbon nanohorns, which are conical in shape[1]. They are often found diverging from a central core in an arrangement call a "dahlia", named for the flower with a similar appearance. These finds reinvigorated carbon nanoscience and have given a new generation of condensed matter

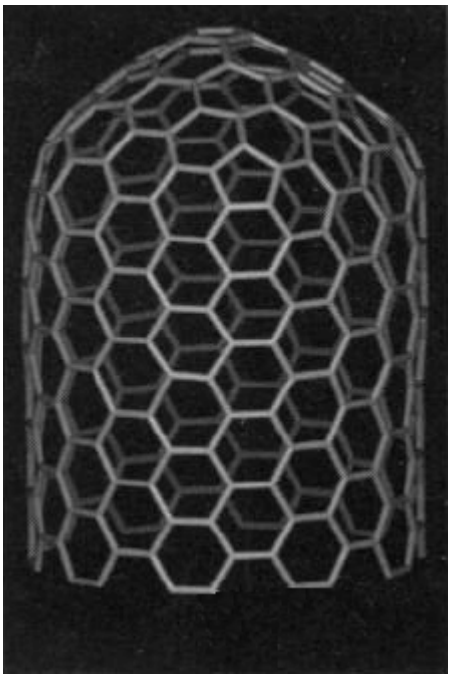

Figure 2.01
Body and cap of a carbon nanotube[8]

scientists a rich landscape of potential research topics. Carbon nanotubes are of particular interest because they offer a high surface area and a uniform pore distribution[1], both of which are important for adsorption applications, and because of their simple geometry.

Section 2.1.1: Carbon Nanotubes

Carbon nanotubes have several unique features that make well-suited for adsorption applications. They are usually on the order of 10Å in diameter and are about 1μm long[7,11,28,30,34]. Once grown, carbon nanotubes spontaneously form bundles, like the one shown in Figure 2.02, due to the van der Waals forces between them[3-9]. These bundles contain anywhere between three and several thousand nanotubes[2], arranged in a triangular lattice with a lattice spacing that depends on the diameter of the component nanotubes, but which is generally about 1.7nm[7-9,22,30]. The extremely high aspect ratio[11,18,25] of carbon nanotube bundles, which can exceed 1000, means that adsorbed films are restricted in motion in some directions but are free to move in others. This immediately drew the interest of condensed matter scientists, who hoped to observe states with reduced-dimensionality, especially quasi-one-dimensional states[1,4-7,9-18,20-22,24,25,28-35], in these films. Because of this special geometry, carbon nanotube bundles were soon the focus of study of many studies.

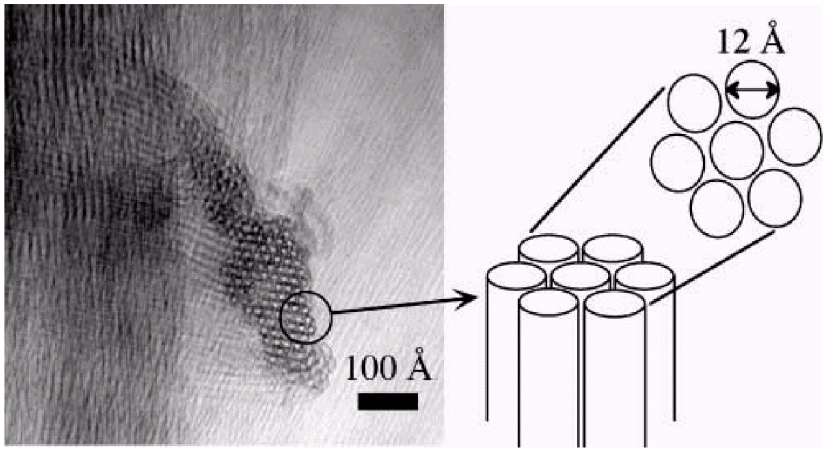

Figure 2.02
TEM images of carbon nanotube (left) and an idealized representation of a carbon nanotube bundle[43]

There are four main types of binding sites found in carbon nanotube bundles, which fall into two categories: external and internal phases[3]. Figure 2.03 shows a cross-section of a carbon

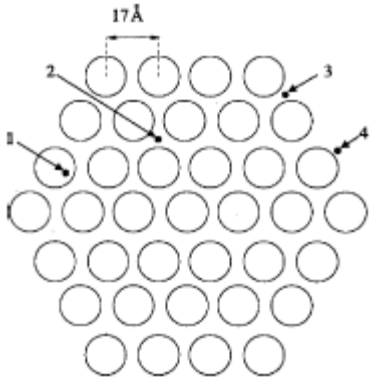

Figure 2.03
Four types of binding sites on an idealized carbon nanotube bundle: 1 – nanotube interior; 2 – interstitial channel; 3 – groove on external surface; and 4 – lateral surface of nanotube on bundle exterior[21].

nanotube bundle and the various binding sites available to adsorbed particles. External phases, like the lateral surfaces of the tubes on the outside of the bundle and the grooves that exist between adjacent tubes, are directly exposed to the adsorbate gas. The lateral surfaces of a carbon nanotube on the outside of the bundle offer a substrate similar to graphene; an adsorbed particle would see only a single sheet of carbon with a binding energy slightly less than that of graphene due to the convex curvature of the nanotube. Conversely, the groove between adjacent nanotubes on the exterior of the bundle offers a unique environment for adsorbed particles. Down in the groove, an adsorbate interacts with the walls of two nanotubes and thus has almost twice as much binding energy as it would elsewhere on the bundle exterior. At the same time, particles in the groove are also restricted in their motion by the close proximity of nanotubes on either side, being able to move easily along the groove but having more difficulty moving up and out of the groove. Adsorption in the groove, then, is of interest because it is a potential location for the formation of the quasi-one-dimensional films mentioned above.

It is also possible for particles to adsorb *inside* the carbon nanotube bundles. The interstitial channels, found between adjacent nanotubes in the interior of the bundle, were once thought to offer much surface area for adsorption, but studies have since shown that they are too small to allow significant uptake[23]. It is possible, however, for particles to adsorb inside the nanotubes themselves. Nanotubes generally have larger diameters than interstitial channels, making it easier for particles to enter. The binding sites inside the tubes also have *increased* binding energies (compared to graphene) due to the concave curvature of the nanotube wall. However, adsorption inside carbon nanotubes is more difficult to observe, compared to uptake in external phases, because of the time needed for the particles to diffuse into the interior.

Figure 2.04 shows the surfaces of constant binding energy in the vicinity of a carbon nanotube bundle. The dark regions in the bottom corners represent individual carbon nanotubes. The method used to calculate these binding energies will be discussed later in this chapter. Of import here is the energy minimum between the two adjacent nanotubes, whose binding energy is twice that of the sites elsewhere on the lateral surface of the nanotubes because particles in the groove interact with both neighboring nanotubes. This strong-binding groove is one of the locations in which researchers expected to observe the formation of novel phases of matter.

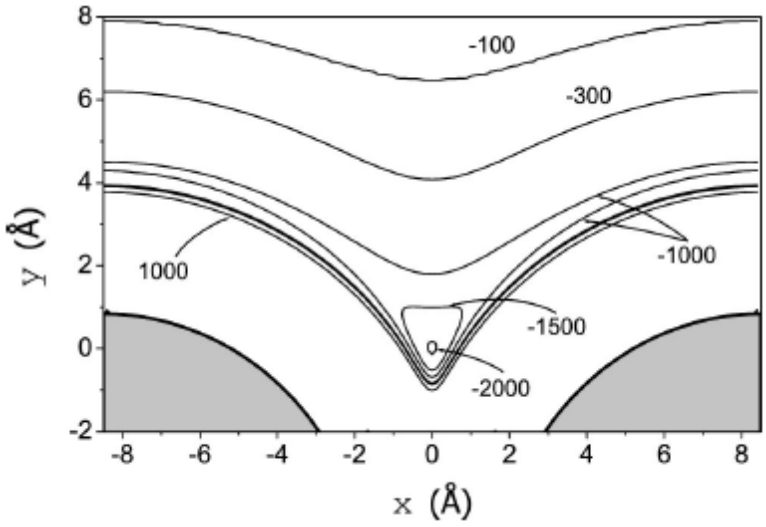

Figure 2.04
The Lennard-Jones potential in the vicinity of the exterior of a carbon nanotube bundle. Note the energy minimum in the groove between two adjacent nanotubes (represented by the gray areas in the bottom left and right corners)[14].

Many theoretical studies considered the adsorption of gas on the external surface of carbon nanotube bundles. Of particular interest was adsorption in the grooves; the strong binding energy and confined space of this part of the bundle made it a likely location for the formation of quasi-one-dimensional phases. A variety of methods have been employed in these adsorption studies, including Grand Canonical Monte Carlo simulations[11-14,26,36] and Kinetic Monte Carlo simulations[3,4,7,10,35]. Simulations predicted that one-dimensional phases of matter would indeed form in the grooves at low coverages. As the coverage increased, additional lines formed parallel to the groove and the 1-D phase transitioned into a 2-D film[3,4,6,9-19].

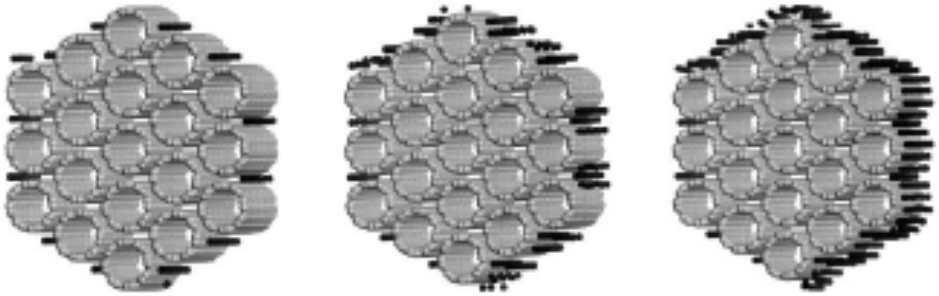

Figure 2.05
External adsorption on carbon nanotube bundles. At low coverages, 1-D phases form in the grooves (left). As coverage increases, these 1-D phases transition to 2-D films (center). At still higher pressures, these films spread to cover the entire external surface of the bundle

The phase transition described above is shown in Figure 2.05. At low pressures (left pane), the majority of the particles settle into the grooves, forming quasi-one-dimensional phases. As the coverage increases, additional lines develop adjacent to the groove (center pane). More and more of these lines form until eventually they spread across the entire exterior surface of the nanotube bundle, thereby completing monolayer coverage (right pane). Many groups also observed the formation of a second 1-D groove phase on top of the monolayer of adsorbed particles, like the one shown below in Figure 2.06. This was only true for small adsorbates, like Ar[12,14,18], Ne[13,14,18], and Kr[14,18], that clung tightly to the structure of the nanotubes and preserved the geometry of the bundle. Larger adsorbates disrupted the potential too much to allow a second 1-D groove phase to form[29]. Experimental results have shown good agreement with these theoretical predictions. Isotherm experiments of the adsorption of noble gases on the external surface of carbon nanotube bundles have shown the formation of a 1-D phase in the groove, which transitions into a 2-D film as it spreads to cover the

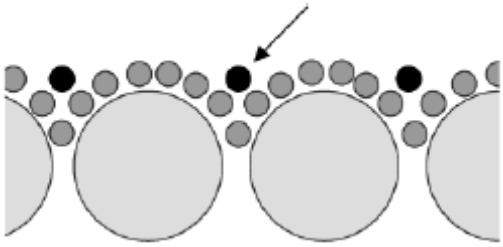

Figure 2.06
An artist's depiction of a second groove phase forming after monolayer has been achieved[24].

bundle[16,18,20-22,24,29]. Even the second layer 1-D groove phase has been observed in the case of Ne adsorbing on the external surface of a carbon nanotube bundle[29].

Most theoretical studies of adsorption on carbon nanotube bundles agreed that adsorption would be limited in the interior of the bundles. It is now widely believed that there is no uptake whatsoever in the ICs[22,26]. Additionally, we have mentioned already that carbon nanotubes have hemispherical cap on either end. When these cap are not actively removed, there is no way for admolecules to enter the nanotube interior. Thus, it is reasonable to neglect adsorption in the interior of the bundle, and to assume that adsorption takes place only in the external binding sites discussed above.

Despite the many studies of gases adsorbing on carbon nanotubes, there are still knowledge gaps to address. The findings described above results from a range of investigations, both experimental and theoretical in nature, that have considered possible adsorption sites in the nanotube bundle, different phases that may form, and even, to a lesser extent, the kinetics of adsorption. Despite this wealth of information regarding adsorption on carbon nanotube bundles, the limitation remains that all of the gases considered in these studies were quasi-spherical adsorbates[3-34]. In order to fully understand the process of adsorption on carbon nanotube bundles, it will be important to study the uptake of more complex molecules in order to determine how the additional freedom of motion will affect both the kinetic and equilibrium characteristics of the system.

Section 2.1.2: Graphite

Another common adsorbent is graphite, which is a series of planar sheets of carbon atoms (individually called graphene). Graphite is a useful substrate precisely because it lacks the complex geometry exhibited by carbon nanotubes. By determining the behavior of different types of admolecules on graphite, it is possible to obtain a baseline from which one can measure the adsorption of that same chemical species on other, more complex adsorbents.

There have been many studies of the adsorption of polyatomic adsorbates on graphite. Many of these works have focused on the phases of matter that can form on the graphitic surface due to the complex interactions between neighboring admolecules. Studies have focused on the

adsorption characteristics of small, rod-like molecules like ethane[45-48] and ethylene[45,47,49,50], while others have considered longer hydrocarbons like propane[51], butane[53-56], and hexane[55-56]. There have even been some studies of extremely long alkanes[57-58] (that is to say, alkanes composed of 15 to 35 chain units).

When considering these polyatomic admolecules, the first difference (compared to quasi-spherical adsorbates) that one must consider is the question of orientation. In the simplest case of a dimer like ethane, there is a measurable angle between the C=C bond in the admolecule and the surface of the adsorbent, whereas in the case of quasi-spherical adsorbates no such distinction is possible. Indeed, an early success in the study of polyatomic molecules was determining the parameters that affect adsorbates' orientation[47,49,52]. It was found that, at low temperatures and coverages, the admolecules would tend to lay flat, with their C=C bonds parallel to the surface, while at monolayer these same particles tended to stand upright, with their long axis perpendicular to the substrate. Several interesting results stemmed from this initial finding. First was the novel phase transition between these two states ("mostly flat" and "mostly upright")[47,49,52]. The other was the discovery that changing the temperature would change the distribution of flat and transverse dimers (ethane, in this case), so that one could find different surface coverages for the same number of molecules[46].

Thus far we have discussed the possible orientations of linear admolecules with respect to the surface. Beyond that, there is the possibility of these particles to change their orientation with respect to each other. Several of these studies found ordered patterns of adsorbates on the surface[45,46,47,50], which could change depending on the parameters on the system. The most common ordered phases were a "herringbone" pattern of flat, linear molecules on the graphitic surface, which could transition to a "parallel" phase, wherein all of the admolecules are aligned. One group[45] found that ethylene formed the herringbone phase because of its stronger quadrupole moment, while ethane tended to arrange itself in a parallel phase due to short-range particle-particle interactions. Another study[56] showed that hexane also formed the herringbone pattern at very low temperatures, but as the temperature increased, a general reorientation to the parallel phase was observed. These investigations demonstrate the importance of particle-

particle interactions, showing how these interactions play a large role in the phases of matter that can form on carbon surfaces. In addition, if linear molecules tend to align themselves in ordered phases on what is an otherwise flat, featureless surface like graphite, then it stands to reason that these or similar quasi-one-dimensional phases might form more easily on carbon nanotubes, whose geometry lends them to linearly-ordered phases.

Despite all of the work done and the great wealth of knowledge that has been gathered, gaps still exist in our understanding of the adsorption of linear molecules on graphite. Although some of findings described above are the products of experimental[46-56,58] studies and others were found through theoretical[45,55-58] investigations, the common theme is that all of these projects focused on the *equilibrium* characteristics of the system in question. The experimental groups used techniques like neutron diffraction[46,50,57,58] to probe the structure of already-equilibrated systems on linear molecules, or heat capacity studies[47,48,51,53,54] to observed phase transitions in the system. Similarly, the theoretical studies relied on Molecular Dynamics simulations to predict phase transitions; while MD simulations do account for time-dependent changes to the system, the time scales used in this technique are so short due to computational limitations that it is impossible to see the entire equilibration process of a given system. Then, the knowledge gap that persists is related to the *kinetics* of adsorption, which will provide an understanding not only of the equilibrium characteristics of a system of linear molecules adsorbing on graphite, but can also show *how* it came to that final state.

Section 2.2: Modeling Adsorption

In order to accurately predict where particles will adsorb and what types of phases will form, accurate calculations of binding energies are necessary. A common model of the energy of interaction between two particles is the Lennard-Jones potential[59], which combines the effects of long-distance attractive and short-range repulsive forces on the overall potential energy of a particle. In most theoretical studies of adsorption, the Lennard-Jones potential is used to find the potential energy at each point in space by summing up the contributions of each individual segment of substrate[7,11-14,16,17,30,32,34,36,37]. The simple geometry of a carbon nanotube makes this calculation relatively easy. The Lennard-Jones potential can also be used to calculate the

interactions between particles in an adsorbed phase. The magnitude of the Lennard-Jones potential[45] can be found by:

$$U_{LJ}(r) = 4\varepsilon((\frac{\sigma}{r})^{12} - (\frac{\sigma}{r})^{6}) \tag{2.01}$$

Where r is the distance between the centers of the two atoms, σ is the length constant and ε represents the strength of the interaction between the particles. The values of σ and ε are characteristic to each element, measured based on interactions within a homogeneous sample of that element. For carbon, which forms the basis for many common adsorbents, the typical values are σ_C=3.4Å and ε_C=28 K[11,30].

The Lennard-Jones potential is plotted in Figure 2.07. In this plot, we see a positive energy of interaction (causing a repulsive force of interaction) for particles inside a radius of σ from the target atom. Outside this radius, the energy is negative and the force attractive, with a stable energy minimum just outside the radius σ. At larger distances, the binding energy approaches zero as the particles cease their interaction.

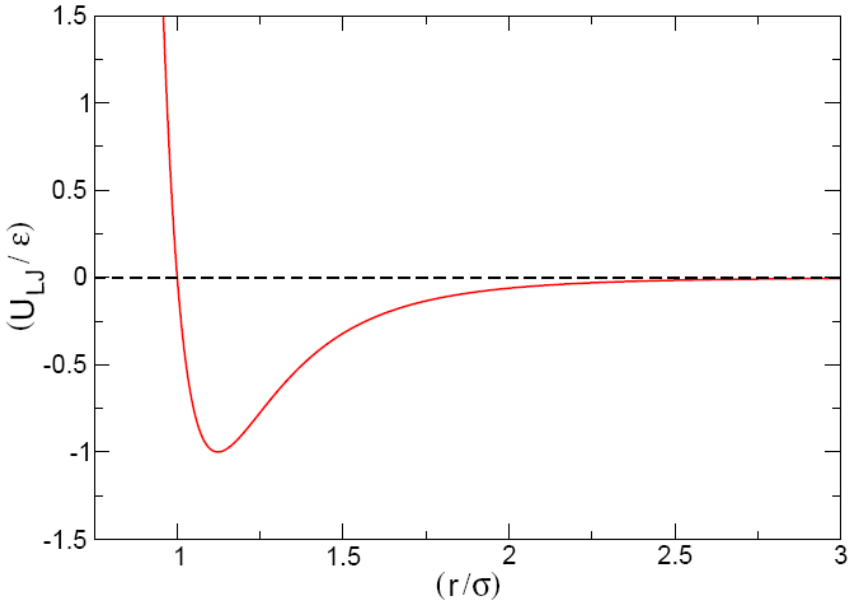

Figure 2.07
A plot of the Lennard-Jones potential[45]. Note the energy minimum for r slightly larger than σ.

When studying the interactions between two particles from two different chemical species (like interactions between the particles of the adsorbate gas and the carbon atoms in the

nanotube, for example), it is necessary to use the "mixed" values of σ_{gC} and ε_{gC}. One method to calculate these values is to follow the Lorentz-Berthelot combining rules[7,11-13,16,17,30,32,34,36,37], whose equations are:

$$\sigma_{gC} = \frac{(\sigma_g + \sigma_C)}{2} \tag{2.02}$$

$$\varepsilon_{gC} = \sqrt{\varepsilon_g \varepsilon_C} \tag{2.03}$$

Where σ_C (σ_g) is the length constant of carbon (the adsorbate gas) and ε_C (ε_g) is the interaction energy of carbon (the adsorbate gas). Through these mixing rules it is possible to calculate reasonable approximations of the binding energy of the substrate.

Another common simplifying assumption is the uniformity of the carbon nanotubes in the bundle. Nanotubes are made up of thousands of carbon atoms, so at the atomic level, these individual atoms give the surface of the nanotube a texture. In order to simplify calculations and simulations, a carbon nanotube is generally modeled as a uniform cylinder[7,11-14,31,32,34,36] in which the corrugation of the carbon atoms has been smeared out to create a continuous and uniform surface.

Section 2.3: Kinetics of Adsorption

We have mentioned above the kinetics of adsorption, and how many investigative techniques, both experimental and theoretical, often overlook this aspect of the equilibration process. For the many insights that can be gained by probing a system at equilibrium, it is often as important to understand how a given system reached its final configuration. There are two groups that have been focusing on this very issue of adsorption kinetics for the past several years: the Migone group, from Southern Illinois University, which collects kinetic data as a part of adsorption studies of gases on carbon nanostructures[41,42]; and the Calbi group, from the University of Denver (previously of SIUC), which uses the Kinetic Monte Carlo algorithm to simulate the behavior of adsorbate gases as they equilibrate on carbon surfaces[3,4,10]. Working in collaboration, these two groups have made significant progress toward closing the knowledge gaps discussed in previous sections.

In a previous collaborative investigation, Kinetic Monte Carlo simulations were used to calculate the fractional coverage of a nanotube bundle as a function of time. These simulations, supported by analytical calculations, predicted that the equilibration time would decrease linearly as the overall coverage increased[3,4,10]. The constant of proportionality in this relation depended exponentially on the quantity $\beta\varepsilon^3$, where β is $(k_BT)^{-1}$, where T is the temperature and k_B is the Boltzmann constant, and ε is the binding energy of the substrate. At the same time, the Migone group performed isotherm experiments with a focus on adsorption kinetics[41,42]. While studying the adsorption of simple gases on the external surface of a carbon nanotube bundle, they found that the waiting time of the system decreased approximately linearly with increases in equilibrium coverage, in good qualitative agreement with theoretical predictions[41,42].

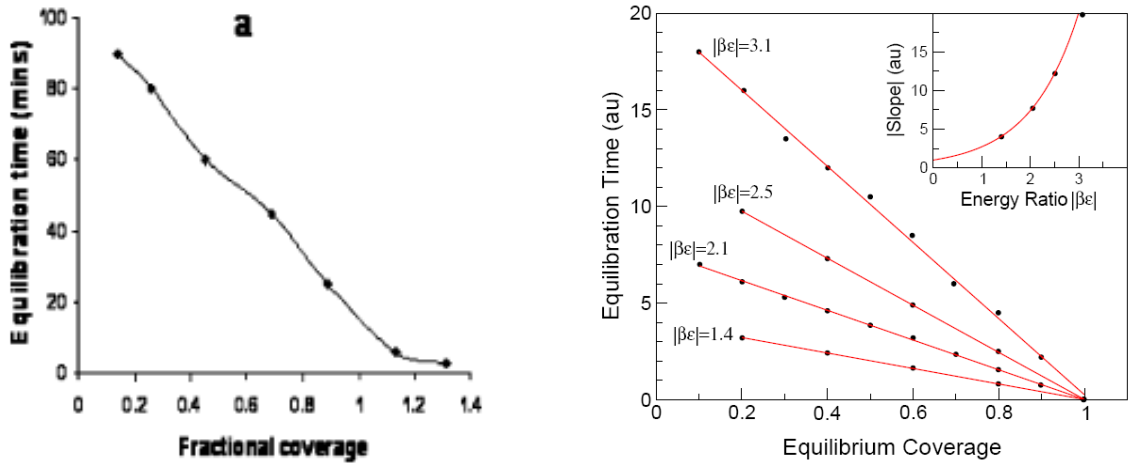

Figure 2.08
Linear relationship between waiting time and final coverage for experimental study (left) and simulation study (right)[3,41].

Figure 2.08 compares the theoretical prediction of the Calbi group (right pane) with the experimental results provided by the Migone group (left pane). The qualitative differences between the two are obvious. Both considered adsorption in external phases of carbon nanotube bundles and both showed decrease in the characteristic time with increased equilibrium coverage.

The raw data from both studies is shown in Figure 2.09. The similarities between the experimental measurements (left pane) and the simulated curves (right pane) are immediately apparent. The computer simulations calculated the fractional coverage as a function of time,

which followed an exponential path. Conversely, isotherm experiments measure the pressure in the cell, which decreases as particles leave the gas to adsorb to the bundle, following an exponential decay curve. The curves are inversions of each other because the simulations measure the particles entering the adsorbed phase, while the experimental results see particles leaving the gas.

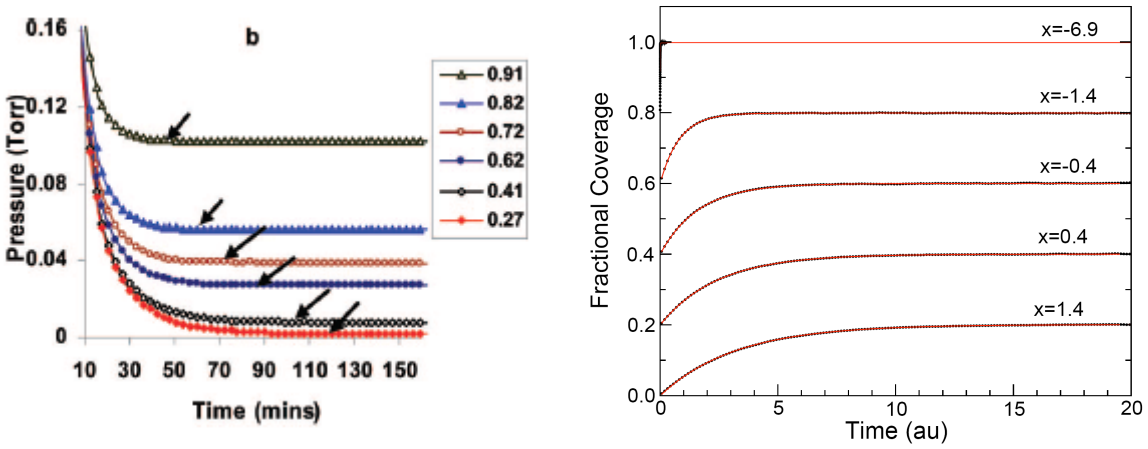

Figure 2.09
Pressure vs. time from isotherm experiments (left) and nanotube coverage vs. time from kinetic simulations. Note the complementary behavior; the experimental results are measuring the loss of particles from the gas, while the simulations focused on the entry of pas particles into the adsorbed phase[3,42].

This initial success impelled further kinetic work. On the theoretical side, there was a temperature-programmed desorption (TPD) study considering the desorption of monomers from a two-dimensional, heterogeneous lattice representing the external surface of a carbon nanotube bundle[60]. At the same time, the original adsorption study was expanded to include the adsorption of monomers on a two-dimensional, heterogeneous lattice[4], and then to consider the adsorption of dimers on the same lattice[61]. The result from the latter can be found in Chapers 5 and 6. On the experimental side, new kinetic results were produced for many systems of increasingly large molecules adsorbing on carbon structures. These new results measured the kinetics of adsorption on carbon nanotube bundles by: quasi-spherical adsorbates[41,42]; ethane[62-65]; propane[65,66]; butane[65,67].

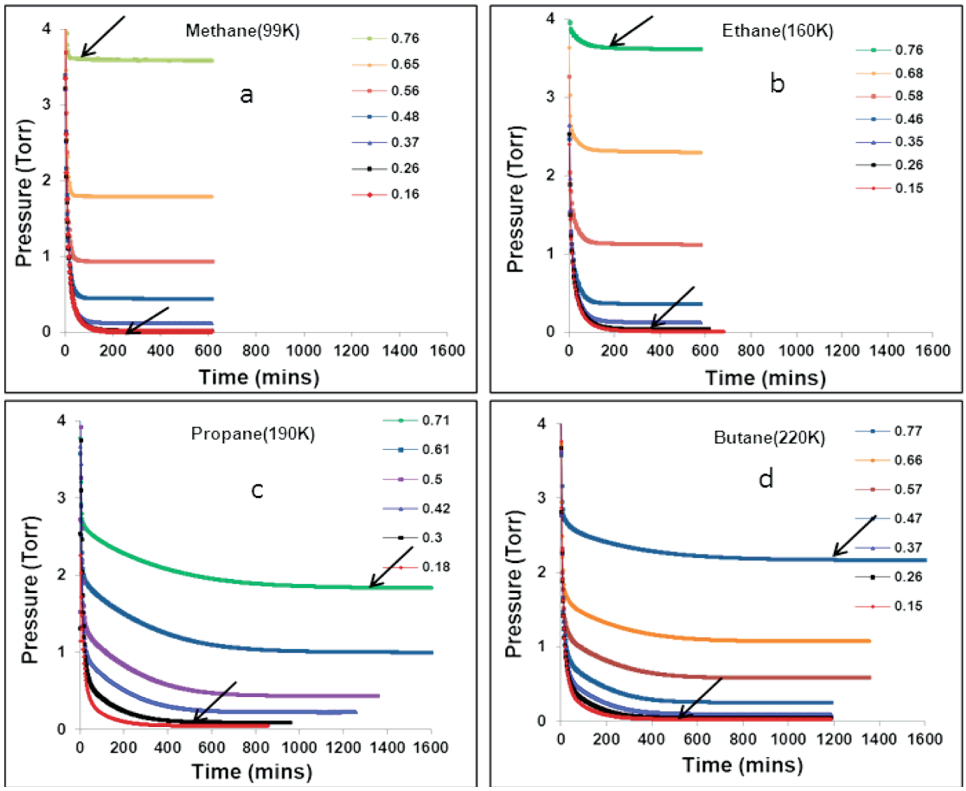

Figure 2.10
Pressure as a function of waiting time for: methane (a); ethane (b); propane (c); and butane (d). Notice that the waiting time decreases as the coverage goes up for the shorter alkanes, methane and ethane, but this behavior reverses for the longer alkanes (propane and butane)[66].

A very intriguing result of the kinetic studies mentioned above is the change in kinetic behavior that occurs when the length of adsorbing alkane is increased. This phenomenon is seen above in Figure 2.10, which shows the kinetic data for the first four alkanes adsorbing on carbon nanotube bundles. The top-left panel (a) shows the pressure as a function of time for methane. As can be seen, the waiting time for low coverages (low pressures) is much longer than it is for high coverages (high pressures). This is in keeping with both our previous theoretical and experimental findings (summarized in Figure 2.08). We see similar behavior in the top-right panel (b), which is the kinetic data for ethane. The decrease is not as drastic, but the waiting time still goes down as the equilibrium coverage increases. However, the complete reversal of this trend is seen in the bottom-left panel (c), where we see that the waiting time for propane continues to

increase as the equilibrium coverage goes up. This new behavior continues for butane, shown in the bottom-right panel (d).

Our past theoretical work with adsorption kinetics led to a greater understanding of the adsorption of quasi-spherical particles on carbon nanotube bundles (and other carbon surfaces). Through our previous work, we elucidated the process through which systems of adsorbates equilibrate, and we developed a strong computational and analytical framework to explain experimental results. The obvious next step, now that we see that linear molecules of increasing length show a reversal of the previous kinetic paradigm, is to continue our simulation scheme and expand it to account for molecular chains. This report details our efforts to understand how increased admolecule complexity, which leads to orientation effects and increased particle-particle interactions affects the kinetics of adsorption. Our goal is to gain a better comprehension of the drivers of adsorption for linear molecules in general, and to explain this particular kinetic behavior for alkanes in particular.

CHAPTER THREE
METHODS AND PROCEDURES

Many competing parameters and processes influence the kinetics of adsorption in any system. We were first prompted to pursue this particular field of study by experimental results of alkanes adsorbing on carbon nanotube bundles, which showed a change in the kinetic behavior of the system as the length of the molecular chain increased. Our goals are two-fold: firstly, we want to explain the change in kinetics observed in the experiments; but we also want to understand the parameters in general that play the greatest role in controlling the kinetics of adsorption. Thus, throughout this study we strike a balance between a specific focus on the behavior of alkanes adsorbing on carbon surfaces and a more generalized understanding of the adsorption of linear molecules that can be applied to other systems.

In order to gain a more complete understanding of the factors that have the greatest effect on the adsorption process, we must approach our work from a variety of different angles, using an array of techniques. Each of the different methods we have used gives us a different insight into the inner workings of these systems. Our use of several techniques in conjunction allows us to constantly check our results. By pursuing multiple vectors of inquiry, we are able to both elucidate the process of adsorption and, at the same time, ensure the quality and validity of our results for experimental comparisons. To this end, we used a combination of computer simulations and analytical calculations to study the kinetics of adsorption.

Section 3.1: Computer Simulation Scheme

The main effort of our study is focused on computer simulations, which allow us to probe the behavior of a wide range of different systems that are too complex for direct analysis. In order to develop our simulation scheme, we needed to model both the molecules that would be adsorbing (the adsorbates or the admolecules) and the surfaces upon which the adsorption would

take place (the adsorbent or substrate). We then applied the Kinetic Monte Carlo (KMC) algorithm to our model, which would allow us to observe the number of adsorbed molecules on the surface as a function of time, from which we could extract the rate of adsorption as well as the equilibrium configuration of the system.

Section 3.1.1: Modeling Adsorbates

The goal of this study is understand the kinetics of adsorption of chain molecules of increasing length. While we are interested in particular in the adsorption of methane, ethane, and propane, we wish the models of these molecules to be as simple as possible so that we can both focus on the parameters that have the *greatest* impact on adsorption kinetics, and so that our results can be extended to other, similar chain molecules.

Section 3.1.1.1: Modeling Methane – Monomers

We first consider the shortest alkane, methane (CH_4). This molecule consists of a central carbon atom that is surrounded by four hydrogen atoms. Because methane spins at a great rate when it is in a gas state, it is both convenient, and mathematically simpler, to treat a methane molecule as a quasi-spherical particle. In our simulations, we neglect any shape of the methane molecule, treating it as a sphere that can adsorb to a surface and diffuse around it, but without any sense of the orientation of the particle. Because of this, there was only one binding energy between the monomer and the surface, and only one value of the interaction energy between neighboring monomers. We assumed the particles would arrange themselves on the surface in order to maximize their adsorption and interaction energies. Methane has an adsorption energy of about 1000K (on graphene), and its particle-particle interaction energy of about 140K. These values are too high for our simulation scheme, so we scaled them down to 100K and 14K, respectively. Thus, we could simulate the behavior of methane directly, or by varying the ratio between the adsorption and interaction energies, we could represent a completely different system.

Section 3.1.1.2: Modeling Ethane – Dimers

The next chain molecule is ethane, which is very similar to methane, except that it is longer. This similarity is why alkanes were of interest to begin with. Its chemical formula is (C_2H_6),

but we consider it to be two quasi-spherical methyl groups bound together. Then, we can imagine our ethane molecule as a dimer, as shown below in Figure 3.01. It serves us well to model ethane as a dimer; not only is it a simple model that contains the keycharacteristics of the alkane, but also many other molecules can also be accurately represented as dimers, giving our work a greater reach.

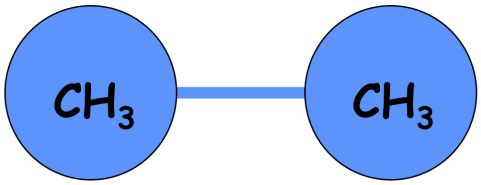

Figure 3.01
A cartoon of an ethane molecule modeled as a dimer.

When we are considering the adsorption of dimers, however, we must make some assumptions about the interactions of the dimers with the surface and with each other. For example, the main difference between a dimer and a monomer is the former's sense of orientation. We can see that dimers can take on different orientations with respect to the adsorbent, while monomers cannot. Then, we must define these possible orientations. Ideally, a dimer should be able to take on any position with respect to a hypothetical surface, which is to the say, the angle between the surface and the dimer should be able to take on any angle between 0° and 90°. However, this is not conducive to our simulation scheme. It adds too many parameters to the system, and as we mentioned previously, we only want to include the parameters that play the most important role in the kinetics of adsorption. Therefore, we limit the orientations of flat molecules to "completely flat" along the surface or "perfectly perpendicular" to it. We posit that, if the dimer were leaning to the side, it would likely obstruct other dimers from slipping between it and the surface, and if there were nothing between this dimer and the surface, it would be energetically preferable for it to lay flat. Furthermore, we kept the option of adding more orientations to the system if it showed that these were necessary to properly model the system, but that did not end up being the case.

The ability of ethane to reorient itself also affects the energies used to model it. An ethane molecule is modeled as two methyl groups, so when it lays flat on the surface, we assign it twice the binding energy of methane (200K on graphene). However, when ethane stands upright on the surface, the bottom methyl group is bound as before, but the upper half of the molecule is significantly farther from the carbon surface. Because of this, the total adsorption energy for an upright dimer 140K, 100K for the bottom particle and 40K for the top particle because of the drop off of electrostatic potential with distance. We used these values for the adsorption energy of our dimers throughout our study. Studying the adsorption kinetics of a system of dimers with a different ratio of flat adsorption energy to upright adsorption energy is something we may pursue in the future, but it is beyond the scope of the present work.

The different orientations of ethane also affect the particle-particle interactions. We mentioned for methane we were using an interaction energy of 14K. While this energy is valid for two flat dimers laying end to end (since both are treated as monomers), it does not hold true for a flat dimer interacting with an upright dimer or for two upright dimers interacting with each other. In the former case, the flat dimer interacts with both units of the upright dimer, so we used a total interaction energy of 21K, since the top unit of the upright dimer is slightly farther away from the flat dimer. For the latter situation, we used a particle-particle interaction energy of 42K because each of the methyl groups in one upright dimer interacts with each of the methyl groups in the other, creating four total bonds.

3.1.1.3: Modeling Propane – Trimers

The final admolecule that we considered in this study was propane (C_3H_8). This particle to be a chain of three units, with methyl groups on either end separated by a methylene group. The difficulty in this situation was that propane has a bend of about 109° in it; this bond is so strong that it is very unlikely that it would change its angle. We had to take this into account in our model.

Similarly to our treatment of dimers, trimers have many possible orientations with a surface. Like before, we had to decide which possible states were the mostly likely and limit our model to those configurations. We selected the flat and upright orientations to maintain the

parallel with dimers. However, we also chose to include a state in which the trimer makes an L-shape with the surface (nicknamed the “ell” state), where two of the units are flat on the surface and the third is standing upright to it. As with dimers, we could have included more states had model required it, but we specifically wanted to keep the number of possible states to a minimum in order to maintain our focus of the most important parameters of the system and to conserve computational resources.

Trimers offered still more complexity when it came to the different energies available in the system. Flat trimers were assigned an adsorption energy of 300K, and an ell trimer was given an energy of 240K, since it is essentially the combination of one monomer and one upright dimer. Upright trimers were a little more complicated; we began with an upright dimer and added another methyl group quite far from the surface, giving it a total energy of 150K. Interaction energies were equally complicated. We continued to have an energy of 14K between interacting units of flat trimers. When a flat trimer interacted with the upright end of an ell trimer, we used an interaction energy of 21K, like we did with dimers. Because the third trimer is so far off the lattice, we neglected its interaction with a flat trimer, and so we used 21K as the interaction energy between a flat trimer and an upright trimer as well. Returning to dimers again, we used 42K for the interaction energy between the upright ends of two ell trimers. Admittedly, the upright half of an ell trimer is not perfectly perpendicular to the substrate, as we discussed previously, but we thought this was a minor assumption in order to simplify our computational scheme. Finally, we used an interaction energy of 49K between the upright end of an ell trimer and an upright trimer, and a binding energy of 70K between two upright trimers. These interaction energies become large quite quickly due to all of the interactions between the units making up these admolecules. There is a particular energetic bias towards trimers that are upright, a situation that will arise as the system approaches monolayer.

Section 3.1.2: Modeling Adsorbents – Surfaces

The next step in setting up our simulation scheme is to model the surfaces upon which the particles will adsorb. Our initial motivation for this study was to consider the adsorption of chain molecules on carbon nanotubes (CNTs), so we wanted to include a CNT bundle as one of

our adsorbents. However, we also wanted to gain a better understanding of how different parameters affect adsorption in general. Because of this, we also wanted to use a simpler substrate that would not have the geometric complexity inherent to CNTs. Therefore, we also considered a flat sheet of graphene as an adsorbent, in order to observe the adsorption behavior of our chain molecules in the absence of surface effects.

In another effort to maintain simplicity (when appropriate), we modeled each of these surfaces as a lattice of discrete adsorption sites. This is a common technique; it is computationally much more difficult to assume continuous adsorption anywhere on the surface, with fairly little benefit. We chose the adsorption energies for these sites based on an average distribution of carbon atoms in the surface, rather than going into the detail of considering surface effects and interactions with individual carbon atoms in the nanotube. This is another technique that is often used, which also greatly simplifies the simulation with a negligible sacrifice of exactness. Our adsorbates can fill these lattices following the lattice-gas model with single-site occupation, meaning a monomer can occupy one site or another, but not half of each, and if one monomer is occupying a given site, another cannot adsorb there too. The system necessarily becomes a bit more complicated for dimers and trimers; a dimer can occupy one or two sites, depending on whether it is upright or flat, and a trimer can occupy one, two, or three sites, again depending on its state. We include particle-particle interactions only between nearest-neighbor adsorbates, that is, between adsorbates in adjacent sites.

Section 3.1.2.1: Modeling Carbon Nanotubes – Simple Model

When modeling adsorption on carbon nanotube bundles, we wanted to maintain our focus on developing the simplest model possible that correctly represents the key characteristics of the system. In the case of CNTs, studies have shown[14] that a strong-binding adsorption site forms in the groove between two adjacent nanotubes on the outside surface of the bundle. Particles in this site would be bound to both nearby nanotube walls and would thus have almost twice the binding energy of a particle elsewhere on the external surface of the bundle. This effect is shown below in Figure 3.02; in this figure, one is looking down along the axis of the nanotube bundle, and the two shaded regions on the bottom two corners represent the nanotubes

themselves. The strong-binding site is clearly visible at the bottom of the groove between the neighboring nanotubes. This is a cross-section of the nanotube bundle; if we assume an ideal infinite bundle, this one strong-binding site would become a line of sites, and it would be this line of sites that would be the most energetically favorable. Thus, our first model for adsorption on a CNT bundle was a one-dimensional, homogeneous lattice of sites, like the one shown below in Figure 3.03. We opted to use a lattice of 200 sites, as an approximation of an infinite lattice.

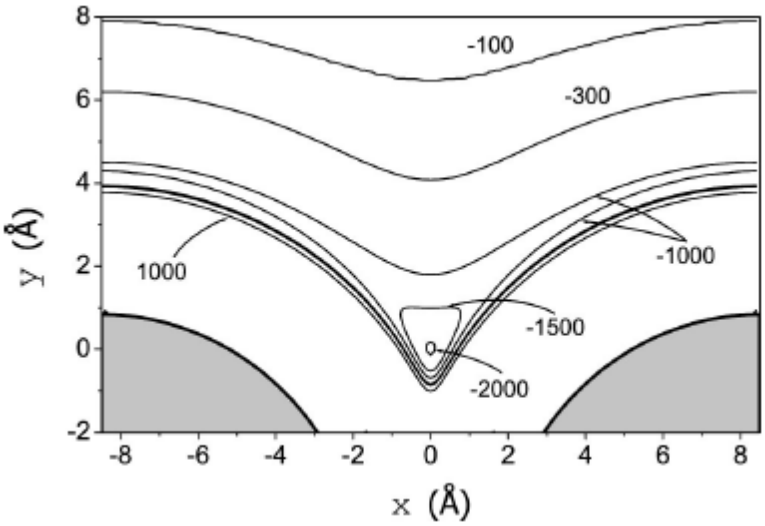

Figure 3.02
Binding energy strengths in the vicinity of a CNT bundle. Note the strong-binding adsorption site at the bottom of the groove formed between adjacent nanotubes (shaded regions)[14].

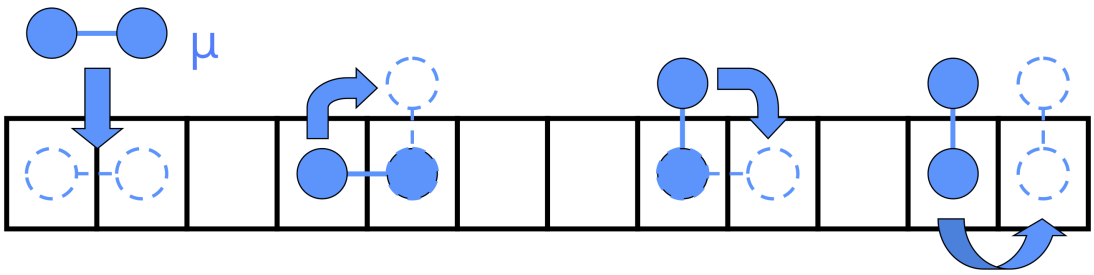

Figure 3.03
A one-dimensional, homogeneous lattice, representing the strong-binding grooves found on the external surface of a CNT bundle. On this lattice, particles can adsorb, diffuse, and change their orientation (where applicable).

Because we are modeling the strong-binding groove, we use an interaction energy of 175K per methyl group (instead of the 100K we used for graphene). It is almost twice as much as we used before, because of the bonds to two different nanotubes, but the curvature of the nanotube wall causes the binding energy to decrease a small amount.

Section 3.1.2.2: Modeling Carbon Nanotubes – Realistic Model

Although the one-dimensional lattice described above gives us a good starting point to understand the adsorption behavior of chain molecules on a carbon nanotube bundle, it lacks some key details that may give us a better understanding of the full adsorption process. We wanted to create a more realistic lattice that might show us some kinetic behaviors that do not appear for the simple, 1-D lattice.

When we reconsider the binding energies on the exterior of a carbon nanotube bundle, we see that, after the groove is filled, particles will begin to spread across the rest of the surface of the bundle. In the left panel of Figure 5.04 (below), we see that there could actually be additional rows of adsorption sites, the strong-binding groove we discussed above, but also adsorption sites binding to the nanotube walls on either side of the groove (the "edges"). Depending on the relative sizes of the adsorbates and the nanotubes, there could be more or fewer edge sites; here we chose to consider one row of edge sites on either side of the groove. In Figure 3.04 (right panel) we show these adsorption sites represented by a 2-D lattice. We used a lattice with three rows of 200 sites each in order to maintain our comparison with the one-dimensional lattice we used previously, and we included periodic boundary conditions to further the approximation of an infinite lattice. As before, the binding energy of the groove was 175K per methyl group in the groove (262.5K per upright dimer) and 87.5K per methyl group of the edges (131.5K per upright dimer) due to the binding with one nanotube wall.

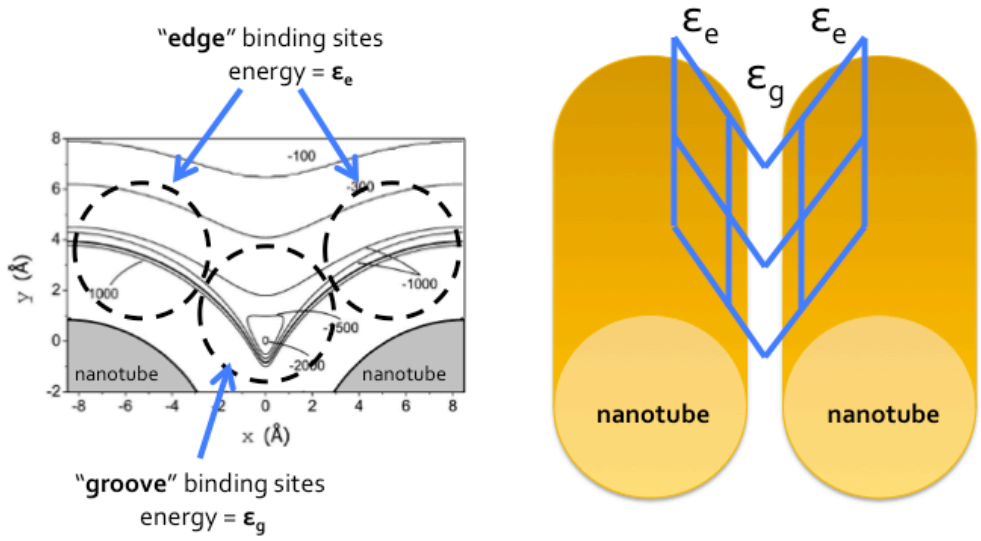

Figure 3.04
Adsorption sites covering the exterior of the CNT bundle (left panel) and how a lattice might model those adsorption sites (right panel)[61]

Section 3.1.2.3: Modeling Graphene

The final surface we wanted to study was a planar sheet of graphene, devoid of surface features. We modeled this surface as a two-dimensional, homogeneous lattice, using six rows of 100 sites in order to maintain the 600 total adsorption sites used for carbon nanotubes. The biggest change we made was to use a triangular lattice rather than a square lattice. We thought this was a more natural shape for our monomers to adsorb in. More importantly, a triangular lattice had a total angle of 120° between adjacent binding sites, which was more conducive to the natural shape of flat trimers (with their 109° bend).

The adsorption energies cited throughout Section 3.1.1 were all for graphene, which is a flat sheet of carbon. Thus our adsorption energy (100K per methyl group) is slightly less than we saw for CNTs, but the lattice allows more nearest neighbor molecules, which means the total binding energy can rise much more quickly.

Section 3.1.3: Kinetic Monte Carlo algorithm

Having developed a framework for the admolecules and adsorbents that we would consider, we were able to implement our simulation scheme, which is based on the Kinetic Monte

Carlo algorithm. This algorithm tracks the number of particles on the surface as a function of time; by tracking the behavior of a system as a series of small changes in state accompanied by small increments in the time variable, we are able to watch the system evolve from its initial to its equilibrium state.

In order to implement the KMC algorithm, we must first know the total energy of every admolecule of the lattice. To find the energy of a given particle, we begin with its adsorption energy. For the homogeneous lattices (1-D and 2-D), this is a fixed amount based on the type of particle, but for the inhomogeneous lattice, we must also consider where on the lattice the particle is bound. To this binding energy we add the interaction energy with any units in neighboring sites. After these energies have been found, and open lattice spaces has been identified as a possible adsorption sites, we calculate the probability of a given change in state (that is, an adsorption event, a desorption event, or a change in orientation) using the following equations:

$$\frac{W_{ads}}{W_{des}} = \exp[-\beta(E_i - \mu)] \tag{3.01}$$

$$\frac{W_{i\to j}}{W_{j\to i}} = \exp[-\beta(E_j - E_i)] \tag{3.02}$$

Here, W_{ads} is the probability of a particle adsorbing in an empty site in the lattice and is dependent on βμ, the effective chemical potential of the system; W_{des} is the probability of desorption of a given particle ***i***, and is dependent on the total binding energy of that particle βE_i**;** and $W_{i\text{-}j}$ is the probability of a particle in a state ***i*** transitioning to a state ***j***, which depends on the energy of each state. With the probabilities of every possible change in state thusly calculated, we select a change of state to occur.

The change in state that actually takes place is the one that satisfies the inequality:

$$\frac{1}{W}\sum_{j=1}^{k-1} W_{ij} < \alpha_1 < \frac{1}{W}\sum_{j=1}^{k} W_{ij} \tag{3.03}$$

Where:

$$W = \sum_{i,j} W_{ij} \tag{3.04}$$

Thus, we select a random number α_1 (between zero and one) and we begin to add up all of the normalized probabilities until our sum surpasses our random number α_1. The change in state whose probability causes our sum to overtake the random number is the one that is implemented in our system, so the most probable changes in state (those with the greatest probabilities) have the greatest chance of being implemented, but other changes in state are also allowed to happen. It is this inherent randomness that allows the system to evolve freely, rather than being forced into a given evolutionary path.

After we have implemented a change in state (by adding a particle to our lattice or removing one, or moving a particle around the lattce), we must also increment the time variable. We do so according to the following equation:

$$\Delta t = -\frac{1}{W}\ln(\alpha_2) \tag{3.05}$$

We select another random number α_2 (between zero and one) and increase the time variable based on that amount. However, we also normalize by the total sum of probabilites. This means that, when there are many probable changes of state, the value of W is quite large, and so the changes in state will occur rapidly (with a small amount of time in between them). One the other hand, when no changes in states are particularly probable, the value of W is much smaller and the evolution of the system proceeds at a slower pace.

After the change of state has been implemented and the time variable has been updated, the algorithm repeats. The energies in the new configuration of the system are again summed up, another change is selected and implemented, and the time increases, and so on. The output of this algorithm, then, is the total configuration of the system at a succession of points in time, from which we can extract kinetic information, like the rate of uptake of the lattice, or equilibrium data, like how many particles are in each orientation at equilibrium.

A different code was needed to implement this algorithm for each of the systems investigated in this study. We used FORTRAN77 because of its ease of use in general and its particular aptness for a repeated set of statistical calculations like we described above. The codes used in this study were written in-house in order to maintain our control of them and to better understand their capabilities and limitations. Appendix A contains a more detailed account of the KMC algorithm.

Section 3.2: Analytical Methods

While our simulation scheme provided most of the results in this study, we used other methods to confirm and inform our simulation data. These alternative methods consisted primarily of statistical mechanical calculations and the manipulation of kinetic equations. Although they represent only a small part of the work we did in this project, these analytical techniques played a key role in our understanding of the kinetics of adsorption.

Section 3.2.1: Equilibrium Calculations

Despite only providing information about the equilibrium state of a system, statistical mechanics played a major role in our study. These calculations did not directly relate to our measurements of adsorption kinetics, but they allowed us to confirm the equilibrium configurations predicted by our simulations. When our simulations showed us unusual or unexpected kinetic data, we were able to trust these results because we knew that the equilibrium values were what they should be.

Section 3.2.1.1: Calculations for a 1-D, Homogeneous Lattice

Because we wanted to include particle-particle interactions in our calculations, we could no longer assume every adsorption site to be independent, as we did in our original calculations for monomers on a homogeneous lattice (Sec. 4.1.1). We had to use a larger unit cell that had the possibility of having multiple adsorbed particles so that we could incorporate particle-particle interactions. Therefore, we used a unit cell of four sites, which would allow us to consider a variety of configurations without being redundant.

We considered every possible arrangement of monomers on the lattice and recorded the number of adsorbed particles, the total energy of the microstate (including both adsorption energy

and interaction energy), and the degeneracy. From these values we were able to predict the total coverage, the total energy, and the energy per particle as a function of chemical potential and interaction energy (as we kept all other parameters constant). We did a similar procedure for dimers. These equilibrium characteristics, which are described in greater detail in Appendix B, were a valuable check on our simulation results.

Section 3.2.1.2: Calculations for a 2-D, Heterogeneous Lattice

Similar calculations were done for a two-dimensional, heterogeneous lattice. In this case, we used a unit cell of six sites, two sites long and three sites (the groove and the two edges) wide. We wanted to use the smallest unit cell possible that still included the key characteristics of the lattice (in this case, the heterogeneity of the binding sites). We again counted all of the possible configurations of dimers on this unit cell and calculated the final coverage and energy per particle for this system. Our calculations for this lattice are found in Appendix C.

Section 3.2.1.3: Calculations for a 2-D, Homogeneous Lattice

The final surface we considered was the planar sheet of graphene, modeled by a triangular lattice. In order to match the geometry of our lattice, we used a unit cell of seven total sites, one in the center, surrounded by a hexagon of six other sites. Again, we were able to identify the different ways that systems of monomers, dimers, and trimers could be arranged on this unit cell, from which we calculated the equilibrium characteristics of each of these systems. The equilibrium calculations for monomers, dimers, and trimers on graphite can be found in Appendices D, E, and F, respectively.

Section 3.2.2: Kinetic Calculations

While most of our analysis focused on the equilibrium configuration of the system, we were able to do some limited work with equations representing the kinetics of adsorption. In our previous work, we were able derive the following equation, which showed how the fractional coverage of a lattice (with adsorbing monomers) increased based on the adsorption process (driven by the chemical potential μ) and decreased based on the desorption of particles (controlled by the binding energy ε_0).

$$\frac{dn}{dt} = \exp(\beta\mu)(1-n) - \exp(\beta\varepsilon_0)n \tag{3.06}$$

This simple equation provided us with much of the insight we gained in our previous work of non-interacting monomers (Chapter 4). Unfortunately, it was not able to include the effect of particle-particle interactions.

We know that, in a system of interacting monomers, the energy per particle on the lattice (and thus the desorption rate) will depend on the total number of adsorbed particles. Examining Eq. 3.06, the obvious change needed to include interaction energy was to allow the energy per particle to be a function of the coverage of the lattice. This improved equation is shown below.

$$\frac{dn}{dt} = \exp\big(\beta\mu\big)(1-n) - \exp\big(\beta\varepsilon(n)\big)n \tag{3.07}$$

However, it was not until we expanded our statistical mechanical calculations, that we were finally able to calculate the energy per particle. Once we had this function, we were able to perform additional analysis on Eq. 3.07 and eventually find the characteristic time of the system as a function of chemical potential and binding energy, within the limitations of several approximations. These results are in Chapter 5. Unfortunately, while we have tried to apply our kinetic equation to dimers and trimers, we have not yet been successful.

CHAPTER FOUR
BACKGROUND INFORMATION AND PREVIOUS RESULTS

Our current study has gone through several phases over the past few years. Our most recent findings are built upon prior results, and our current analysis relies heavily on the framework that we built in the previous phases of our work. We will give a brief but thorough recounting of our previous work, which was the subject of a Master's thesis and several publications[3,4,10], in order to help explain and motivate the work we have done for this dissertation.

Section 4.1: Non-Interacting Monomers on a 1-D, Homogeneous Lattice

This work, which focuses on the kinetics of adsorption of chain-molecules of increasing length on carbon surfaces with different geometries, began as a study of the adsorption kinetics of quasi-spherical adsorbates on carbon nanotubes. We wanted to help elucidate the process of adsorption of these small particles on carbon nanotube bundles. In particular, we sought to identify potential adsorption sites in and around the nanotube bundle and to determine it how long the process of adsorption would require for each of these potential binding sites (that is, how much time is needed for the system to reach equilibrium). Because of the very large aspect ratio of carbon nanotubes, it was logical to use a one-dimensional lattice to represent adsorption sites in a carbon nanotube bundle. Adsorbed particles are often confined by the nanotube walls, whether these adsorbates are inside a carbon nanotube or adsorbed in the strong-binding groove that exists between adjacent nanotubes on the exterior of the bundle. We used a homogeneous lattice, meaning every lattice site had the same binding energy, based on the assumption of an ideal nanotube bundle. And we modeled our adsorbates as monomers because we wanted to compare with experimental results from systems using noble gases and other quasi-spherical admolecules, like methane and Freon.

At this stage of our work, we wanted to use the simplest model possible to explain the adsorption kinetics of monomers on carbon nanotube bundles, seeking to identify the parameters that have the greatest influence on the kinetics. Therefore, we chose to neglect particle-particle interactions and surface heterogeneity. We would include these factors later in order to better understand the role they play in the equilibration of the system, but only after we had developed an understanding of the basic behavior of the system.

Using a simple model for adsorption had the added benefit of several analytical tools that allow us to understand not only the behavior of the system, but also the drivers of that behavior. These techniques helped us to better understand the equilibrium and kinetic characteristics of our systems as well as allowing us to verify our simulation results. The only drawback of these analytical methods is that they only work for simple systems, more specifically, systems without particle-particle interactions or surface heterogeneity. When these factors are included, it becomes impossible to find closed-form solutions to these equations. By allowing us to confirm the veracity of our simulation results for simple systems, however, we knew that we could trust our simulation results when these factors were later introduced.

Section 4.1.1: Analysis of Neutral Monomers on 1-D, Homogeneous Lattice

Because we chose to neglect nearest-neighbor interactions in this initial part of the study, we were able to treat each binding site independently. This reduces the system to a series of N (in this case, 600) individual binary systems, each of which could be empty (with zero energy) or be occupied by a single particle (with energy ε). The expected fractional coverage of this system was found thusly:

$$n_{eq}(T,\mu) = \frac{1}{1+e^{\beta(\varepsilon-\mu)}} \tag{4.01}$$

We derived this equation via the partition function using the standard statistical mechanical method. Here, the expected equilibrium fractional coverage n_{eq} has been found as a function of energy and chemical potential (ε and μ, respectively) and of the inverse of the temperature β (where β is defined as $(k_BT)^{-1}$), where T is the temperature and k_B is the Boltzmann constant.

We also developed a simple kinetic equation model describing the rate at which the fractional coverage of the lattice increases:

$$\frac{dn}{dt} = W_a(1-n) - W_d n \tag{4.02}$$

Where W_{ADS} = exp(βμ) and W_{DES} = exp(βε) as discussed in Chapter 3 (and are constant). Because we assume the system is connected to an infinite reservoir of particles, we require μ to have a fixed value, and neglecting nearest-neighbor interactions results in a constant value for the energy ε. Then, we can approach this equation as a first-order, linear differential equation, with the solution:

$$n(t) = n_{eq}(1 - e^{-t/\tau}) \tag{4.03}$$

This is the kinetic behavior we predicted from our simulations. We expected a exponential-style decay both from experimental results as well as from our intuition. Thus, we are most interested in the characteristic time τ of the system. We can rearrange Equation 4.03 to become:

$$-\ln(1 - n(t)/n_{eq}) = \frac{1}{\tau} t \tag{4.04}$$

By plotting the logarithm of the fractional coverage as a function of time, we are able to extract the characteristic time as the reciprocal of the slope of the line produced. This method is commonly used in experiments to quantify an equilibration time for a given system.

At the same time, as part of the calculations that produced Equation 4.03, we were able to develop an expression for the characteristic time τ that depended on W_{ADS} and W_{DES} (from Equation 4.02). By rearranging this expression, we were able to show that:

$$e^{-\beta\varepsilon}\left(1 - \left\langle N \right\rangle\right) = \tau \tag{4.05}$$

Our preliminary calculations therefore predicted a linear relationship between the equilibrium fractional coverage <n> and the characteristic time τ, with the constant of proportionality in this relationship dependent on the strength of the binding energy and on the temperature of the system. With these predictions made, we set about performing our first simulations to compare to these analytical results.

Section 4.1.2: Kinetics of Neutral Monomers on 1-D, Homogeneous Lattice

As mentioned in Chapter 3, our first simulations modeled non-interacting monomers adsorbing on a one-dimensional, homogeneous lattice. We implemented a code applying the Kinetic Monte Carlo algorithm to this system and ran a battery of simulations to observe the kinetic behavior of this system as the binding energy, temperature, and chemical potential changed. We found that the equilibrium coverages indicated by our simulation code matched our calculations of the equilibrium characteristics of the system. Similarly, we discovered an exponential decay function in the fractional coverage as time progressed, just like we predicted with our kinetic calculations. Because our simulated results matched so well their predicted values, we can trust other simulation results for system for which little analysis and equation manipulation is possible.

Figure 4.01 (below) shows the fractional coverage as a function of time for a system on non-interacting particles adsorbing on a one-dimensional, heterogeneous lattice. The red lines are the curves predicted by our kinetic calculations (Equation 4.03), while the small black dots are the output of the simulations discussed in this section. As can be seen, there is very good agreement between the behavior our calculations predict and what our simulations report.

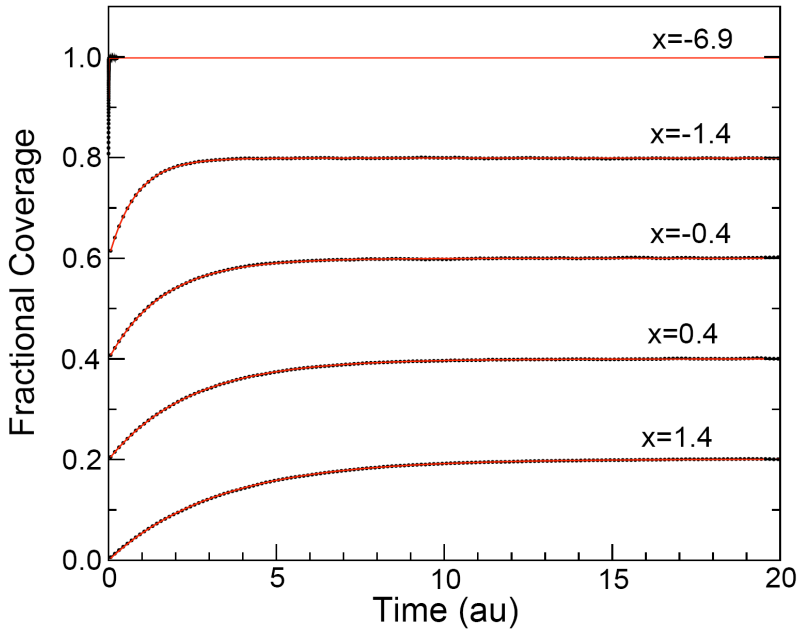

Figure 4.01
Total fractional coverage as a function of time for a 1-D homogeneous lattice for various chemical potentials, where $x = \beta(\varepsilon - \mu)^3$

We note here that it is possible to solve Eq. 4.02 using non-zero initial conditions, which adds a term to Eq. 4.03 representing initial coverage. The initial conditions do not affect the kinetic behavior of the system, and after producing Figure 4.01, we assumed an empty lattice to at the beginning of the time-evolution to avoid any further confusion.

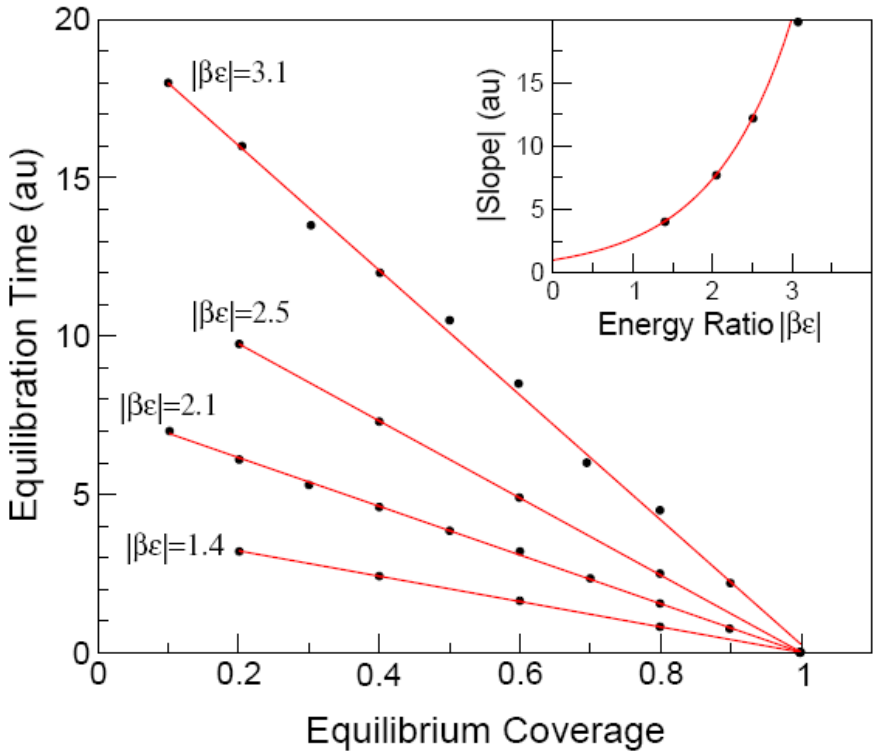

Figure 4.02
Equilibration time versus equilibrium coverage for a 1-D homogeneous lattice for several values of $\beta\varepsilon^3$

Because there was such good agreement between our calculations and simulations at every point in time during the evolution of the system, it was no surprise that we also observed a strong correlation between the kinetic behavior (that is to say, the characteristic time) of the simulated systems and that predicted by our kinetic calculations. Figure 4.02 (above) shows the characteristic time τ as a function of equilibrium fractional coverage. Again, the red lines represent the values predicted by our equilibrium calculations (Eq. 4.05) while the black dots show the characteristic times measured from our simulation results (Eq. 4.04). We see that the waiting time decreases linearly with final coverage, and that the slope of this line depends on the quantity $\beta\varepsilon$, meaning that the longest equilibration times should be expected for systems with high binding energies or low temperatures. This stems from the fact that such systems would require low chemical potentials, and thus would have slower kinetics.

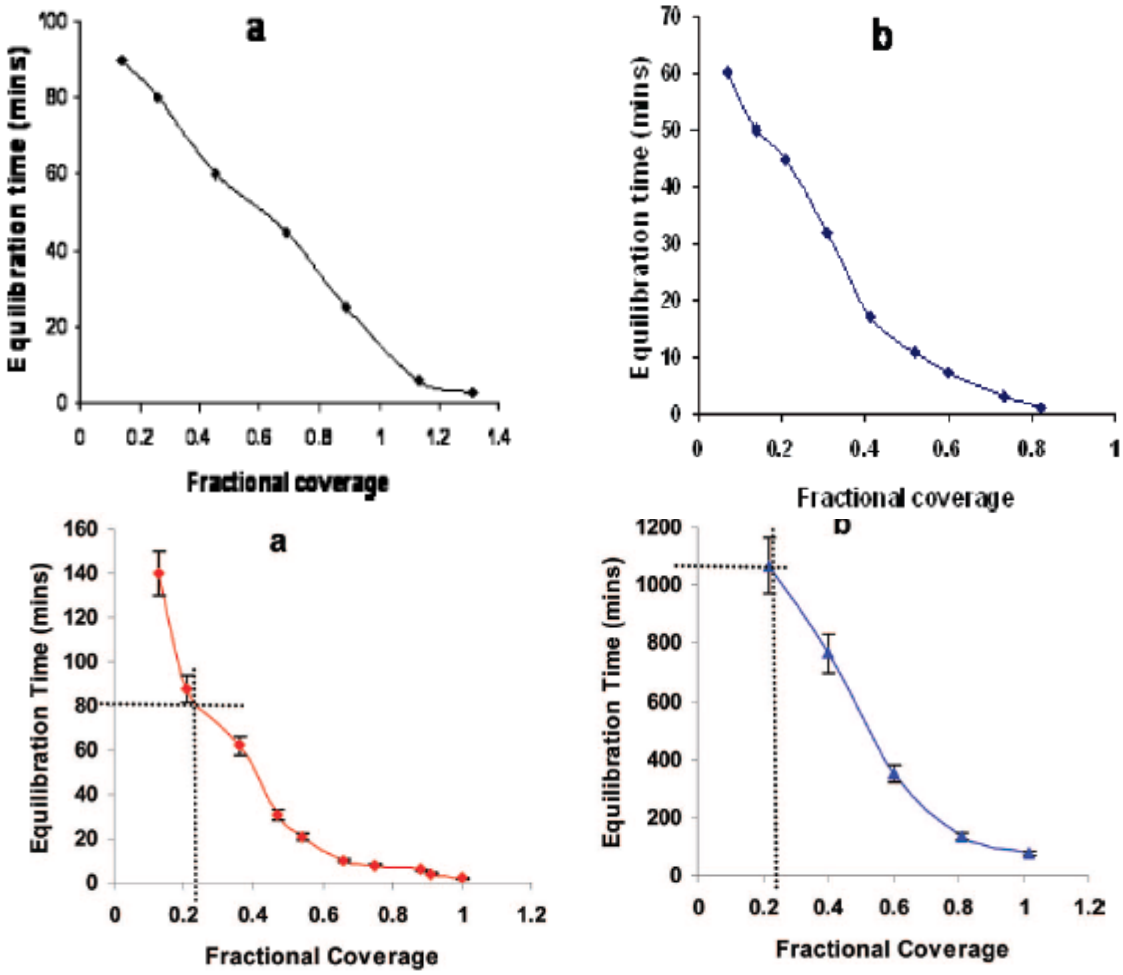

Figure 4.03
Experimental measurements of equilibration time versus equilibrium coverage for CH_4 (top left), Ar (top right), H_2 (bottom left) and CF_4 (bottom right)[42].

These preliminary results matched well to the corresponding experimental data, shown above in Figure 4.03. In the figure above, we see data from gases of simple adsorbates, each of which can be modeled as a quasi-spherical particle, adsorbing to the external surface of a carbon nanotube bundle. Firstly, we see that the curves are monotonically decreasing as the fractional coverage goes up, and in fact these curves are fairly linear in appearance. We would consider them in agreement with the linear relation predicted by our calculations; the fact that they curve slightly actual creates better agreement with our results for monomers on a two-dimensional, heterogeneous lattice, which we will discuss in more detail in Section 4.3. Furthermore, when

considering the details of these experiments, we see that the slope of the line in the panel on the bottom right is several orders of magnitude larger than the slope of the line on the bottom-left, and in those two experiments, done on H_2 and CF_4, we know that the latter has a significantly higher binding energy with the surface. Thus, we see very good agreement between our calculations, simulations, and the initial experimental data regarding quasi-spherical particles adsorbing on carbon surfaces.

Section 4.2: Interacting Monomers on a 1-D, Homogeneous Lattice

We eventually included nearest-neighbor interactions in our simulations of monomers adsorbing on a 1-D, homogeneous lattice. Our results can be seen below in Figure 4.04. Here we have used ε as the magnitude of the adsorption energy (thus a positive value), and we have allowed the interaction energy to be ±10% of that value. When the interaction energy is negative, the particles are attracted to each other (red curve), while a positive energy in actuality corresponds to a repulsion (blue curve).

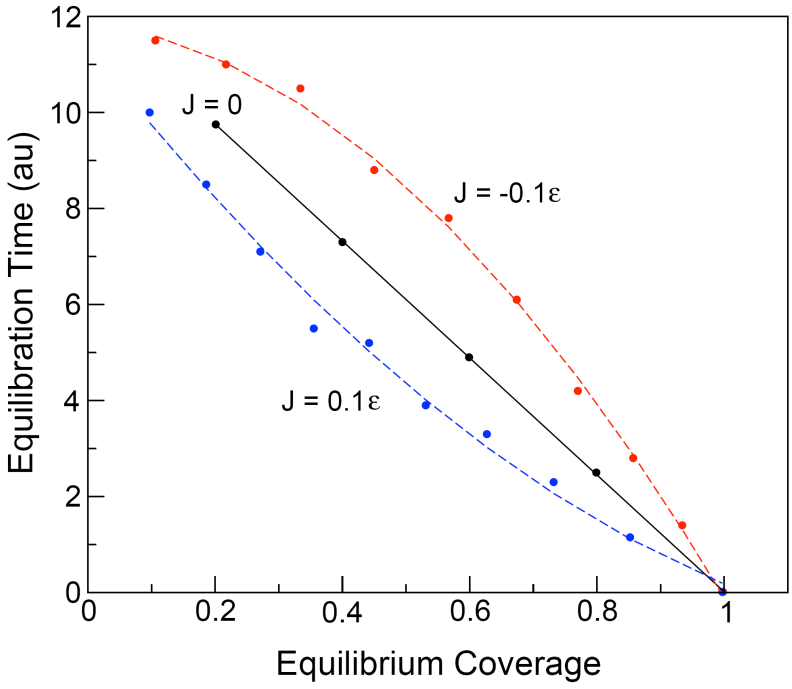

Figure 4.04
Equilibration time versus coverage a system with no particle-particle interactions (center line), attractive interactions (top), and repulsive interactions (bottom)[3]

The behavior we see here in Figure 4.04 is expected, given what we found previously for monomers adsorbing on a 1-D, homogeneous lattice. We saw, for the non-interacting case, that the waiting time increased with the magnitude of the binding energy. Attractive nearest-neighbor interactions increase the effective energy of particles on the surface, so it is expected that the waiting time would increase. Similarly, repulsive interactions decrease the magnitude of the energy (meaning a greater chemical potential is needed to force the particles onto the surface), and so here it makes sense that the kinetics would speed up.

At this point in our study, we increased the strength of our interaction energies but were unable to show an increase in equilibration time with coverage. This does not mean that no increase existed, but rather that, at this early point in our work, our computational and theoretical techniques were insufficient to demonstrate this behavior. We were later able, however, to better understand the adsorption behavior of monomers on a homogeneous lattice; our full results are discussed in Chapter 7.

Section 4.3: Neutral Monomers on a 2-D, Heterogeneous Lattice

In another previous work, published in 2009[4], we considered a system of monomers adsorbing on a two-dimensional, heterogeneous lattice, representing the exterior surface of a carbon nanotube bundle. This scheme is discussed at length in Chapter 3; the lattice consists of three rows of 200 adsorption sites each, with the adsorption sites in the center row (“the groove”) having a greater binding energy (about 50% more) than the sites on the other two rows (“the edges”). Particles are able to adsorb to and desorb from any site on the lattice, and can diffuse freely by jumping from one site to the any unoccupied neighboring site.

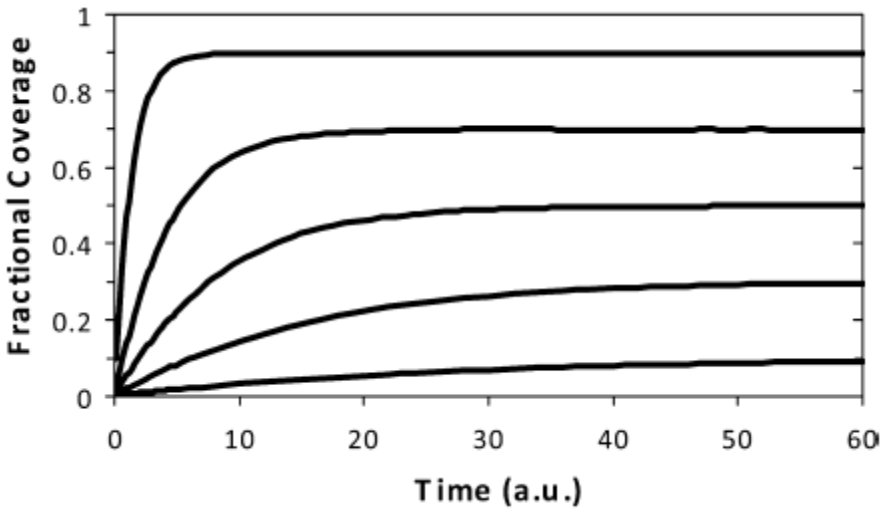

Figure 4.05
Fractional coverage versus time Equilibration time for a single species of monomers adsorbing on a 2-D, heterogeneous lattice[4]

Above, in Figure 4.05, we show the fractional coverage versus time for several systems of monomers adsorbing on a two-dimensional, heterogeneous lattice. We see that, while the curves are still generally exponential in shape, it is clear that they are not truly exponential decay functions. It seems that the coexistence of adsorption sites with different binding energies has made a small but important change in the kinetics of adsorption, compared to the case of monomers adsorbing on a one-dimensional, homogeneous lattice. In particular, the system reaches the highest coverages faster than we would have expected, compared to the pseudo-exponential decay curve we had seen previously.

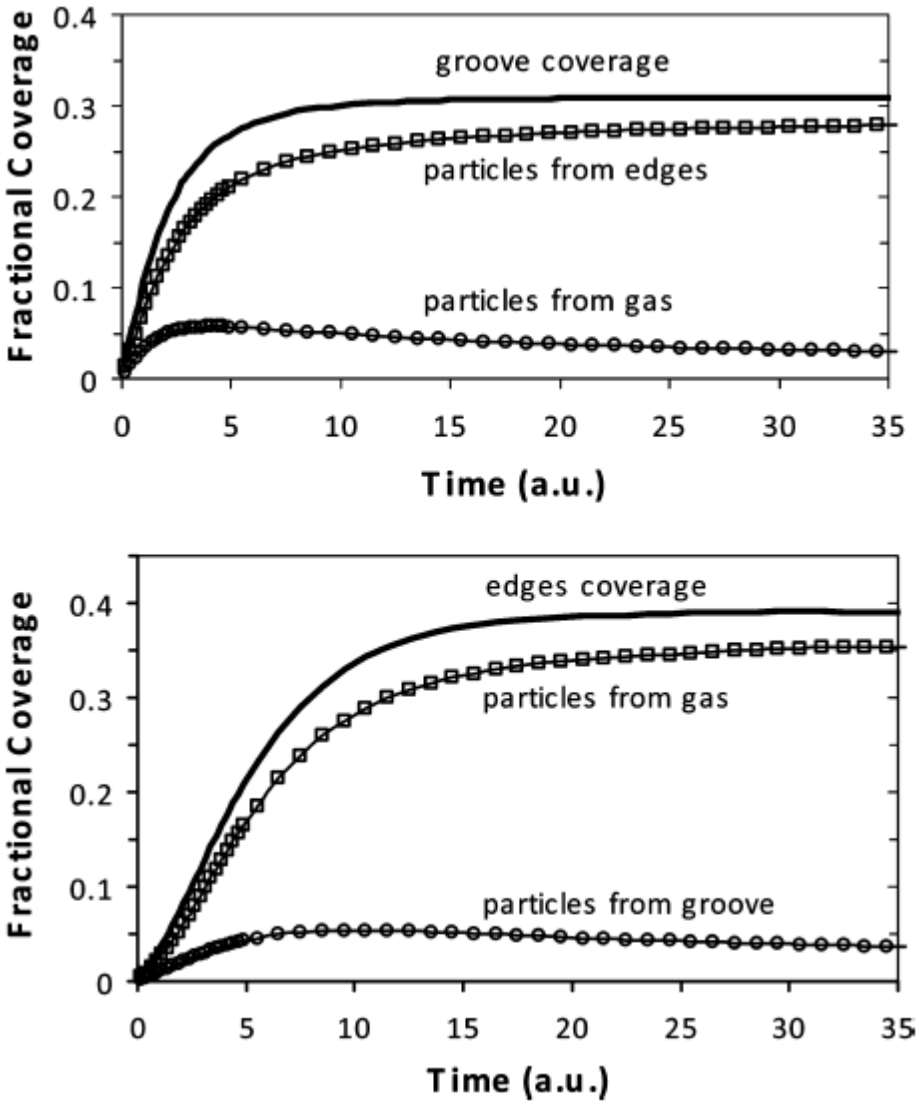

Figure 4.06
The fractional coverage of the groove (top panel) and the edges (bottom panel) as a function of time. The majority of the particles originated in the edges, meaning most particles adsorbed to this weaker-binding phase and then diffused to the rest of the lattice rather than adsorbing directly[4].

We studied this effect in more detail above in Figure 4.06. In the top panel, the solid line shows the total coverage of the groove as a function of time, with the other two lines showing origins of the particles contributing to this overall coverage. It can be seen that the majority of the particles in the strong-binding groove in fact adsorbed on the edges and then diffused into the groove, with only a few particles adsorbing directly from the gas onto the groove. The exact

opposite is shown in the bottom panel, showing the coverage of the edges as a function of time. Here, we see that the edges are filled mostly with particles that adsorbed directly, with only a small flux of particles from the groove. This means that the vast majority of the particles on the lattice are adsorbing on the edges, where the sites are more numerous and more sparsely populated, both of which meaning there are many more adsorption sites available.

The driver of this behavior is the fact that there is a single chemical potential (because it is a single gas species) driving adsorption into two different types of adsorption sites. The chemical potential must be great enough to achieve the desired coverage of the weak-binding sites, but as a result the kinetics will be greater for the strong-binding sites (if only the strong-binding sites were present, a smaller chemical potential would be required, and equilibration would be slower). We see here that adsorption will be faster in all available sites, and a filling effect will come into play in systems where a transfer of particles from the weak-binding sites to the strong-binding sites will increase the rate of equilibration (and decrease the waiting time) for the system as a whole. We will see again this process of adsorption in a weaker-binding (but more accessible) state and transition to the stronger-binding state preferred at equilibrium in our study of dimers adsorbing on a one-dimensional, homogeneous lattice.

When we look at the characteristic time as a function of equilibrium coverage, as seen below in Figure 4.07, we see that the curve for this heterogeneous system falls between the curves for a homogeneous system of adsorption sites with the strong binding energy of the groove (dotted line – top) and the weaker binding energy of the edges (dotted line – bottom). This is a consequence of the “filling effect”, where the fast kinetics of the weaker-binding sites lead to a process by which the stronger-binding sites are filled more quickly by diffusion from the weaker binding sites than through direct adsorption from the gas. We also notice that there is a small curvature to the curve for our hybrid system, meaning the filling effect plays a greater role at higher coverages.

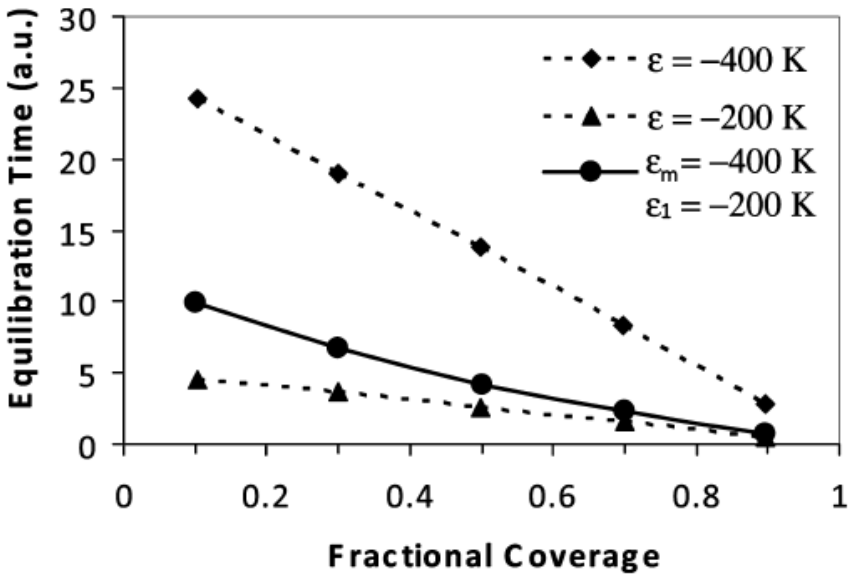

Figure 4.07
Equilibration time vs. coverage for a 2-D homogeneous lattice of strong-binding sites (diamonds), a 2-D homogeneous lattice of weak-binding sites (triangles), and a 2-D heterogeneous lattice (circles)[4]

Finally, we included particle-particle interactions to observe what this added effect would change the kinetics of adsorption. The equilibration time as a function of fractional coverage can be seen below in Figure 4.08. We see firstly the more pronounced curvature of the curve for the non-interacting case (solid line). This makes an even better match for the experimental data shown in Figure 4.03, which was in fact from a system of monomers adsorbing on a carbon nanotube bundle. Attractive interactions (dotted line – top) cause the curve to bow upward. This stems from the fact that the particle-particle interactions make it more likely that an adsorbed particle will remain on the lattice, so a lower chemical potential is required to reach equilibrium; this lower chemical potential translates into slower kinetics, and thus a longer waiting time. We were not able to show the waiting time increasing with coverage for this system, although that neither proves nor disproves that this behavior could develop given sufficiently-strong nearest-neighbor interactions, but rather that our simulation scheme was unable to perform the necessary calculations with the computational assets available. For the largely hypothetical case of repulsive interactions, the net binding energy per particle is decreased, which means a greater chemical

potential is required for the system to reach a given equilibrium coverage, which in turn leads to faster kinetics and smaller waiting times.

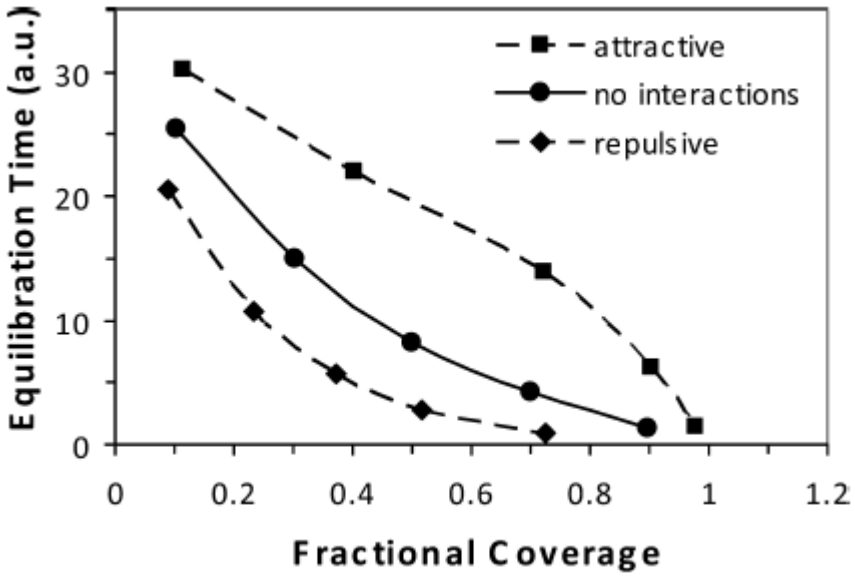

Figure 4.08
Equilibration time versus coverage for adsorption on a 2-D, heterogeneous lattice with no particle-particle interactions (middle curve), attractive interactions (top curve), and repulsive interactions (bottom curve)[4]

The key to this system's behavior is the heterogeneity and distribution of the adsorption sites. The groove has a significantly stronger binding energy, so particles naturally tend to gather there before spreading to the rest of the lattice. However, adsorption is equally likely in every unoccupied site, so the greater number of edge sites means that particles will adsorb in the edges more than the groove. This leads to the "filling effect", meaning particles tend to adsorb in the more numerous, weaker-binding sites and then diffuse into the stronger-binding sites. This process allows for a faster filling of the lattice than direct adsorption (without diffusion) can accomplish alone.

Section 4.4: Conclusions from Previous Work

We know, however, that not all adsorbates can be treated as monomers. We have seen experimental results that show that, while ethane also sees decreasing equilibration time with coverage, propane and the longer alkanes exhibit radically different kinetic behaviors. These longer hydrocarbon chains show an *increase* in equilibration time with coverage, the exact

opposite of what we have observed for methane, the simplest alkane. In this study, we want to see if our model will also predict this increase in characteristic time, and to use our results to explain *why* this change in kinetic behavior occurs. Beyond our interest in hydrocarbons, we are also interested in *how* the parameters of a system affect its kinetic behavior, so that we might find certain conditions in which dimers or even monomers might exhibit an increase in waiting time with coverage, even if those parameters are non-real for hydrocarbons.

CHAPTER FIVE
ADSORPTION ON A ONE-DIMENSIONAL, HOMOGENEOUS LATTICE

As we begin our work considering the adsorption on carbon surfaces of molecular chains of increasing length, we begin where we left previous work. Thus, we continue to use a one-dimensional, homogeneous lattice upon which our particles can adsorb. This is the simplest lattice possible, since it removes the possible added effects of energetic heterogeneity and even complex surface distributions, allowing us to focus on the parameters that most affect the kinetic behaviors of the system. We consider first interacting monomers, and then move on to dimers and trimers.

Section 5.1: Review of Monomers on a 1-D Homogeneous Lattice

We made several important discoveries in our work with the adsorption kinetics of monomers. First was the connection between the characteristic time τ

and the energy ratio $\beta\varepsilon$, where β is $(k_BT)^{-1}$ and ε is the binding energy of the system. We found that as the magnitude of $\beta\varepsilon$ increased, either by an increase in binding energy or a decrease in temperature, the characteristic time becomes larger. This increase in characteristic time is due to a decrease in the speed of the evolution of the system; a system with a greater adsorption energy or a lower temperature would have a lower desorption of adsorbed particles, so a lower chemical potential is needed to reach a given coverage, which results in slower kinetics and a longer waiting time. Another key finding was the relationship between the characteristic time and the coverage of the lattice; we found that the waiting time required for the system to reach equilibrium decreased as the equilibrium coverage went up. These two findings (both shown in Figure 4.02) are at the heart of our understanding of the kinetics of adsorption for all of the systems considered in this study.

We also studied the effect of particle-particle interactions in our previous work, although not in great detail. The inclusion of these interactions caused the characteristic time of the system to tend upward for a given equilibrium coverage (Fig. 4.04), which was due to the fact that the nearest-neighbor interactions increased the effective energy of the particles on the lattice, which increased their characteristic time (based on the reasoning outlined in the previous paragraph). Despite the characteristic time curve bending upward, we were not able to observe the waiting time actually increase as the coverage went up. Part of this current work is to determine what parameters, if any, are necessary to cause the system to exhibit this behavior.

Finally, we will briefly recount the filling effect that we observed for monomers adsorbing on a two-dimensional, heterogeneous lattice. In that model, the surface consisted of a strong-binding central line of adsorption sites flanked on either side by a weaker-binding line of sites. We knew that particles would prefer the central line (the “groove”) at equilibrium because of its energetic advantage, but would eventually fill both regions of the lattice. What we found, however, was that while particles preferred to stay in the strong-binding groove, there were actually more opportunities for adsorption in the edge sites. This led to the “filling effect”, by which the fastest process through which particles can make their way to the strongest-binding sites is not through direct adsorption, but by moving through an intermediate state (one that is easier to reach via adsorption). The result of the filling effect is an increase in the kinetics of adsorption and a decrease in characteristic time for the system. We observed a similar phenomenon when dimers adsorb on a homogeneous lattice.

Section 5.2: Dimers on 1-D, Homogeneous Lattice

Our next step is to study the adsorption of dimers on a one-dimensional, homogeneous lattice. We begin with non-interacting dimers, again hoping to determine a baseline behavior for these admolecules. After gaining a better understanding of the kinetic behavior of neutral dimers, we will add the effect of nearest-neighbor interactions in order to determine how their inclusion affects the kinetics of adsorption. Our findings for dimers (both neutral and interacting) adsorbing on this simple lattice will also give us some perspective when we move on to consider dimers adsorbing on more complex surfaces in Chapters 6 and 7.

Section 5.2.2: Neutral Dimers Adsorbing on a 1-D, Homogeneous Lattice

We begin our work with dimers on a one-dimensional, homogeneous lattice of 200 adsorption sites. Each site is identical to the others; however, there is heterogeneity in the system stemming from the particles' ability to change their orientation with respect to the lattice. As we have mentioned before, these particles can lay flat on the surface or stand perpendicularly to it; the flat state havs approximately 50% more adsorption energy that the upright state, but requires more surface space. While there other possible orientations of the particles with respect to the lattice (that is, they could stand up at an angle between 0° and 90°), we ruled out these other potential states in order to focus on the most important parameters that would have the greatest impact on the kinetic behavior of the system. At this initial stage of the investigation, we also neglected nearest-neighbor interactions.

Section 5.2.2.1: Equilibrium Behavior of Adsorbed Dimers

We have created an isotherm, shown below in Figure 5.01, of a system of dimers adsorbing on a one-dimensional, homogeneous lattice. Using a range of values for the pressure, we allow the system to equilibrate and plot the final coverage versus the chemical potential. We are thus able to compare our simulation results to the coverages predicted by our statistical mechanical treatment of the system. This plot, shows good agreement between our simulated (sim) and calculated (calc) results, both for the total number of dimers adsorbed to the lattice (green), but also considering the contributions of both flat (blue) and upright (red) dimers. With our simulation scheme thusly verified, we can move forward with an analysis of the kinetic aspects of our simulation results.

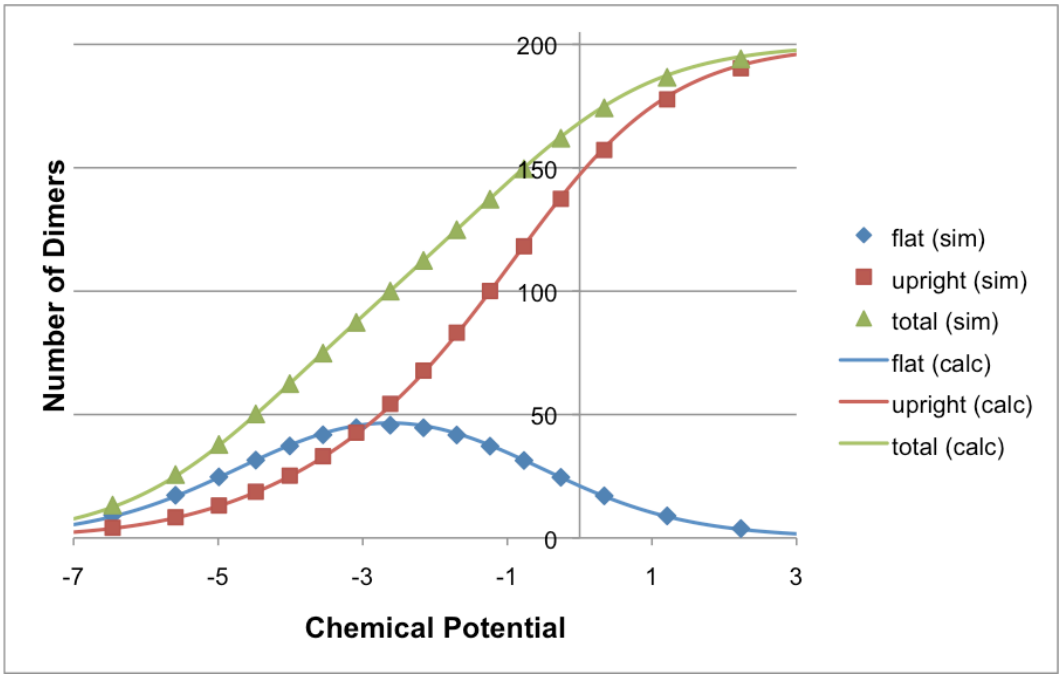

Figure 5.01
Isotherm of dimers adsorbing on a 1-D, homogeneous lattice. Flat dimers account for most of the coverage at low values of the chemical potential, with a transition to transverse dimers at high coverages.

Section 5.2.2.2: Overall Kinetic Behavior of Adsorbing Dimers

Our first simulation results can be seen below in Figure 5.02, which shows the total number of particles on the lattice as a function of time for a representative sample of equilibrium coverages. The black points show where each system reaches its characteristic time, which is determined by assuming each system to be a pseudo-exponential-decay function and finding the value at which the exponential term decays to e^{-1}. We find this value by plotting $\ln(1-N/N_{eq})$ versus time and measuring the slope of the line produced, as discussed in Chapter 4 (Eq. 4.04). The dotted line guides the eye and gives an impression of the kinetic behavior of the system. We see that the characteristic time decreases rapidly as the equilibrium coverage goes from low to moderate coverages, and then decreases at a slower rate as the equilibrium coverages increase from moderate to high. In all cases, however, the waiting time decreases with coverage across the spectrum of equilibrium coverages. This is the same behavior that has been observed for ethane.

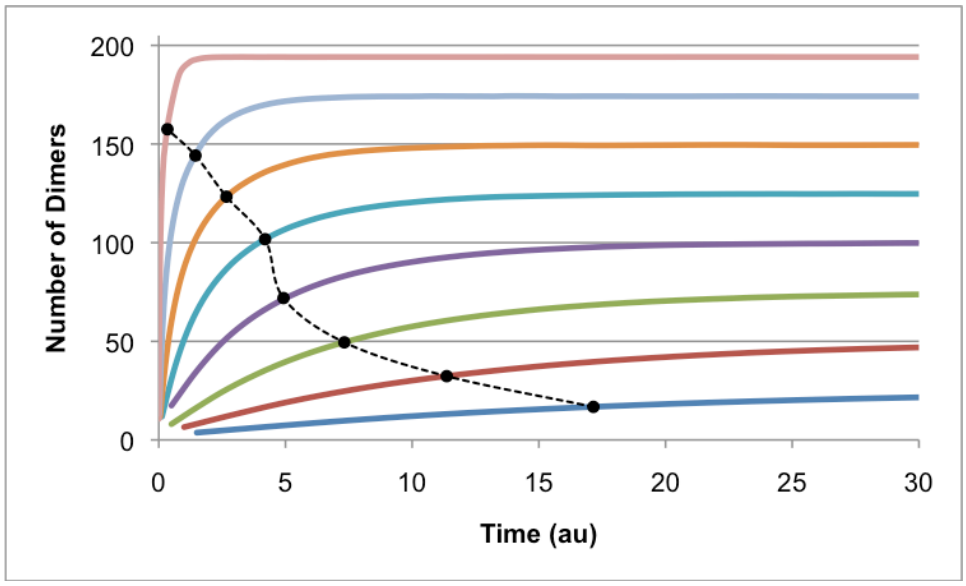

Figure 5.02
Number of particles versus time for a range of equilibrium coverages. As the number of dimers adsorbed at equilibrium increases, the waiting time for the system to reach equilibrium decreases.

Section 5.2.2.3: Kinetic Behavior of Adsorbing Dimers (Low Coverage)

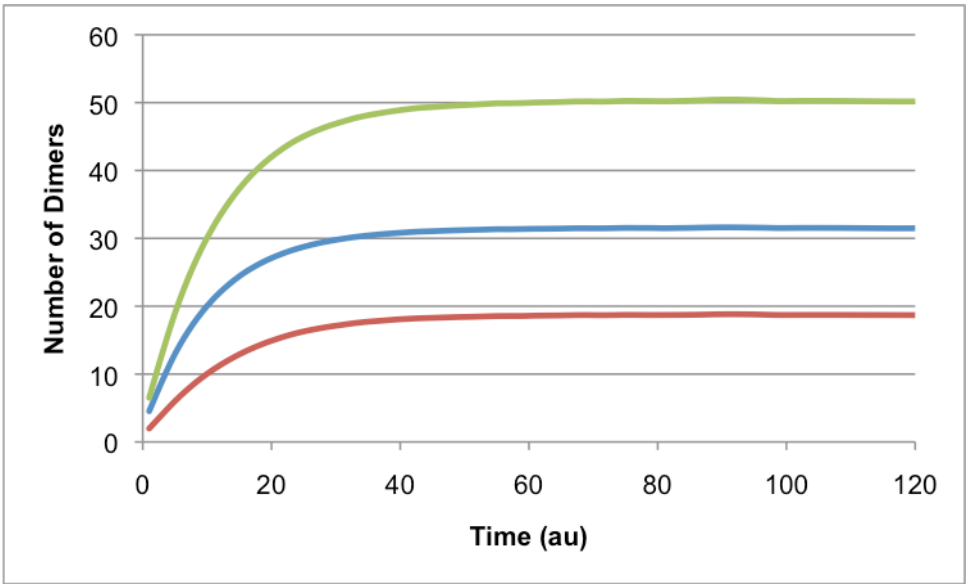

Figure 5.03
Number of dimers adsorbing on a 1-D homogeneous lattice reaching a low equilibrium coverage. Throughout the evolution, the total coverage of the lattice (green) is dominated by flat dimers (blue), with only a few dimers in the upright configuration (red).

Figure 5.03 (above) shows the number of dimers adsorbed on our one-dimensional, homogeneous lattice as a function of time for a system with a low equilibrium coverage. In this system, only 50 dimers are adsorbed at equilibrium (green curve), compared to a maximum of 200 that can occupy the lattice at monolayer. Only about 40% of the lattice is covered at equilibrium, so space is not a factor, and we see that the admolecules tend toward the flat orientation (shown in blue) because that is the energetically preferable orientation. We can see in all cases that the number of molecules in each state increases monotonically as the system evolves from an empty lattice to its equilibrium configuration.

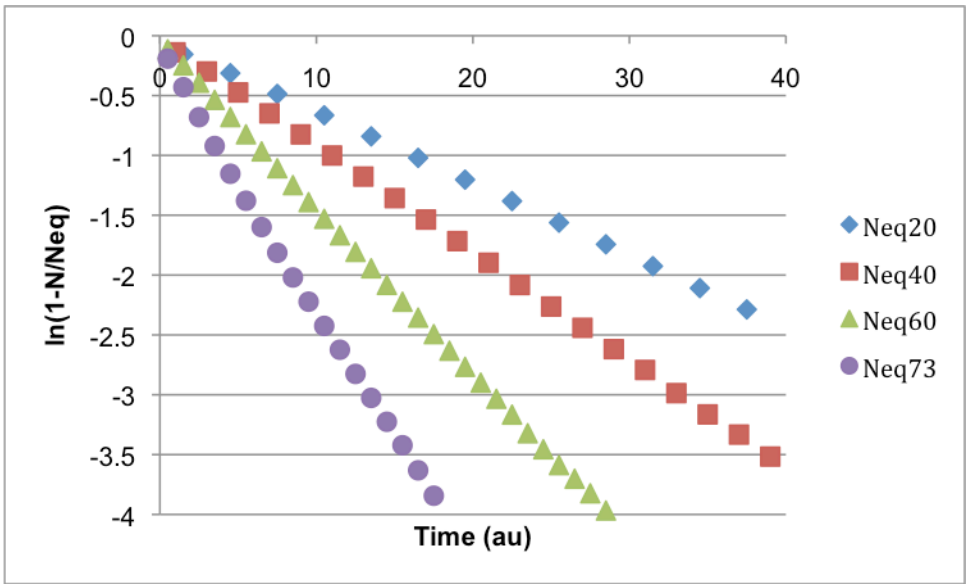

Figure 5.04
The rate curves for low coverages of dimers on a 1-D, homogeneous lattice. The linear curves means that the kinetics of each system is governed by a single rate.

As we see now in Figure 5.04 (above), the typical rate curves for the lower coverages of dimers adsorbing on a one-dimensional, homogeneous lattice. Shown here are the curves for systems with 25, 50, 75, and 100 dimers at equilibrium (blue diamonds, red squares, green triangles, and purple circles, respectively). These correspond to equilibrium fractional coverages of: 20%, 40%, 60% and 73%. As can be seen, the rate curves are almost perfectly linear in each case, meaning that the evolution consists of a single process that runs at a single rate. This agrees with what we observed in Figure 5.06, where both the number of flat dimers and the

number of upright dimers increased steadily to equilibrium. Our observations further concur with what we have seen when we break apart the rate curve for the system reaching 50 particles at equilibrium, as we have done below in Figure 5.05. There, we that the rate of increase of the number of flat dimers (red squares) as well as the increase in the number of upright dimers (green triangles), are approximately equal to the overall rate of equilibration of the system as a whole (blue diamonds). The total rate is an average of the two components; we will soon show why the rate at which the number of upright dimers takes longer to equilibrate (as demonstrated by its slower rate) than the number of flat dimers.

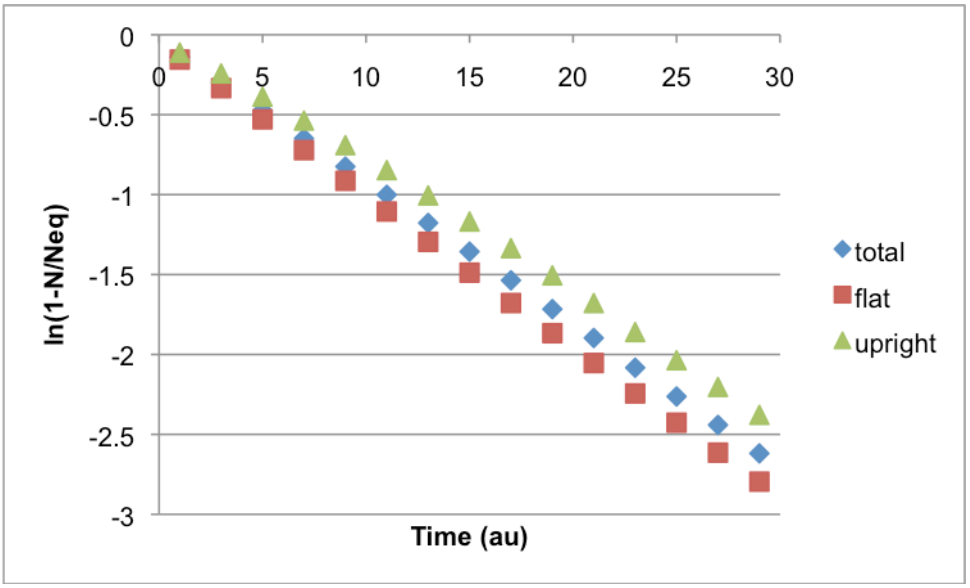

Figure 5.05
Rate curves for a system of 50 dimers (adsorbed at equilibrium) broken out into its component parts. We see that the overall rate (blue), which is linear, is in fact made up of the contributions of its two component parts, flat dimers (red) and upright dimers (green), both of which are linear.

Section 5.2.2.4: Kinetic Behavior of Adsorbing Dimers (High Coverage)

While the equilibration process for systems with a low coverage at equilibrium seems rather straightforward, we see many more features when we consider systems with many more adsorbed particles at equilibrium. We will explore some of this behavior in this section.

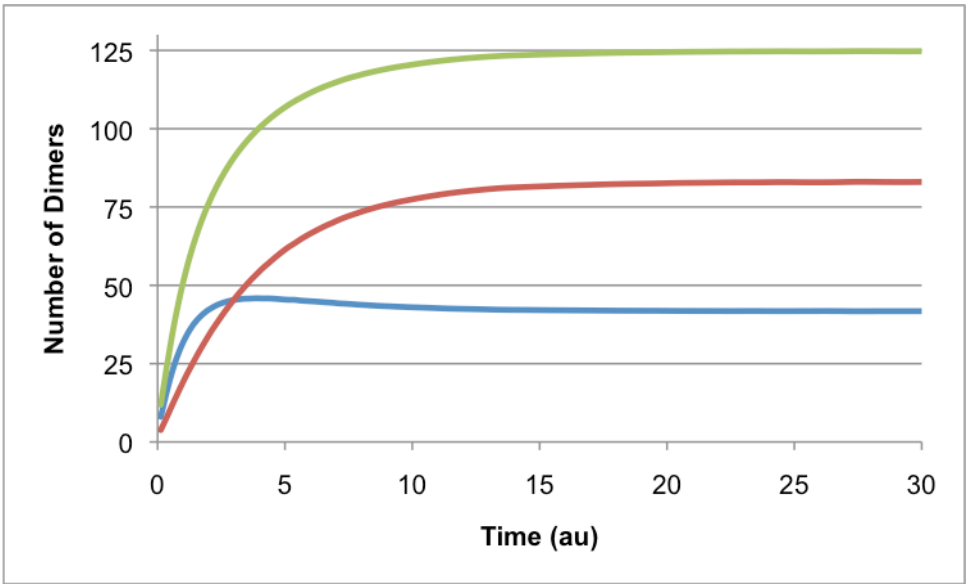

Figure 5.06
The number of adsorbed dimers as a function of time for a system of moderate coverage at equilibrium. Though the total number of particles (green) and the number of upright dimers (red) both increase monotonically, we see an overshoot begin to form for the number of flat dimers (blue), with the peak occurring at about 4 time units.

When we increase the chemical potential of our system, causing it to reach a higher coverage at equilibrium, we notice the formation of an overshoot in the number of flat dimers (blue), while the number of upright dimers (red) and the total number of adsorbed particles (green) both increase monotonically, as we saw before. This overshoot begins to form when the lattice reaches 80% fractional coverage, and is already easily seen when the fractional coverage reached 83%, as shown above in Figure 5.06. Although 83% of the lattice is covered, the lattice only holds 125 admolecules at this point, or about 63% of the total number at equilibrium, due to the fact that many of the particles are still in the flat configuration. When the chemical potential is increased such that the system adsorbs 186 dimers at equilibrium, for a total fractional coverage of 98%, we see that the overshoot is far more pronounced, reaching a value far greater than the equilibrium value before falling away to almost nothing. The overshoot for this very high coverage system also occurs earlier in the evolution; for the system in question, whose evolution is shown below in Figure 5.07, we see that the overshoot occurs at about 0.2 time units. We will study the overshoot in greater detail in Section 5.2.2.5.

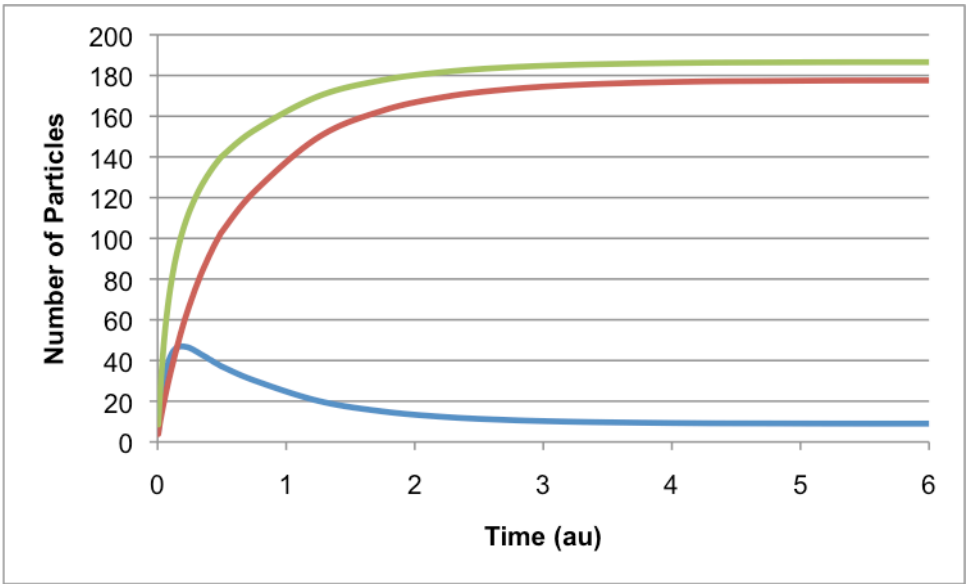

Figure 5.07
Number of adsorbed dimers as a function of time (1-D, homog) for a system with a very high equilibrium coverage. The number of flat dimers (blue), reaches a high overshoot very early in the evolution; upright dimers then take over and dominate the lattice at equilibrium.

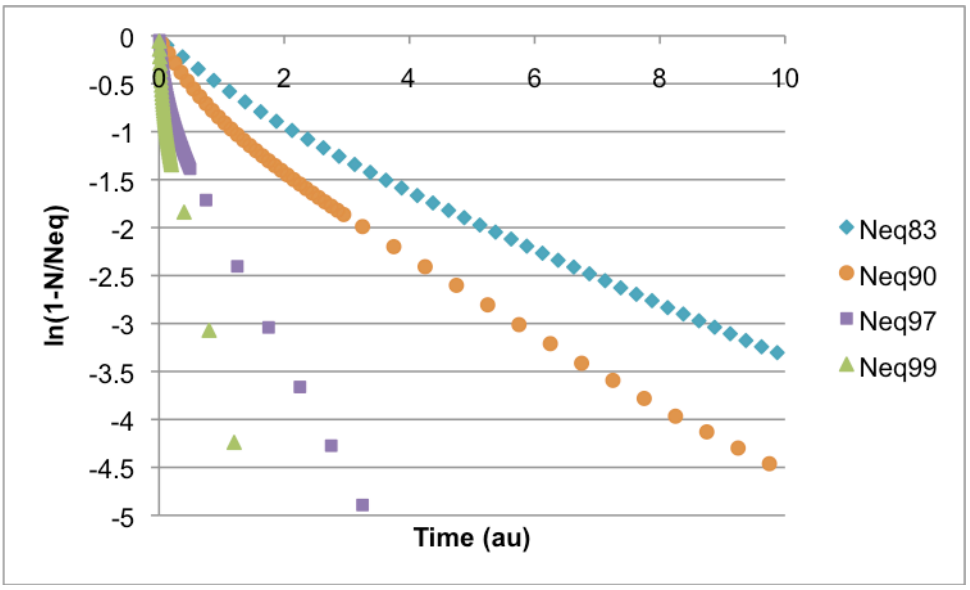

Figure 5.08
Rate curves for dimers adsorbing at higher equilibrium coverages. Instead of the linear curves seen for lower coverages, we now see a pronounced bend or kink in the rate curves for higher coverages.

When we look at the rate curves for the highest coverages of dimers adsorbing on a one-dimensional, homogeneous lattice, as we have shown above in Figure 5.08, we see a pronounced bend. Because there are two distinct regions to each curve, each with its own slope, we can surmise that there are in fact two separate processes taking place here. The characteristic time of the entire system, then, would have to be the characteristic time of the slower process, which must be the limiting factor for the system to reach equilibrium. We will discuss these processes in more detail in the following sections.

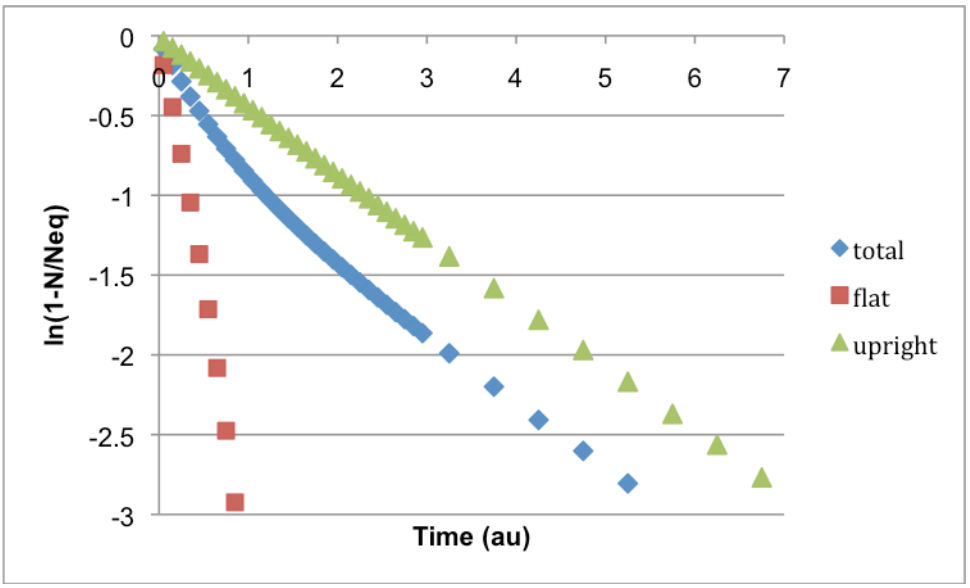

Figure 5.09
Rate curve for a system reaching 90% fractional coverage at equilibrium, broken out into its component rates. We see the total rate is initially quite high, boosted by the high rate of the flat dimers; once the flat dimers hit their overshoot, however, the total rate abruptly bends to match the rate of the upright dimers.

We again break the rate curves down into their component parts. We see here in Figure 5.09, showing our results for a system with 90% fractional coverage at equilibrium, that the bending rate curve of the total number of dimers (blue) is made up of a very fast rate for flat dimers (red) and a relatively slower rate for upright dimers (green). Because our method of measuring the rate assumes an equilibrium value, we were forced to measure the rate of the flat dimers relative to the maximum value seen at the overshoot, since in many cases the flat dimers spent a majority of their time with a coverage above what they will have at equilibrium. We see

that the rate of increase of the number of flat dimers is very high, but occurs for a very brief time. After about 1.3 time units, the rate curve for flat dimers abruptly disappears, as the overshoot is reached. At the same time, the rate curve for the total system bends to follow the rate curve of the number of upright dimers. This is the main rate that denotes the time necessary for the system to equilibrate. However, we know that the system also just reached overshoot, so the number of flat dimers on the lattice should be falling. Then, this rate is not actually the adsorption rate of upright dimers onto the lattice, but rather includes the entire process of flat dimers reorienting themselves into the upright state along with some continued adsorption of upright dimers. All of this together is the second process through which the system evolves to equilibrium. This idea is explored in greater detail in Section 5.2.2.5.

Section 5.2.2.5: Comments on the Overshoot

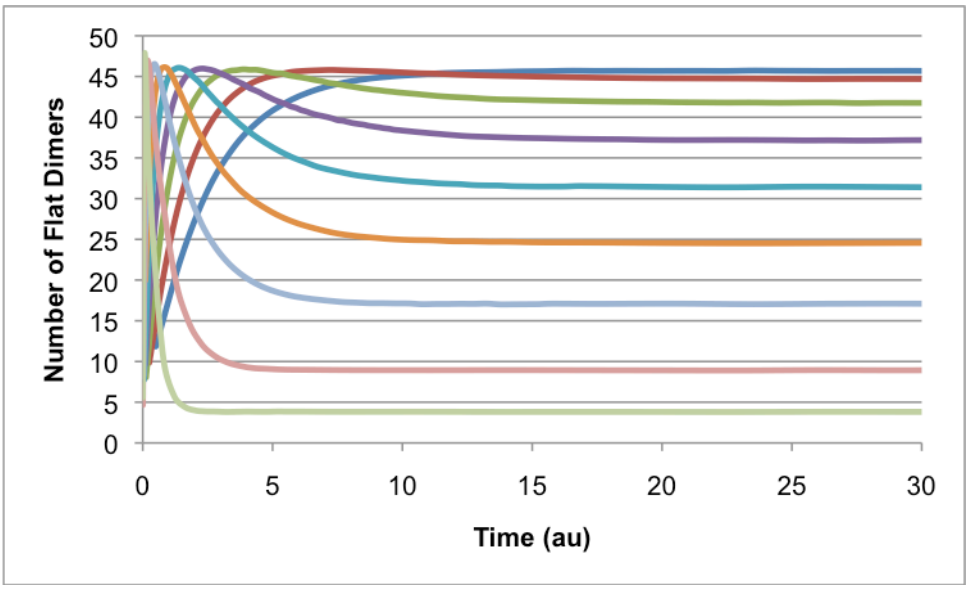

Figure 5.10
The number of flat dimers as a function of time for systems with high total coverages at equilibrium. An overshoot develops for the number of dimers, occurring increasingly early in the evolution of the system, but always with a peak at about 46.

When we plot the number of flat dimers as a function of time for systems with more than 100 particles (more than 80% fractional coverage) at equilibrium, as shown above in Figure 5.10, we see the development of an overshoot in the coverage of flat dimers. As the final coverage of

the system increases, this overshoot occurs earlier in the evolution of the coverage and falls off more quickly; as the total coverage goes up, the number of flat dimers at equilibirium is lower because transverse dimers make up a greater proportion of the coverage. It makes sense that the dimers would reach an overshoot earlier at higher coverages because the higher coverage is driven by a stronger chemical potential, which speeds up the flux of particles onto the surface. What is more surprising is that, despite the increasing pressure and coverage, the height of the overshoot is almost constant, ranging from 45.8 to 47.9. We would consider all of these values to be within the margin of error for each other, since our method of averaging data points gives us a small degree of uncertainty of the exact value of a given data point. When trying to make sense of this behavior, we returned to the isotherm of this system, shown in Figure 5.01, and we realize that this small range of peak values of the overshoot in fact centers around the peak value of the number of flat dimers seen in the isotherm, which is 46.6, as given by our statistical mechanical calculations.

Since the maximum number of flat dimers at equilibrium (via the isotherm in Figure 5.04) is approximately equal to the maximum number of flat dimers at any point in the temporal development of the system (based on the overshoots shown in Figure 5.10), we wondered if the relative numbers of flat and upright dimers would maintain this proportion throughout the time-evolution of the system (and not just at the overshoot). In order to test this hypothesis, we plotted the number of flat dimers in one of our simulations as a function of the total number of dimers on the lattice; this produced a parametric curve, as the number of flat dimers and the total number of adsorbed dimers are both dependent on time. We then compared these points to the curve representing the number of flat dimers predicted at equilibrium (as a function of the total number of adsorbed dimers) by our calculations. Our results can be seen in the following figures.

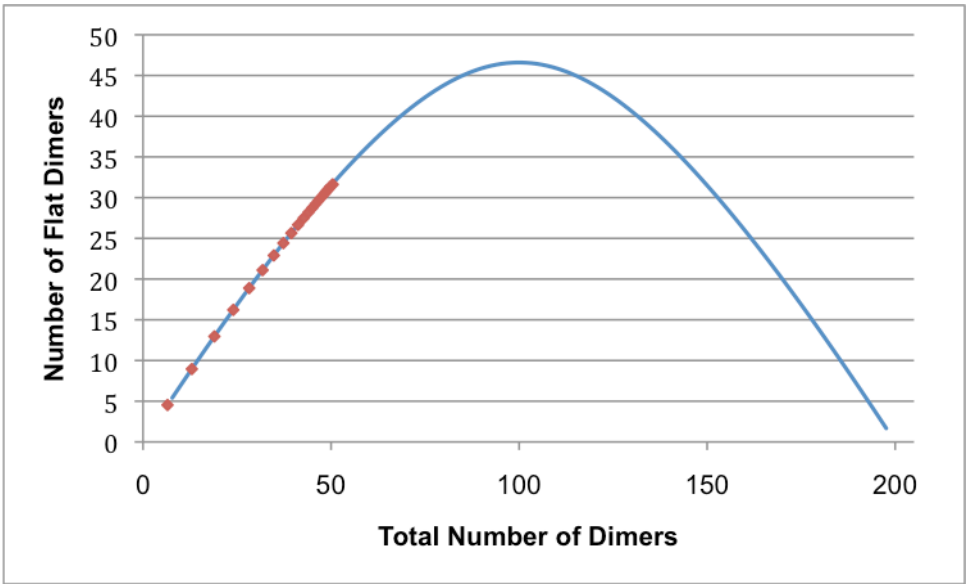

Figure 5.11
Number of flat dimers versus the total number of adsorbed dimers at equilibrium (blue curve) and at different points in time (red points) for a system equilibrating to 50 admolecules (40% fractional coverage).

Figure 5.11 shows the number of flat dimers as a function of the number of total adsorbed dimers for a system equilibrating to 50 admolecules. As can be seen, throughout its time evolution, the system maintains the same ratio of flat dimers to total dimers as an equilibrated system would have. Another way to consider this is that, while the chemical potential drives the continued flux of new particles onto the surface (up to the appropriate number of particles at equilibrium), these particle continuously reorient themselves to maintain a sort of pseudo-equilibrium in all points in time along its temporal development. This is important to us, since the Kinetic Monte Carlo algorithm assumes that the system is in an semistable equilibrium throughout the evolution of the system. We should also note that we could have done the same comparison using the number of upright dimers as a function of the total number of adsorbed dimers, but because we are interested in the number of flat dimers, it was convenient to use this value.

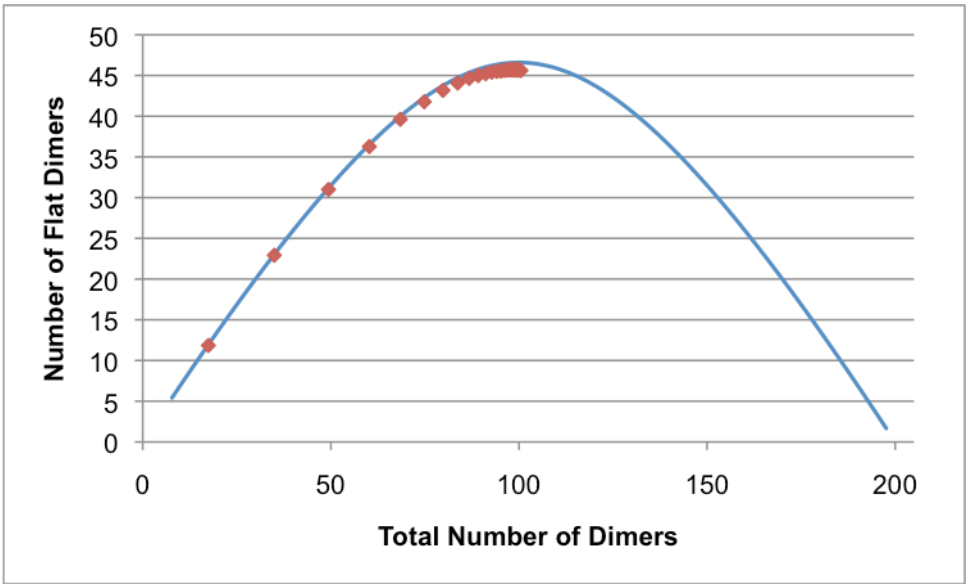

Figure 5.12
Number of flat dimers versus the total number of adsorbed dimers at equilibrium (blue curve) and at different points in time (red points) for a system equilibrating to 100 admolecules (73% fractional coverage).

We made a similar comparison of the relative number of flat dimers for a system that reached 100 total adsorbed dimers at equilibrium. As can be seen above in Figure 5.12, there is again good agreement between the relative number of flat dimers as a function of time (points) and how many would be in an equilibrated system (curve). What is interesting about this system is that it was the last one that did not exhibit an overshoot; as can be seen, the number of flat dimers increases to the maximum value and stops (as the system reaches equilibrium).

We continued our comparison for a system equilibrating to 125 particles, shown below in Figure 5.13. This was the first system to show an overshoot in its time evolution, and the overshoot can be seen here as well, as the number of flat dimers increases as the total number of adsorbed dimers goes up, continuing this way until it reaches a peak value and then falling back to a lower value, which it will maintain at equilibrium. We have shown thusly the origin of the overshoot observed in the number of flat dimers.

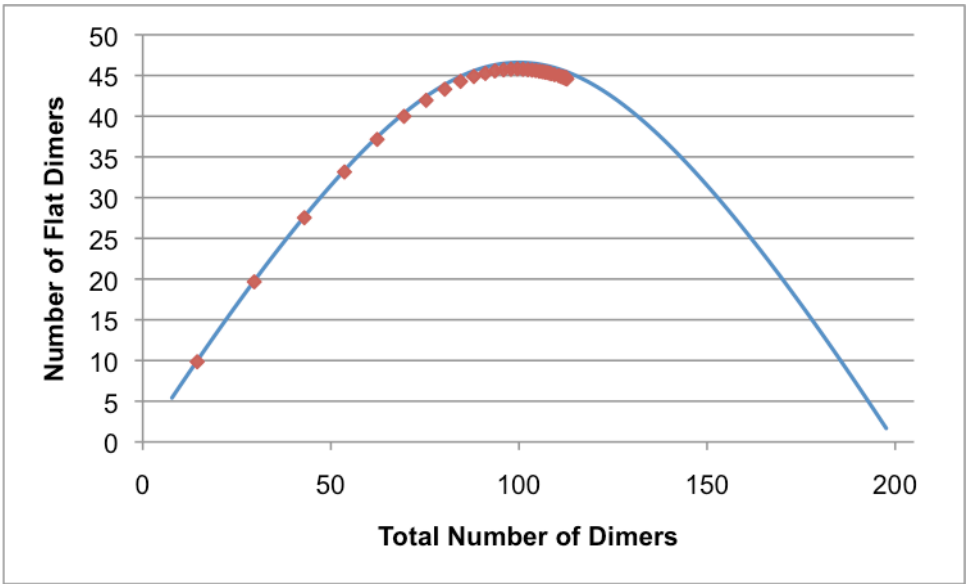

Figure 5.13
Number of flat dimers versus the total number of adsorbed dimers at equilibrium (blue curve) and at different points in time (red points) for a system equilibrating to 125 admolecules (80% fractional coverage).

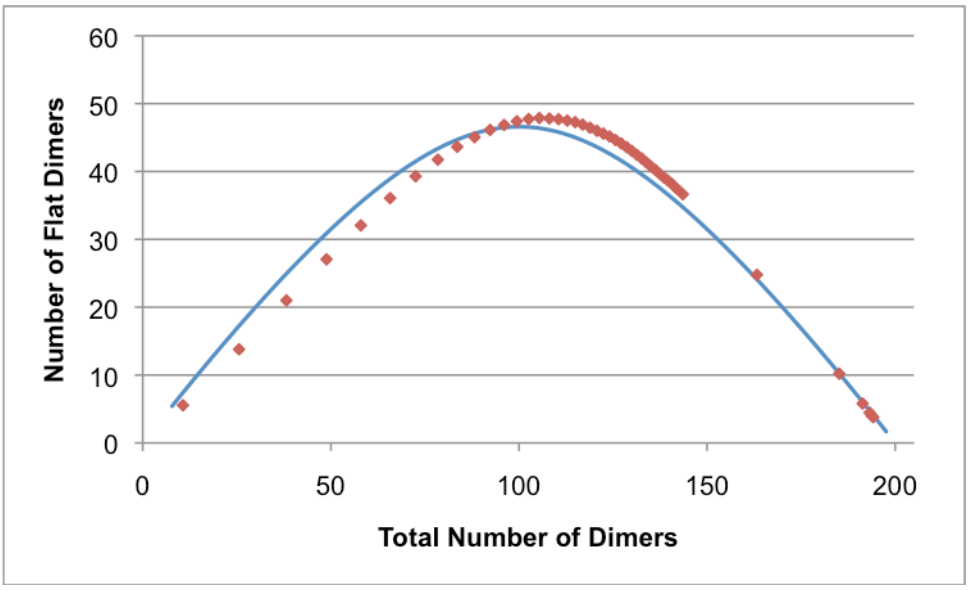

Figure 5.14
Number of flat dimers versus the total number of adsorbed dimers at equilibrium (blue curve) and at different points in time (red points) for a system equilibrating to 195 admolecules (99% fractional coverage).

We consider one more system, this one with the highest number of adsorbed particles at equilibrium that we considered, shown above in Figure 5.14. For this system, which is approaching monolayer coverage, we see the number of flat dimers follows closely predicted value, the agreement is not as close as we'd seen for other systems. We believe that the relation breaks down due to the very high chemical potential of the system, which drives a very fast adsorption process. As a result, the system does not have the time it needs to fully reestablish equilibrium at every step along its evolution.

We mentioned before that we saw an overshoot develop in the adsorption of a binary mixture of monomers on a homogeneous lattice. We determined that this overshoot developed from the difference between the adsorption rates of the two competing species. In that situation, the weaker-binding species needed a stronger chemical potential to reach a given coverage, which drove a faster initial adsorption, leading to an overshoot in the coverage. While our two "species" here (flat and upright dimers) do indeed have two different binding energies, they must have the same chemical potential (as they are indistinguishable in the gas phase). Furthermore, they are more strongly connected, as there is a balance not only in total adsorption energy (and, later, interaction energy), but also a trade-off in the lattice space required (as flat dimers require more space). Finally, there is the ability of the admolecules to reorient themselves on the lattice, meaning there is a possibility that there will be a general shift of flat dimers standing up to become upright or upright dimers laying down to become flat, which may further complicate the kinetics of adsorption. We will explore this transition between phases, and how it affects the adsorption process, in the following section.

Section 5.2.2.6: Comments on the Filling Effect

In Sections 5.2.2.3 and 5.2.2.4 we considered the number of adsorbed dimers as a function of time. Systems with a high equilibrium coverage exhibited an overshoot in the number of flat dimers in the system, after which the number of flat dimers decreased slowly while the total number of adsorbed dimers continued to go up. While the direct adsorption of upright dimers is still taking place, there is also the possibility (indeed, the inevitability) of a change of state, meaning some of those flat dimers are disappearing because they are reorienting themselves

and turning into upright dimers. We have seen previously, in our study of a single species of monomers adsorbing on a heterogeneous lattice, that the existence of two different states with two different binding energies lead to a “filling effect”, where the strongest-binding sites are filled not only by direct adsorption but by being “filled in” through the process of diffusion from weaker-binding states. In the same way, we expect to see a general transition from upright (weaker-binding) to flat (stronger-binding) dimers, at least at lower coverages, when space is not limited. At higher coverages, however, when the limited capacity of the lattice to hold a finite number of adsorbed particles comes into play, we may see very different behavior. We wanted to understand the role played by the reorientation of adsorbed particles, and how this process affects the overall kinetics of the system.

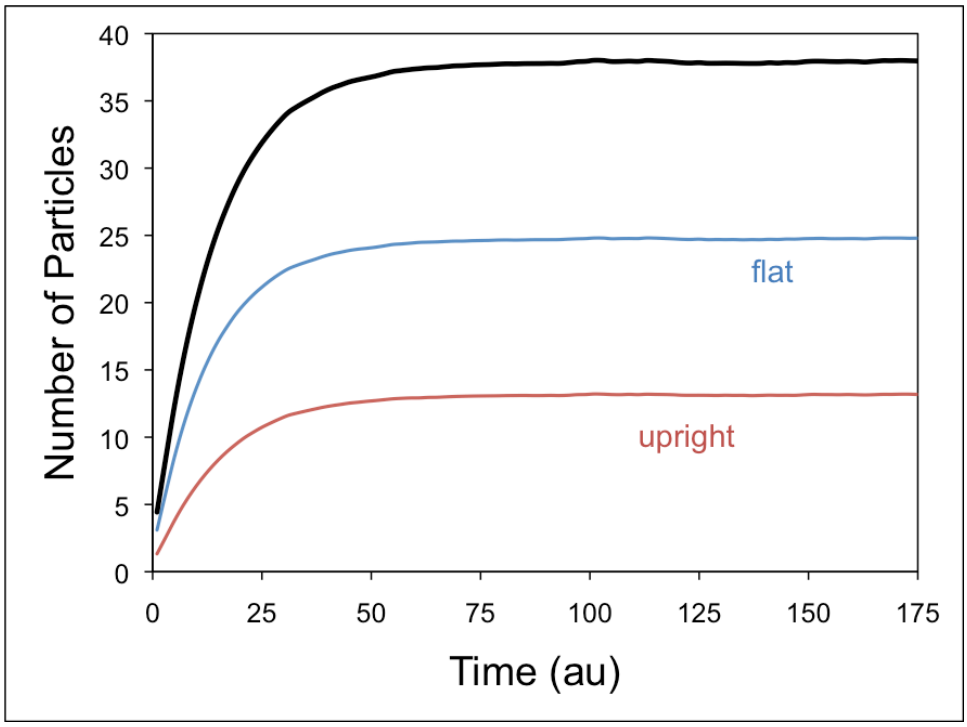

Figure 5.15
Number of dimers as a function of time for a system with an average of 37.5 adsorbed particles (31% fractional coverage) at equilibrium. Most of the particles are in the flat orientation because it is energetically preferable.

In order to observe the filling effect, we return to considering the number of adsorbed particles as a function of time, as we did in Sections 5.2.2.2 and 5.2.2.3. A typical example of this

is seen in Figure 5.15, for a system reaching 31% fractional coverage at equilibrium (a low-coverage system). As we have seen and discussed before, with space readily available on the lattice, both the flat (blue) and upright (red) dimers increase in number until they reach their equilibrium values. However, in addition to simply tracking the number of particles in each orientation, we also tracked the orientation in which each particle originally adsorbed. That way we could look at a flat dimer, for example, and know whether it was flat because it had adsorbed that way, or because it found itself in that state through a reorientation on the surface. A plot of our results can be seen below in Figure 5.16.

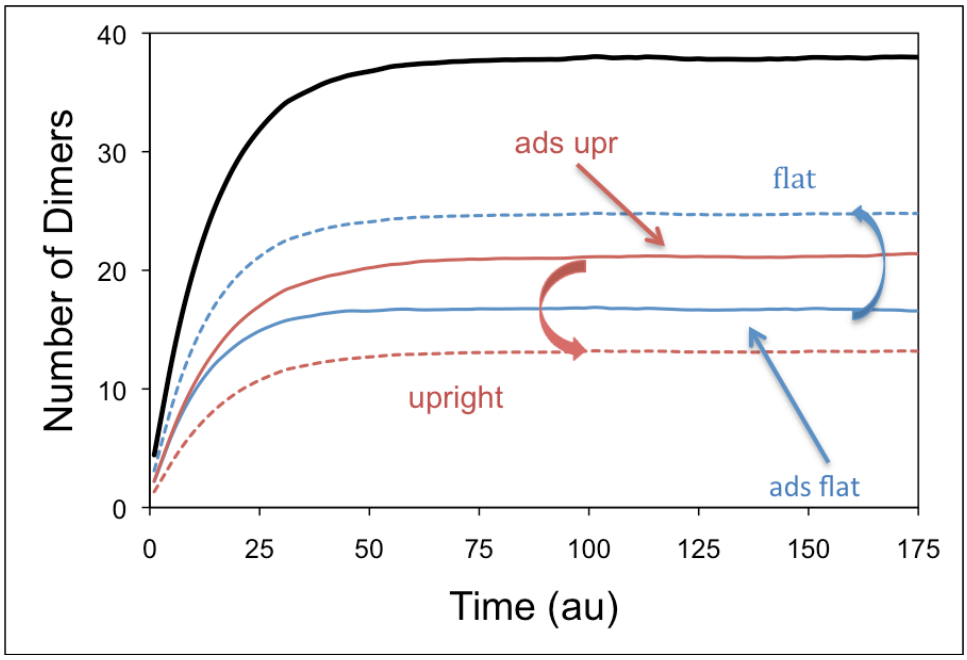

Figure 5.16
Number of dimers that were in each state on the lattice (dotted lines) compared to the number of dimers that adsorbed in each state (solid lines). We see evidence of a net transition from the upright to the flat orientation[61]

When we look at how many particles adsorbed in each orientation on the lattice, compared to how many end up in each state, we see evidence of a general transition of particles from the upright to the flat state. There are significantly more particles on the lattice that adsorbed in the upright state (red solid line) than there are particles in that state (red dotted line); the loss of these upright particles points to a net transition to the flat state. Conversely, there are more

dimers that are flat (blue dotted line) than there are dimers that adsorbed flat (blue solid line), and the increase in the number of flat dimers comes from gains equaling the losses in upright dimers. This is the very filling effect that we expected to find. Notice as well that this transition is steady throughout the time-evolution of the system. Recall from Section 5.2.2.3 (Figure 5.08) that the rate curves for these low-coverage systems are linear throughout their evolutions, meaning that the evolution is proceeding at a single rate because a single process is taking place. We believe that the process here includes both the adsorption from the gas to the lattice (into both possible orienations) *and* the transition from upright to flat dimers.

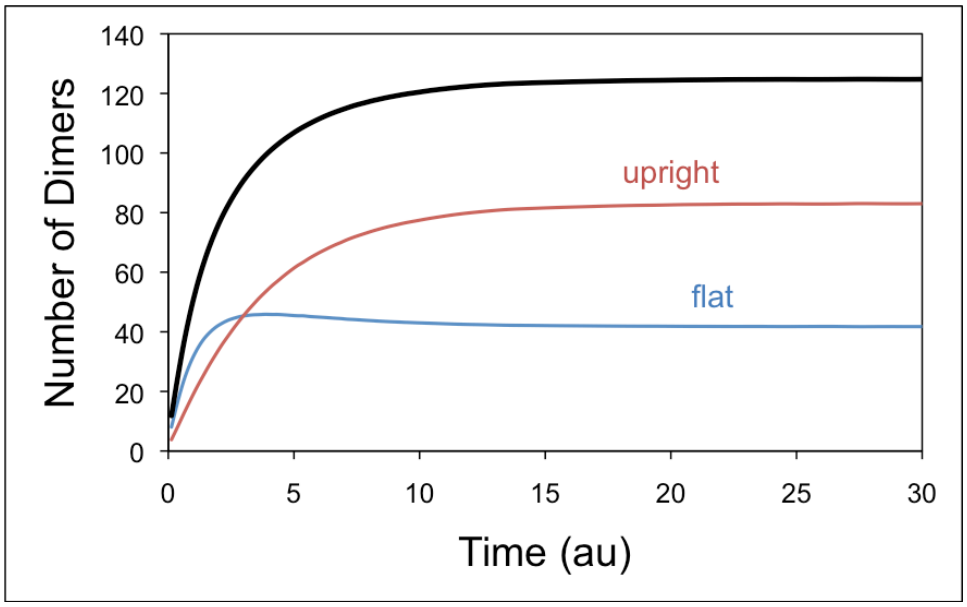

Figure 5.17
Number of dimers as a function of time for a system reaching 125 particles at equilibrium. Notice the overshoot in the number of flat dimers.

Now, we look at a system reaching 125 admolecules at equilibrium (83% fractional coverage), shown above in Figure 5.17. Here, the number of flat dimers (blue) exhibits an overshoot, while the upright dimers (red) make up a greater contribution to the overall number of admolecules. When we look at the states in which each particle originally adsorbed, as seen below in Figure 5.18, we see that, even with upright dimers dominating the lattice, there are still a small number of upright dimers that are reorienting themselves to become flat (Note: it is not a

few specific dimers, but rather, of all the dimers reorienting themselves in both directions, there is on average a net conversion of a few upright dimers to flat).

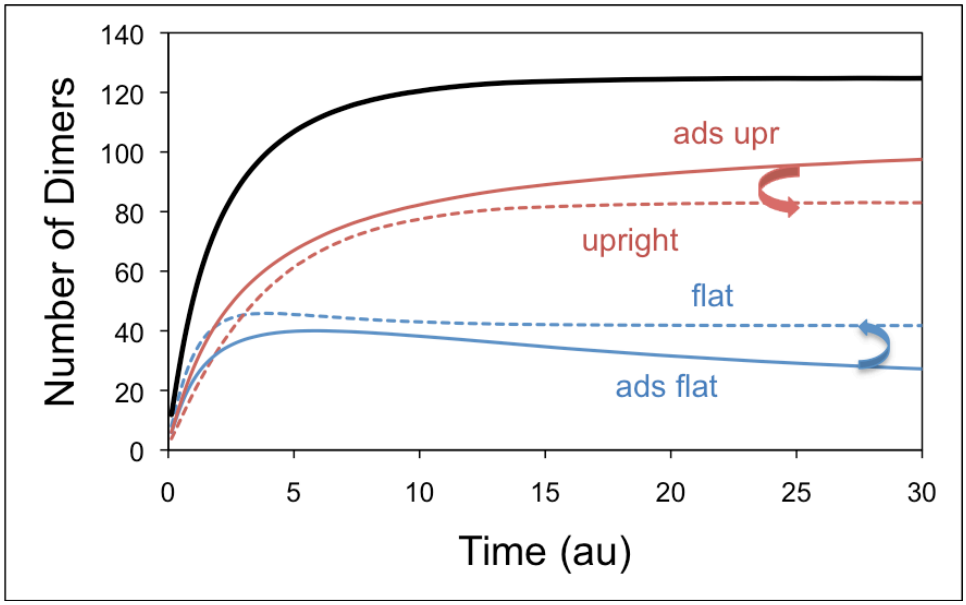

Figure 5.18
Number of dimers that were in each state on the lattice (dotted lines) compared to the number of dimers that adsorbed in each state (solid lines). Note the overshoot both in the number of flat dimers and the number of dimers that adsorbed flat.

We also notice here that the number of dimers adsorbing flat (blue solid line) and the number of dimers adsorbing upright (red solid line) are identical at the initial stages of the time evolution of the system (when the lattice is mostly empty). This makes sense, as there are as many places for a flat dimer to adsorb as there are for an upright dimer. However, as the lattice begins to fill, there is a statistical shift in favor of upright dimers. For example, the space occupied by a single upright dimer is enough to block one upright dimer from adsorbing, but it takes away two possible adsorption sites for a flat dimer. Similarly, a flat dimer keeps two upright dimers from adsorbing, but also blocks three other flat dimers. Thus, as time goes by and the lattice begins to fill, it necessarily becomes more difficult for flat dimers to adsorb than upright dimers. We see this behavior in Figure 5.18, where after about 2 time units the number of particles adsorbed as upright quickly outstrips the number that adsorbed flat.

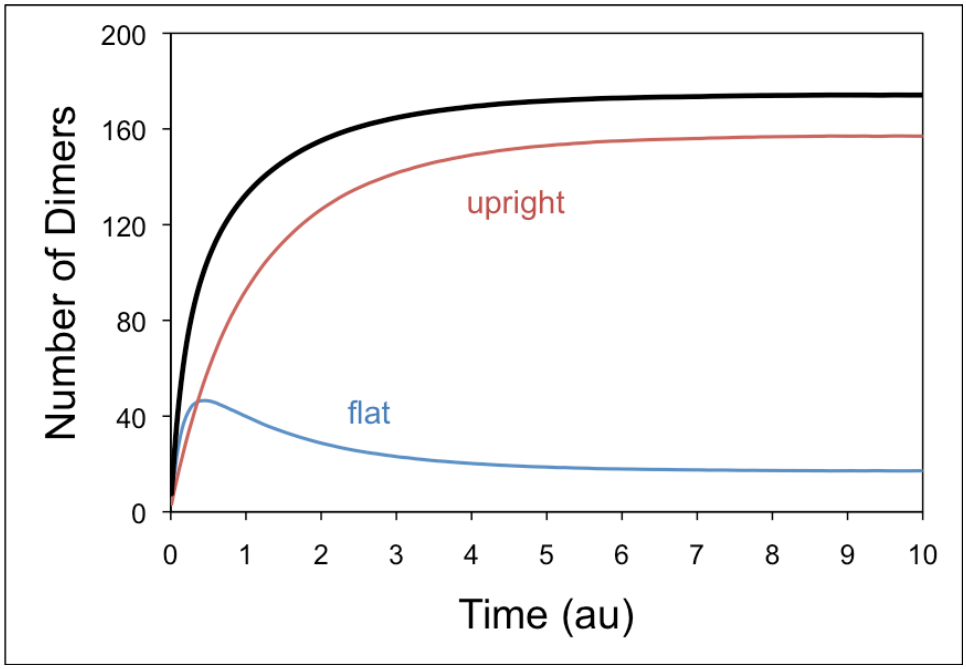

Figure 5.19
Number of dimers that were in each state on the lattice for a system reaching 162 particles at equilibrium. The overshoot in the number of flat dimers is now quite distinct.

Finally, we consider a system with a high number of adsorbed particles at equilibrium (162, with a fractional coverage of 93%). There is now a pronounced overshoot in the number of flat dimers, as shown above in Figure 5.19. When we look at the states in which those dimers are adsorbing, we see that the filling effect continues in order for the overshoot to occur. Looking at Figure 5.20 (below), we see a transition from the upright orientation to flat, which occurs very early in the time evolution of the system. Shortly after the overshoot is achieved, however, we see a reversal of this behavior. For most of the evolution of the system, and continuing through equilibration, there is actually a net transition of flat dimers to upright dimers. In this system there is very little exposed surface area (only about 7%), so space is at a premium. As flat dimers stand up, it is far more likely that the open site they create will be taken by an adsorbing upright dimer, keeping them from returning to their energetically preferred orientation.

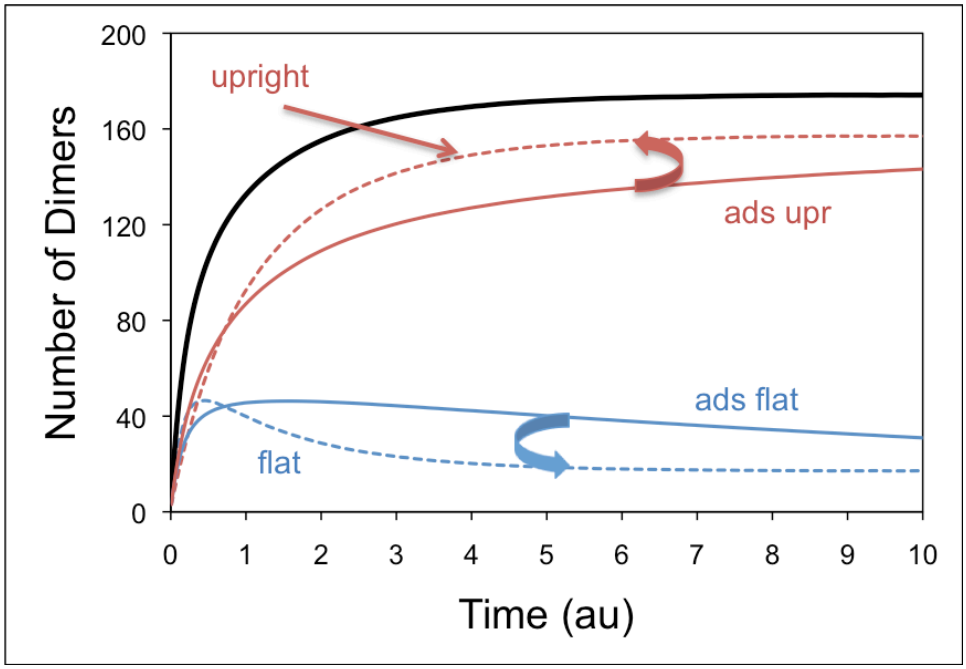

Figure 5.20
Number of dimers that were in each state on the lattice (dotted lines) compared to the number of dimers that adsorbed in each state (solid lines). Note the overshoot both in the number of flat dimers and the number of dimers that adsorbed flat.

Section 5.2.3: Interacting Dimers on a 1-D, Homogeneous Lattice

All of our discussion thus far has focused on non-interacting dimers. We have worked to thoroughly understand this simplest system, in order to better know what to expect from systems to which the influence of nearest-neighbor interactions has been added. The interaction energies we have used here are similar to the nearest-neighbor interactions for ethane, and so we have measured the strength of our particle-particle interactions in comparison to this basic set of interactions between two flat "monomers" (each representing half of a flat dimer), between a "monomer" and a upright dimer, and between two upright dimers, as discussed in Chapter 3.

Section 5.2.3.1: Equilibrium Characteristics

Our first step after adding nearest neighbor interactions was to ensure that our computer simulations were representing these admolecules in the same way we understand them to behave. Again, we developed a statistical mechanical model of the system to predict what the equilibrium coverage of the lattice should be for a given chemical potential (as well as what the

contributions of flat and transverse dimers should be). We then compared these predicted values with a sampling of our simulation results in order to ensure that our simulations were in fact converging to the correct equilibrium values. A comparison between our calculated isotherms (lines) and our simulated isotherms (data points) is shown below in Figure 5.21. As can be seen, we had good agreement between our simulation results and our theoretical calculations across the spectrum of chemical potentials and interaction energies. The statistical mechanical calculations used here can be found in their entirety in Appendix B.

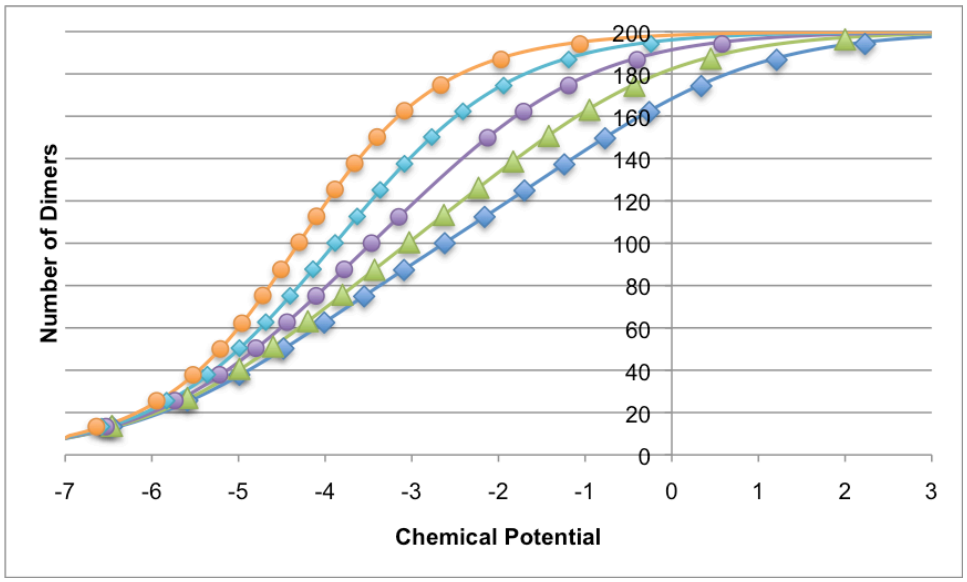

Figure 5.21
Calculated (lines) and simulated (points) isotherms of interacting dimers adsorbing on a one-dimensional, homogeneous lattice. The right-most curve (blue) shows the non-interacting case, while the curves to the left show integer multiples of the base interaction energies of ethane.

When we inspect the isotherms, we see that the curves shift to the left and become steeper as the magnitude of the interaction energy goes up. The dark blue curve shows the non-interacting case, shown previously in Figure 5.04. The green curve represents the system including nearest-neighbor interactions approximately equal to the typical values for ethane. The purple, light blue, and orange curves represent twice, thrice, and four times this amount, respectively. The leftward shift in the curves is not unexpected. As the increased interaction energies make it easier for adsorbed particles to stay on the surface, a lower chemical potential is

required to reach a given coverage. We also see the curves get steeper, which is to say, that there is a greater change in the number of particles per change in the chemical potential. Again, the interaction energies are contributing more to maintaining the coverage of the lattice, and the interaction energies favor ever more coverage (a tightly packed lattice is a lower total binding energy), and so a smaller change in chemical potential is required to increase the equilibrium coverage of the lattice.

Section 5.2.3.2: Kinetic Behavior of Interacting Dimers on a 1-D, Homogeneous Lattice

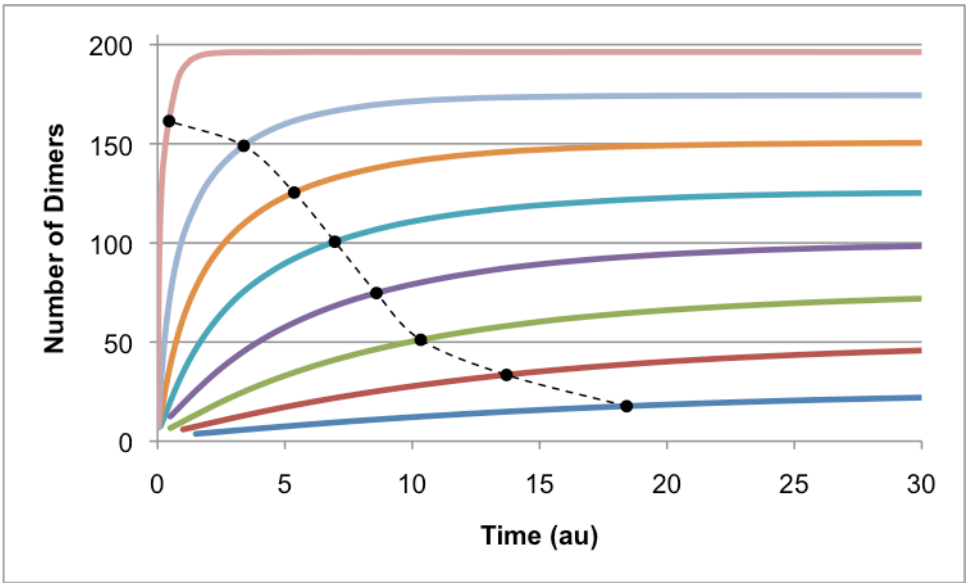

Figure 5.22
Total number of adsorbed particles as a function of time for a system with typical interaction energies for ethane. The black points show the characteristic time for each curve; notice the monotonic decrease in characteristic time as equilibrium coverage increases.

We begin by plotting the number of particles as a function of time. Figure 5.22 (above) shows the total number of adsorbed dimers as a function of time for a representative sample of equilibrium coverages, for a system with interaction energies consistent with ethane. As before, the points show when each curve reaches its characteristic time, while the dotted line guides the eye. We can see a monotonic decrease in the equilibration time as a function of coverage, which is what we know to be the case for ethane. Qualitatively, the characteristic times here are similar to what we saw for the non-interacting case (Figure 5.05), with one trend downwards in

characteristic time for low-coverage systems (here, the bottom three curves), and another downward trend for intermediate coverages, with the characteristic time approaching zero for the highest coverage.

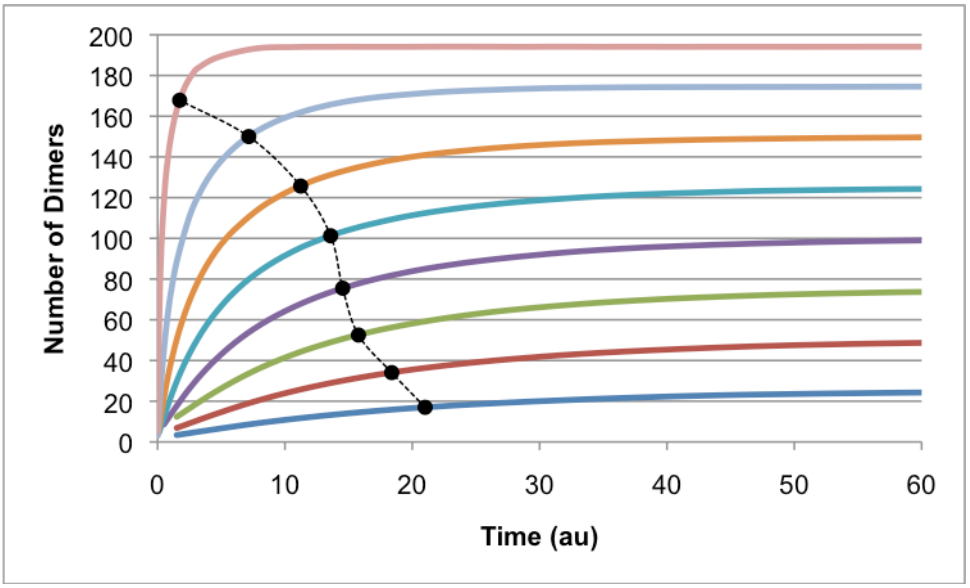

Figure 5.23
Total number of adsorbed particles as a function of time for a system with twice (2xR) the typical interaction energies for ethane. The black points show the characteristic time for each curve; now the characteristic times begin to bow outward for high-coverage systems.

We next considered a system with twice the "real" interaction energies. Again, we have plotted the total number of admolecules as a function of time, with the characteristic times shown for reference, in Figure 5.23 (above). We see that the characteristic time for the low-coverage systems increases only a small amount, and the characteristic time for monolayer is still almost zero. It is in the range of medium-to-high coverages, however, that we observe the kinetic behavior begin to change. Where before there was an almost linear decrease in characteristic time as the final coverage went up, we now see a "bulge" begin to form, as the characteristic times for these systems (100-175 adsorbed dimers, 70-90% fractional coverage) increase to a much greater extent than other systems.

We increase the strength of the nearest-neighbor interactions again, this time to thrice (3xR) the real values for ethane, and examine the number of adsorbed particles as a function of

time. As shown below in Figure 5.24, the characteristic time for the very highest- and lowest-coverage systems are largely unchanged, but the slight bowing-out of the characteristic times of the high-coverage systems (seen previously in Figure 5.26) have now developed into an outright increase in the characteristic time as the equilibrium coverage goes up. This is contrary to what we know experimentally about some common dimers (in particular, ethane) and is opposite to all of the kinetic behavior we have seen thus far.

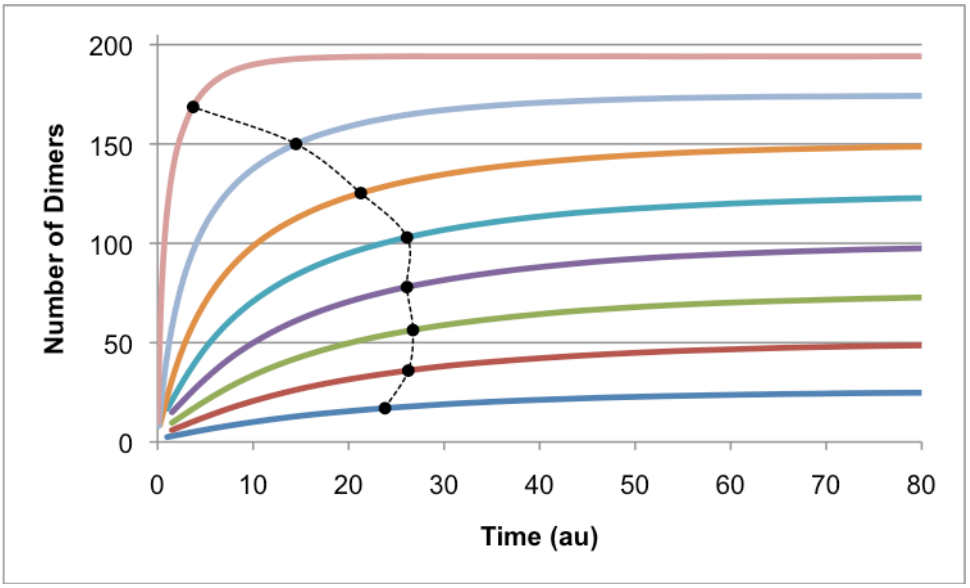

Figure 5.24
Total number of adsorbed particles as a function of time for a system with thrice (3xR) the typical interaction energies for ethane. The black points show the characteristic time for each curve; now the characteristic times actually increase with equilbrium coverage.

Our last system under consideration includes particle-particles interaction energies that are four times our baseline values (4xR). We show the number of adsorbed particles as a function of time, along with the characteristic times of each curve (black points), below in Figure 5.25. Here, there is a clear increase in the characteristic time with increases in the equilibrium coverage of the system. As we mentioned before, this is the reverse of the behavior we expected (and found) for ethane. It seems, then, that particle-particle interaction energies play a significant role in the kinetic behavior of a system. In the following sections we will expound upon this point.

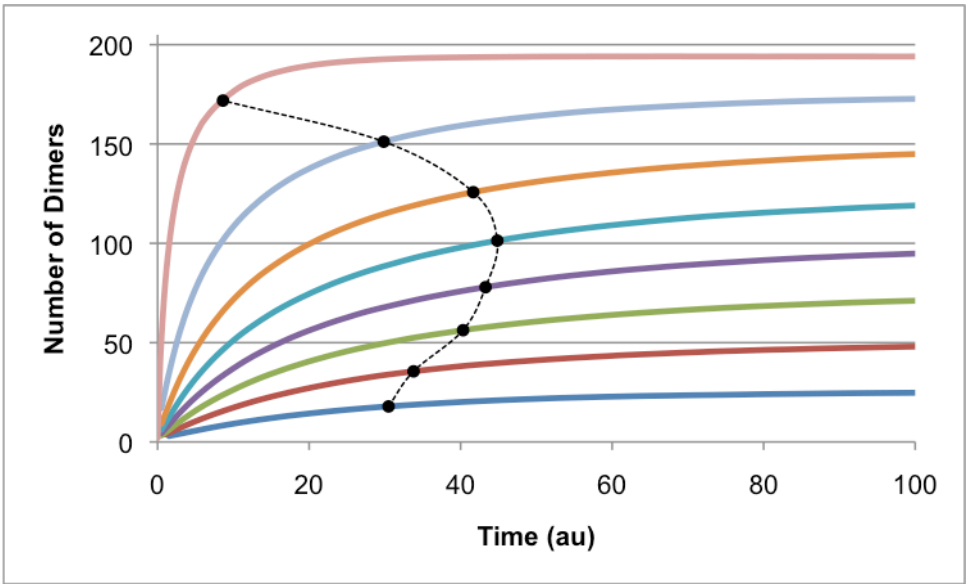

Figure 5.25
Total number of adsorbed particles as a function of time for a system with four times (4xR) the typical interaction energies for ethane. The black points show the characteristic time for each curve; now the characteristic times begin to bow outward for high-coverage systems.

When we were considering the adsorption of non-interacting dimers, we went into great detail regarding the rates for the system, and looking at the details of the graphs of the numbers of dimers as a function of time. We have not included all of those figures for our treatment of interacting dimers because it seemed redundant. A plot showing the number of flat, transverse, and total adsorbed dimers as a function of time (for a given equilibrium coverage) looks about the same regardless of the strength of the interaction energies in the system; only the time scale varies significantly, which we have shown in our figures above. But having studied closely these aspects of the evolution of these systems for the non-interacting case, we did not feel it necessary to reproduce all of our work for all of the interacting cases as well.

Section 5.2.4: Characteristic Times for Dimers

We now consider the characteristic time as a function of the total number of admolecules at equilibrium for dimers adsorbing on a one-dimensional, homogeneous lattice (shown below in Figure 5.29). We notice firstly that there is little change in the characteristic time at either end of the spectrum. We expect the particle-particle interactions will have little effect on systems with

extremely low equilibrium coverage; with so few particles on the lattice, it is unlikely that any particle will find itself a nearest-neighbor with any other particle, and thus the inclusion of nearest-neighbor interactions is moot. On the other hand, we also see very little change in the characteristic time for the highest coverage, which approaches zero regardless of the interaction energies. A very large chemical potential is needed to force the system into a state approaching monolayer, and this high flux of particles onto the surface seems to largely overwhelm any effect of interaction energies; the particles are held on the surface due to the strength of the chemical potential.

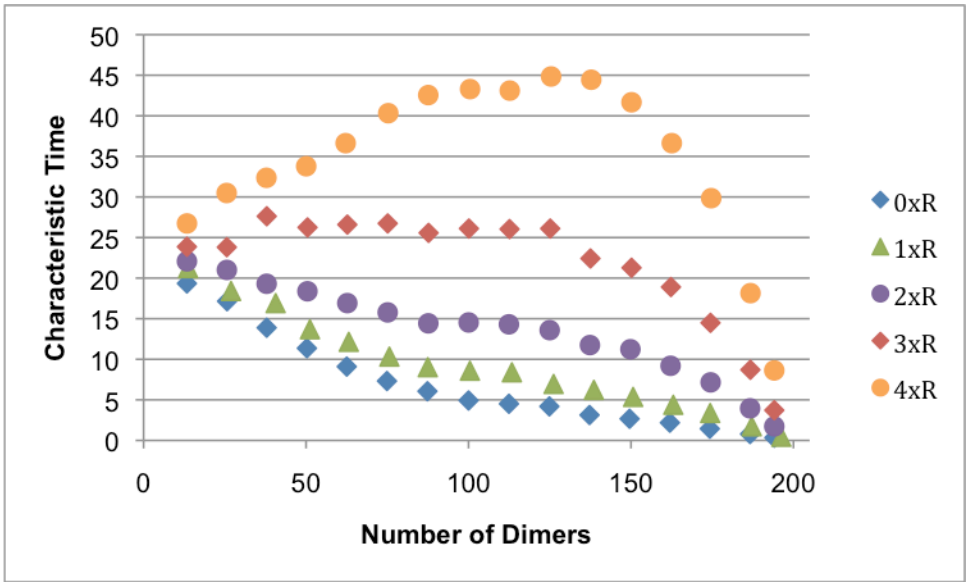

Figure 5.26
Characteristic time versus equilibrium coverage for interacting dimers on a 1-D, homogeneous lattice. When the particle-particle interactions become sufficiently large, the kinetic trend reverses.

When we inspect the curves in Figure 5.26, we can identify other trends that are not limited to the extrema. For example, we can see a largely linear relationship between the characteristic time and the number of dimers across the range from 12 to 87 adsorbed dimers. This region corresponds to equilibrium fractional coverages of 10 – 65%; they also represent the systems in which there is no overshoot, but rather the numbers of flat and upright dimers simply increases through the mechanism of the filling effect. We see that this linear relationship is

maintained regardless of the strength of the interaction energies; however, for the non-interaction case up through the inclusion of twice the baseline energies, in relation has a negative slope, but as the strength of the interaction energies increases, it eventually reverses itself and has a positive slope. In this region, flat dimers play a greater role, and there is an even mixture of flat and upright dimers on the lattice.

The other region of note includes systems with equilibrium coverages of 100 to 175 adsorbed particles. This region also shows a linear relationship between the characteristic time and the number of adsorbed particles for the non-interaction and real-interactions cases. However, the characteristic times in the region soon begin to tend upward, and as the strength of the interaction energies increase, we see the characteristic times actually begin to increase with coverage, reaching a peak that rises quickly and moves to the right (towards higher-coverage systems). This is the region that drives the reversal in the kinetic behavior (the increase in characteristic time with coverage, rather than the decrease that we have seen until now). We will discuss below what we believe the be the driver of this behavior.

Despite this large swing in the number of particles on the lattice (almost half of the total number that can fit on the lattice), this region of 100 to 175 adsorbed dimers only accounts for 65% to 95% of the fractional coverage of the lattice. From this we can gather a few things. The lattice is already quite crowded in this region, and the addition of many more particles (with nearly as much increase in fractional coverage) necessitates a great deal of rearrangement on the lattice to make room. Furthermore, this is the region wherein the upright dimers begin to take over. This is important because upright dimers are inherently more affected by nearest-neighbor interactions; two neighboring upright dimers have two methyl groups to interact with another two methyl groups, giving them much more interaction energy than two flat dimers laying “nose to nose” with only one methyl group to interact with another one methyl group. Then, an increase in the number of particles necessitates a large amount of reorientation in order to make room, but the strong bonds from the interaction energies mean that the chemical potential does not need to increase as much, meaning there is not a great increase in the flux of particles onto the surface to drive adsorption. We believe it is this smaller increase in chemical potential, coupled with the

increased need for reorientation (and the increased capacity for reorientation, entropically speaking) that causes the characteristic time to increase with coverage.

CHAPTER SIX
ADSORPTION ON A TWO-DIMENSIONAL, HETEROGENEOUS LATTICE

After gaining as much information as we could from a one-dimensional, homogeneous lattice, we needed to expand our lattice in order to develop a more realistic simulation model. In general, most films exist in two dimensions, and so adding a second dimension to our adsorption lattice was the natural first step. As we have mentioned before, we were originally inspired to do this work by the question of adsorption of gases on carbon nanotube bundles, so the obvious choice was to use a two-dimensional lattice that recreates the adsorption site distribution on the external surface of a CNT bundle. However, while we are interested in understanding the adsorption of molecules on CNT bundles, we also know from our previous work with monomers that the kinetics of adsorption rely heavily on the binding energies of the adsorption sites on the adsorbent. Then, the next step is to consider how the kinetics of adsorption change if different regions of the lattice have different binding energies. We are able to address both questions by using a two-dimensional, heterogeneous lattice.

Section 6.1: Adsorption of Monomers on a 2-D, Heterogeneous Lattice

Our previous results for monomers adsorbing on a two-dimensional, heterogeneous lattice have already been discussed in Sections 4.3 and 5.1. We have discussed the filling effect, which stems from the quick adsorption to a weaker-binding state followed by diffusion from the weaker-binding state to a stronger-binding one. This process serves to speed up the equilibration of the system and decrease the characteristic time; it is paralleled by dimers' ability to change their orientation from a strong-binding flat configuration to a weaker-binding upright state, and vice versa. We have also seen that the inclusion of particle-particle interactions in a system of dimers can cause the characteristic times to increase for a given coverage, although we have not observed this same behavior for systems of monomers adsorbing on a 2-D, heterogeneous lattice.

Section 6.2: Adsorption of Dimers on a 2-D, Heterogeneous Lattice

Having already considered monomers on a two-dimensional, heterogeneous lattice, we wanted to investigate the behavior of dimers adsorbing on this same lattice. In particular, we sought to determine whether the adsorption kinetics of dimers undergoes the same changes, when going from a homogeneous to a heterogeneous lattice, that we saw for monomers.

As we mentioned in Chapter 3, these dimers can adsorb and desorb anywhere on the lattice, either in the flat or upright configuration, and can change orientation with respect to the lattice (that is, change from flat to upright or vice versa). We returned again to non-interacting dimers, but we would later add nearest-neighbor interactions.

Section 6.2.1: Non-Interacting Dimers on a 2-D, Heterogeneous Lattice

We began this phase of our study by investigating the adsorption of non-interacting dimers on a two-dimensional, heterogeneous lattice. Our greatest interest was in how the heterogeneity of the lattice paired with the inherent heterogeneity of the dimers (due to their multiple orientations with respect to the surface) affected the kinetics of adsorption. This would prove an important baseline for determining how the kinetics of adsorption of neutral dimers changes when going from a homogeneous to a heterogeneous lattice, and later would also be a basis of comparison for the changes brought on by the inclusion of nearest-neighbor interactions.

Section 6.2.1.1: Equilibrium Calculations for Dimers on CNTs

Our first step was to verify the results of our simulations. We did this by running our simulations for a range of values of the chemical potential, and then comparing the equilibrium values that we found to those predicted by our statistical mechanical calculations. By showing that our simulations produced the correct equilibrium configuration of the system, based on temperature, chemical potential, and other parameters, we knew that the data on kinetics that our simulations provided was also correct. The statistical mechanical calculations used here can be found in their entirety in Appendix C.

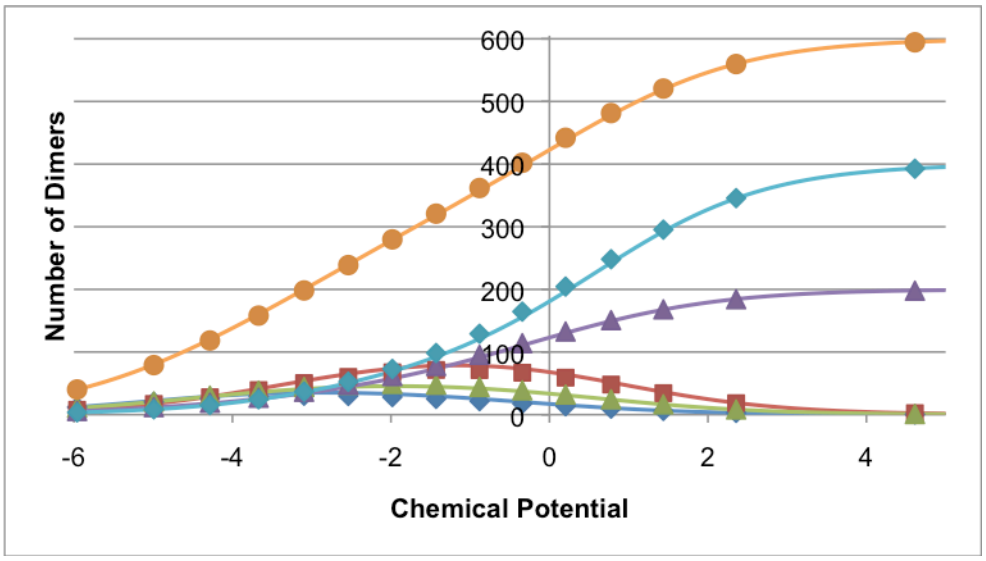

Figure 6.01
Number of particles as a function chemical potential for neutral dimers adsorbing on a 2-D, heterogeneous lattice. We see that the flat configurations (dark blue, green, and red) rise with chemical potential before falling away as the total coverage increases, while the upright states (purple and light blue) increase monotonically, as does the total coverage (orange).

Figure 6.01 (above) shows the number of dimers adsorbed at equilibrium as a function of chemical potential. We see that the coverage of the lattice is dominated by flat dimers for low values of the chemical potential. These dimers can be in three possible states: flat along the groove, the strongest-binding state (dark blue curve); flat along the edge, the weakest-binding state for a flat dimer (red curve); or laying across the groove, with one end in the groove and the other in an edge site, in an intermediate state (green curve). We see that, as the chemical potential increases, each one of these states reaches a peak value, in turn according to the strength of its binding energy. We also see that these peaks are of different heights, which is a function of the number of binding sites available. In a lattice of three rows of 200 sites, there can be a maximum of 100 dimers solely in the groove, but there can be as many as 200 dimers laying across the groove or on the edges. Despite these slight differences in the peaks of the different variations, we see that these different possible states of flat dimers behave in general quite similarly, in that they rise together, peak at comparable heights and at comparable chemical potentials, and then fall away together.

We see the same similarity of behavior in the upright dimers, which can stand upright in the groove (purple curve) or on the edges (light blue curve). Again, there are more edge sites, so there are more upright dimers on the edges at equilibrium. However, the number of upright dimers in each state rises at approximately the same rate.

We also note that the last peak of flat dimers occurs when there are 320 total dimers on the lattice (out of 600 total sites). This corresponds to a fractional coverage of about 77%, meaning we again see a general reorientation from flat to upright dimers occurring between 77% and 95% fractional coverage, similar to what we have seen for dimers on other surfaces.

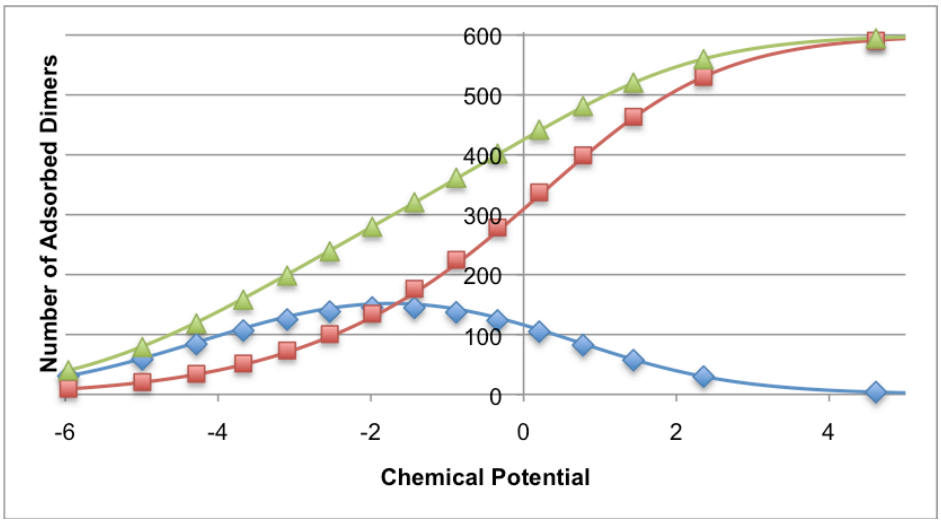

Figure 6.02
Number of dimers adsorbed at equilibrium versus chemical potential. The blue curve shows the contribution of *all* flat dimers, the red curve shows *all* upright dimers, and the green curve shows the total number of dimers adsorbed at equilibrium for each value of the chemical potential.

We have mentioned in the preceding discussion that there is not a large difference between the various sub-states available for flat and upright dimers. It seems that the dimers tend to share a similar equilibrium behavior, regardless of where they might adsorb on the lattice. This is shown quite well in Figure 6.02 (above), which shows the same isotherm we discussed in Figure 6.04, but with all of the flat dimers counted as one (blue curve) and all the upright dimers counted together (red curve), with the total coverage is shown in green. The isotherm we see

here is not qualitatively dissimilar from what we saw for dimers adsorbing on a one-dimensional, homogeneous lattice, save for the scaling due to the size difference between the two surfaces.

Section 6.2.1.2: Kinetic Behavior of Dimers Adsorbing on a 2-D, Heterogeneous Lattice

Having thusly verified that our simulations were giving us accurate data, we set about studying the kinetic behavior of these systems of dimers adsorbing on a two-dimensional, heterogeneous lattice. Like before, our simulations provided us with the number of particles in each orientation as a function of time, from which we could extract information pertaining to the characteristic time of the system as well as the phases through which it passes as it evolves toward equilibrium.

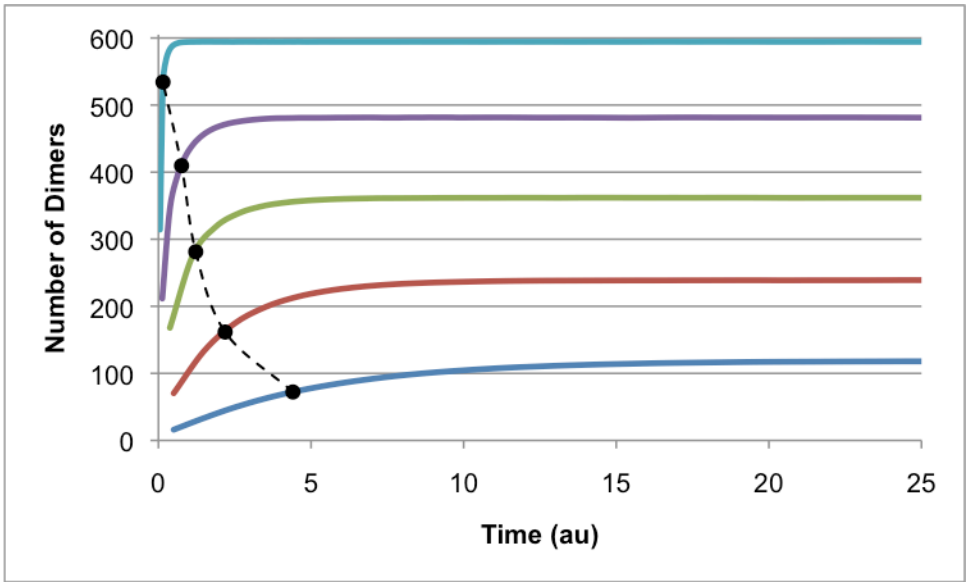

Figure 6.03
Total number of adsorbed particles as a function of time for several systems of neutral dimers adsorbing on a 2-D, heterogeneous lattice. The characteristic time decreases as the coverage goes up (black points).

The total number of adsorbed particles as a function of time is shown above in Figure 6.03. Qualitatively, this graph is very similar to what we saw for dimers adsorbing on a one-dimensional, homogeneous lattice. We see the characteristic time decrease as the equilibrium coverage goes up. As we have found previously, the characteristic time decreases rapidly as the

system goes from low coverages to moderate coverages, and then decreases more slowly as the system goes from moderate to high coverages.

Next, we looked at the contributions of each possible orientation of the dimers on this lattice. We show the number of particles in each state as a function of time in Figure 6.07 (below). The total coverage (orange) is a pseudo-exponential decay function, as we have seen before. The dimers making up this total coverage are evenly distributed into the various possible states, as seen by the close packing of the other curves at the bottom of the graph, representing the number of dimers in each of the possible states in this system.

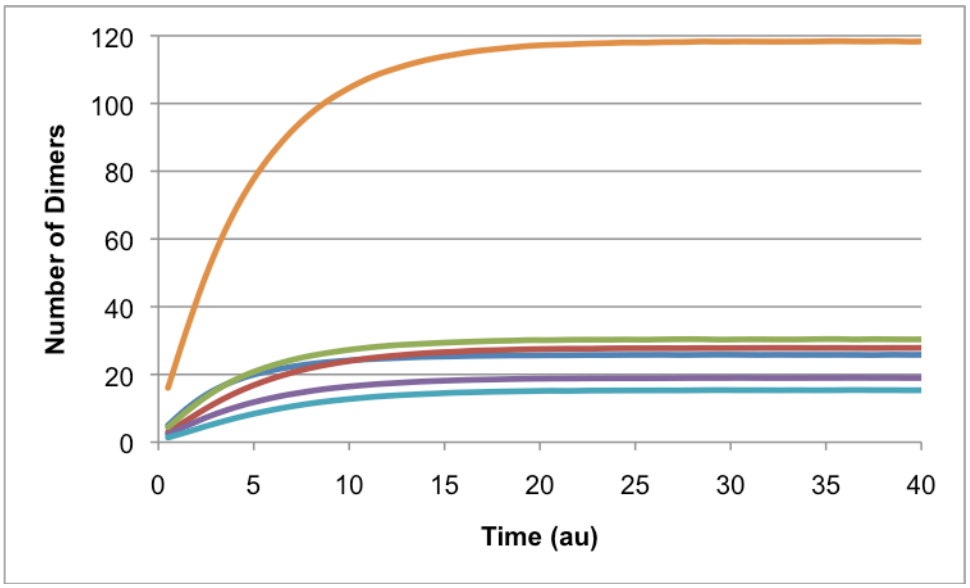

Figure 6.04
Number of particles as a function of time for a system of neutral dimers adsorbing on a 2-D, heterogeneous lattice. The curves at the bottom are tightly packed, meaning that the dimers in this system are evenly distributed among the several available states rather than preferring one or more in particular.

It is difficult to discern much detail from Figure 6.04 because the curves are so close together. We have zoomed in on this detail of the graph in Figure 6.05 (below) in order to better show the contribution of the number of dimers in each available state in the system. We see that initially in the time-evolution of the system, the greatest number of dimers are laying flat in the groove (dark blue curve), which makes sense as this is the most energetically favorable state. It is likely that these dimers filled the groove so quickly through a filling effect like we observed

before. However, these dimers lying flat along the groove are soon overtaken by dimers laying flat partly in the groove and partly on the edges (green curve). This state sacrifices some of the binding energy in order to allow more particles into the flat orientation. All along, there are still a comparable number of particles laying flat on the edges (red curve). Meanwhile, there are a smaller number of dimers standing upright n the groove (light blue curve) and on the edges (purple curve). Again we can see a slight anomaly very early in the evolution of these upright dimers, particularly in the curve of upright dimers in the groove (light blue), which is due to dimers reorienting themselves from this state into one of the flat states, driving the filling effect.

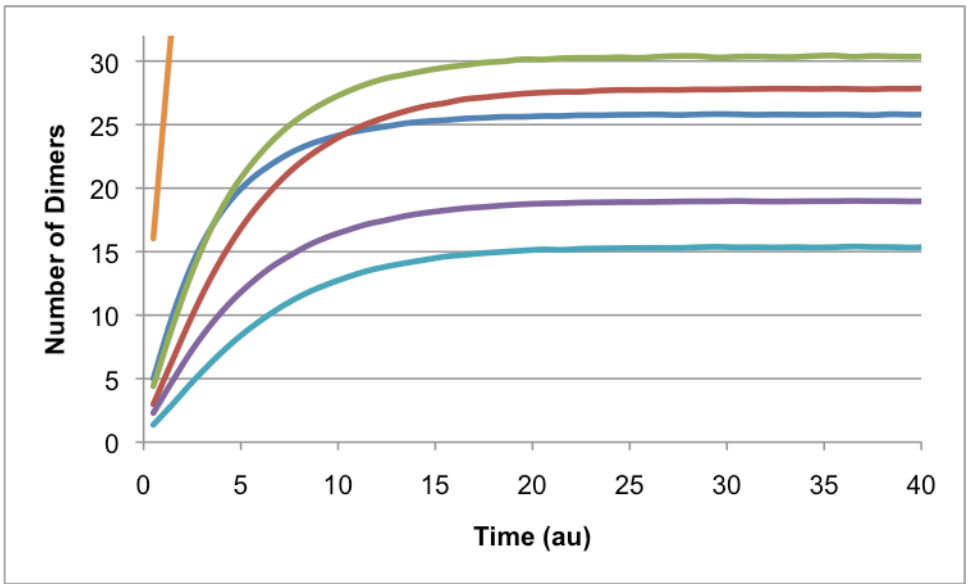

Figure 6.05
Number of dimers as a function of time for a system of dimers adsorbing on a 2-D, heterogeneous lattice, zoomed in to show the contributions of each sub-state of the dimers. Note that the dimers in flat orientations (dark blue, green, and red) behave very similarly to one another, as do the dimers in the upright orientations (light blue and purple).

Another important point to draw from Figure 6.08 is the similarity in the kinetic behaviors of the dimers in the flat sub-states (dark blue, green, and red) and in the upright sub-states (light blue and purple). As we noticed in the isotherms for this systems (shown in Figures 6.04 and 6.05), there does not seem to be a great difference between considering the contributions of each individual sub-state, each separated from the rest, or considering all of the flat dimers as one group and all the upright ones as another. Similarly, we discussed in Figure 6.08 how one group

of flat dimers was briefly preferred over another group of flat dimers, but in the end, all of the flat dimers made comparable contributions to the overall coverage of the lattice at equilibrium. This indicates that the heterogeneity of the lattice, expressed by the availability of adsorption sites with different binding energies, is not as important as the heterogeneity of the adsorbates, who, through their ability to stand perpendicularly to the lattice or lay flat upon it, create not only a difference in the available binding energies but also an interplay between the total binding energy and the number of particles on the lattice and the fractional coverage of that lattice.

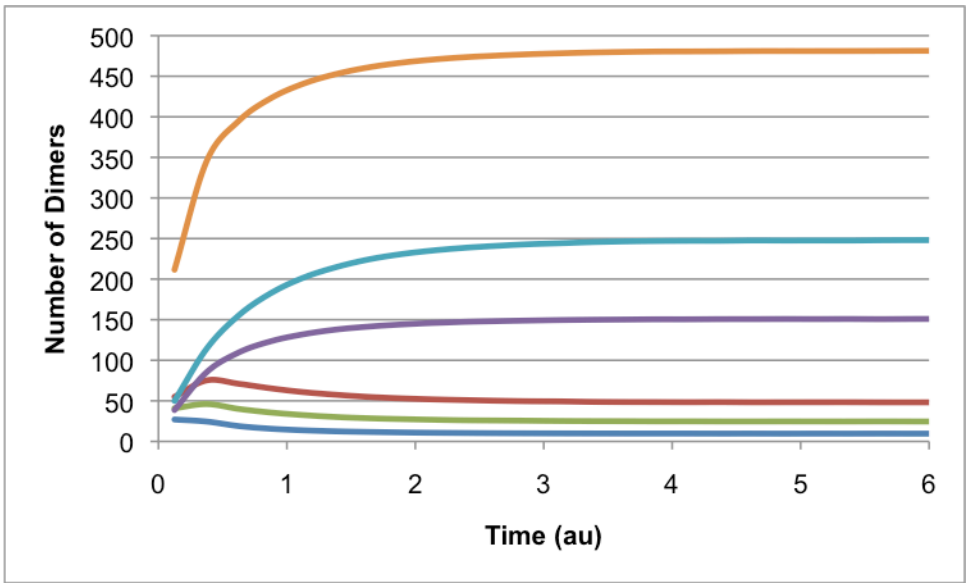

Figure 6.06
Number of particles as a function of time for a system of neutral dimers adsorbing on a 2-D, heterogeneous lattice. Note that, as before, the dimers in flat orientations (dark blue, green, and red) behave very similarly to one another, as do the dimers in the upright orientations (light blue and purple).

When we consider very high coverages of dimers adsorbing on a two-dimensional, heterogeneous lattice, we see similar behavior we what we saw for lower coverages. Above, in Figure 6.06, we show the number of particles in each sub-state as a function of time for a system with 480 adsorbed dimers at equilibrium, representing a fractional coverage of 94%. We see that the dimers in the flat states (dark blue, green, and red) each exhibit an overshoot that reaches a different peak; we know that these different peaks at the overshoot coincide with the peak number of particles in each flat state shown in the isotherm in Figure 6.04. We discussed the

overshoot thoroughly in Section 5.2.2.5. We notice again that the dimers in the flat states all seem to behave in a similar manner, despite small differences between them. Similarly, we see that the dimers in the upright states (light blue and purple) also behave similarly; the number of transverse dimers on the edges only reaches a greater contribution because there are twice as many edge sites as there are groove sites.

Section 6.2.2: Interacting Dimers on a 2-D, Heterogeneous Lattice

Having gained as much knowledge as we could about neutral dimers adsorbing on a two-dimensional, heterogeneous lattice, we added nearest-neighbor interactions in order to see how this factor would affect the kinetics of adsorption. The main difference here is that a flat dimer can now interact with a total of six nearest neighbors (three for each end) and a upright dimer can interact with four nearest neighbors, whereas there were only two possible nearest neighbors in a one-dimensional lattice. Furthermore, although a upright dimer has fewer possible nearest neighbors, these particle-particle interactions favor transverse dimers because *both* methyl groups in a upright dimer can interact with nearest neighbors, while only one methyl group of a flat dimer can bond with each neighbor. As before, we considered both the equilibrium configurations and kinetic behaviors of this system.

Section 6.2.2.1: Equilibrium Characteristics of Interacting Dimers Adsorbing on a 2-D, Heterogeneous Lattice

We again verified our computational scheme by comparing the equilibrium coverages produced by our simulations to the values predicted by our statistical mechanical calculations. The total number of adsorbed particles at equilibrium as a function of chemical potential is shown below in Figure 6.10. The non-interacting case is shown in dark blue, and each curve to the left represents the inclusion of half of the interactions typical for ethane. Therefore, the green curve shows the most accurate depiction of ethane adsorbing on CNTs, the light blue curve is a system with twice the nearest-neighbor interactions as ethane, and so forth. There is very good agreement between our calculations and simulations across the range of interaction energies that we used. This means that we correctly incorporated particle-particle interactions into our

calculations and our computational scheme. The statistical mechanical calculations used here can be found in their entirety in Appendix C.

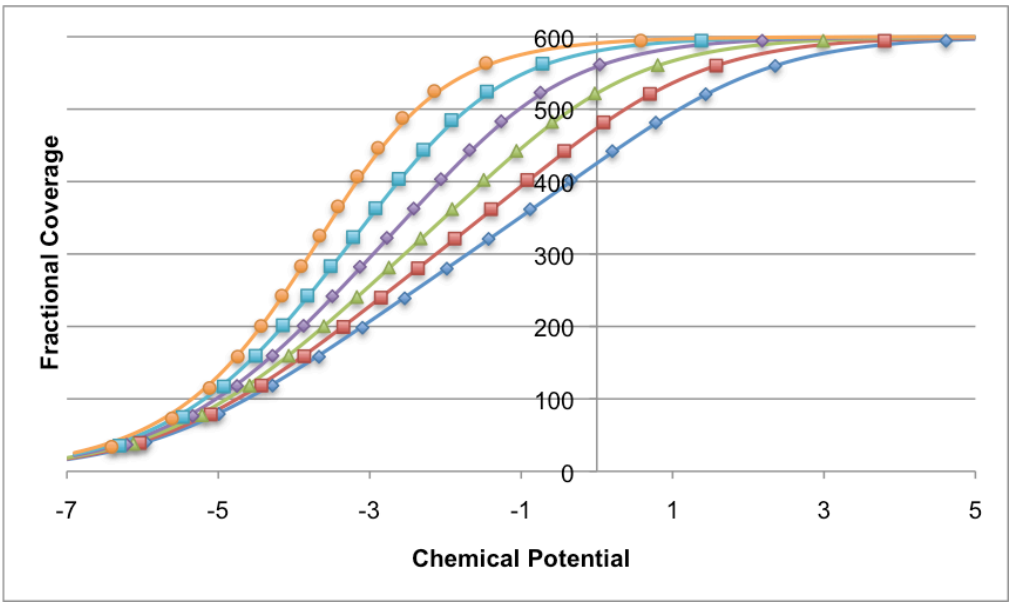

Figure 6.07
Number of particles versus chemical potential for interacting dimers adsorbing on a 2-D, heterogeneous lattice. The neutral case is shown on the far right (dark blue curve), and as the interaction energies are increased (by steps corresponding to half of the typical values for ethane), we see the curves shift to the left and become steeper.

As we further inspect the curves in Figure 6.07, we notice that the curves shift to the left as the magnitude of the particle-particle interactions increases, meaning that a lower chemical potential is required to reach a given coverage. This change occurs because the stronger total binding energy holds more of the adsorbed molecules on the surface, so less chemical potential is necessary. We also see that the number of particles rises more quickly with respect to the chemical potential as the interactions are increased, which shows that greater interaction energies require much smaller increases in the chemical potential to boost total coverage, due to the fact that it is much more energetically advantageous to have more particles on the lattice because of the strong binding in general and the preference in the interaction energies for upright dimers in particular.

Section 6.2.2.2: Adsorption Kinetics for Interacting Dimers on a 2-D, Heterogeneous Lattice

We now turn to the kinetics of these systems of interacting dimers adsorbing on a two-dimensional, heterogeneous lattice. By plotting the total number of particles as a function of time, we are able to extract information regarding the speed with which the system equilibrates, from which we can gain a better understanding of the adsorption kinetics. Below are a few of the systems we simulated that best highlight the changes in kinetics as the interaction energies increase.

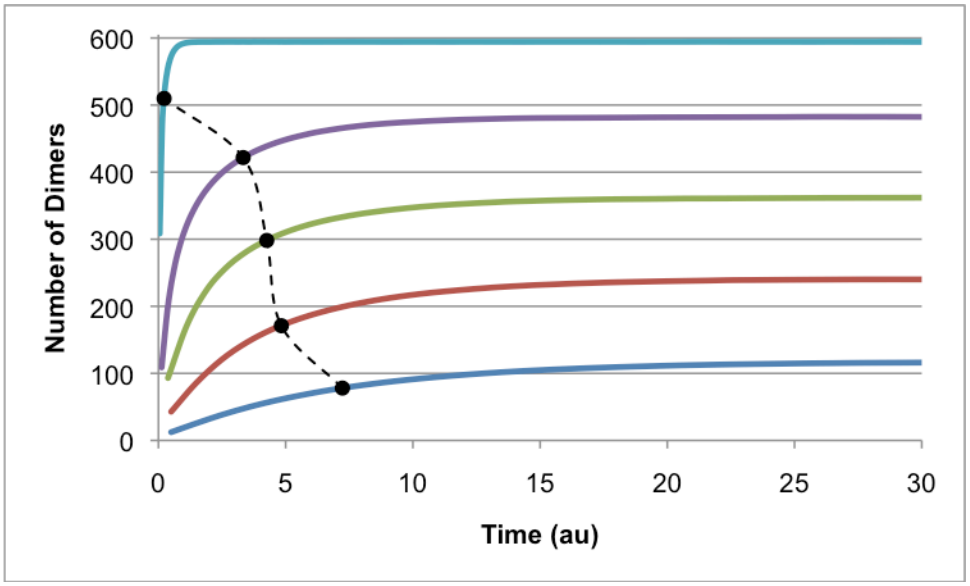

Figure 6.08
The number of particles as a function of time for a system of interacting dimers adsorbing on a 2-D, heterogeneous lattice. The characteristic time (black points) decreases as the equilibrium coverage goes up, but we see the curve begin to bow out for moderate and high coverages.

When we look at a system with interactions of strength comparable to the accepted values for ethane (shown above in Figure 6.08), we see that the characteristic time (black points) still decreases as the equilibrium coverage goes up. This is similar to the non-interacting case in that there is still a decline in the characteristic time at the lowest coverages, and the characteristic time still goes to zero as the system approaches monolayer, but we see here that the curve begins to bend outward as it goes from moderate to high coverages. While there is still a decrease in characteristic time, it is much slower than we saw for the case of neutral dimers.

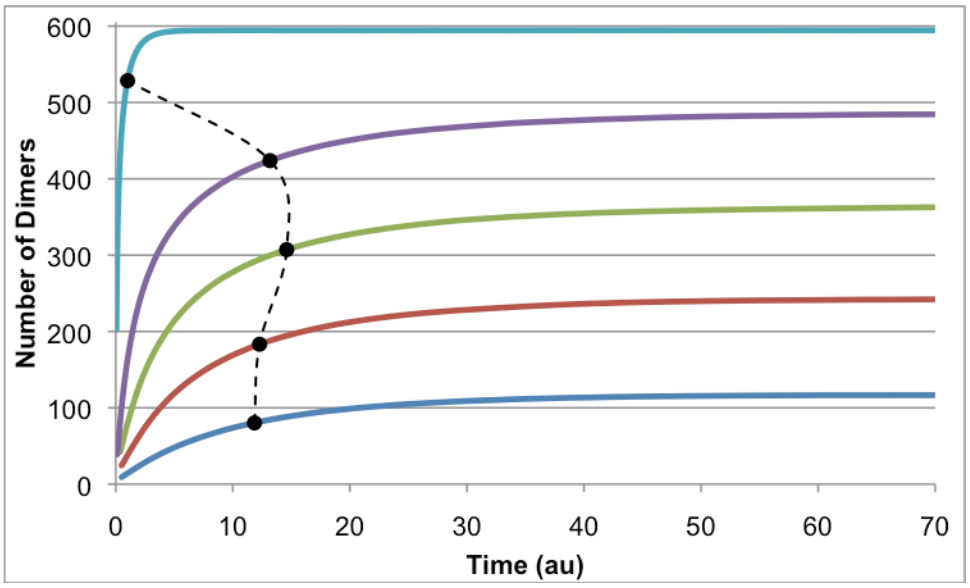

Figure 6.09
The number of particles as a function of time for interacting dimers adsorbing on a 2-D, heterogeneous lattice. Now with twice the particle-particle interactions for ethane, the characteristic time increases slightly as the equilibrium coverage goes up.

Now we consider a system with twice the magnitude of the typical interaction energies for ethane, shown above in Figure 6.09. We see that the characteristic times for the lowest coverages have increased, but only a small amount. Similarly, the waiting time for monolayer is still approximately zero. The greatest change in characteristic time, compared to cases discussed previously, occurs for the systems with moderate to high interaction energies. These are the systems in which the lattice is first is covered by flat dimers (through the filling effect) and then undergoes a general shift from flat to upright dimers. We believe it is this process of reorientation that slows down the evolution and causes the increase in the characteristic time.

Section 6.2.3: Characteristic Times for Interacting Dimers on a 2-D, Heterogeneous Lattice

We now consider the characteristic time as a function of equilibrium coverage for all systems of interacting dimers, shown in Figure 6.10 (below). As we noticed from the time-evolution curves, the characteristic times are very close for very low coverages (when the lattice is sparsely populated and so nearest-neighbor interactions play a small role) and for the highest coverages (where the chemical potential is so high that it overpowers any energetic effects). We

also note from the curves above that there are generally two regions of kinetic behavior, one for systems with fewer than 300 particles at equilibrium and another for systems with a higher coverage than this at equilibrium. This corresponds the behavior shown in the isotherm for this system (Fig. 6.02). There, we saw that below 300 particles (approximately), the lattice is dominated by flat dimers and the number of flat dimers increases with chemical potential, while above that coverage the number of flat dimers falls as the chemical potential continues to rise and upright dimers end up covering most of the lattice. This makes sense that we would see one kinetic behavior for systems of mostly flat dimers and another for systems that must undergo a general reorientation from flat to upright.

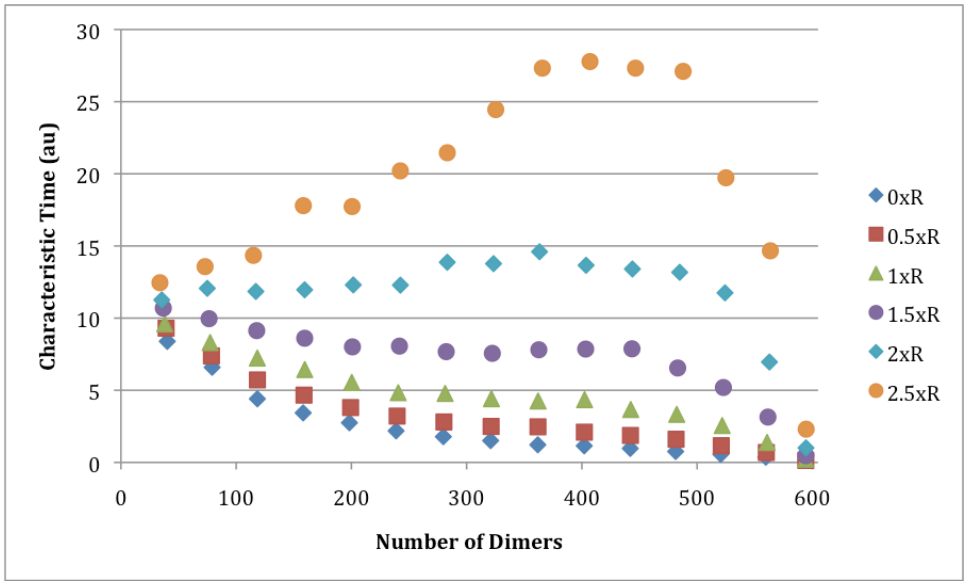

Figure 6.10
Characteristic time as a function of the number of adsorbed dimers at equilibrium, for interacting dimers adsorbing on a 2-D, heterogeneous lattice. The characteristic time decreases with coverage for interacting dimers that model ethane; when the particle-particle interactions are greater than that threshold, the characteristic time actually increases with coverage.

Beyond the kinetic changes that occur by changing the chemical potential in a single system, we are also interested in the effect of changing the magnitude of the interaction energies to create an entirely new system. The greatest change in the kinetic behavior occurs at the threshold of the “real” interaction energies for ethane. Below this value, the characteristic time decreases as the equilibrium coverage, albeit at different rates between systems and even within

a given system. On the other hand, systems with particle-particle interactions greater than this threshold demonstrate an increase in characteristic time with coverage. Thus, we have shown a decrease in the characteristic time versus coverage for ethane adsorbing on carbon nanotube bundles, which matches the experimental data we have. However, we predict that a different gas, one with greater nearest-neighbor binding energies than ethane, might in fact show an increase in waiting time with coverage when adsorbing on CNTs.

The peak characteristic time seems to occur in the range of 80-90% fractional coverage, when the adsorption of additional particles mostly depends on the reorientation of particles on the lattice in order to make space. This process require little extra chemical potential to boost the kinetics (because the change is so energetically advantageous), but requires more time in the sense of increased diffusion/reorientation on the lattice.

CHAPTER SEVEN
ADSORPTION OF ALKANES ON GRAPHENE

The main focus of our study was to understand how molecular length affects the kinetics of adsorption. To this end, we considered alkanes of increasing length adsorbing on graphene, thereby removing the effect of surface geometry in order to better isolate the effect of molecular length.

Section 7.1: Adsorption of Monomers on Graphene

We began with the simplest alkane, methane, modeled as a monomer. While this model is similar to what we have discussed in previous chapters, it provides an important baseline for the rest of our study. As before, we used a combination of analytical calculations and computer simulations to explore the kinetics of the adsorption of these molecules, this time on a flat, homogeneous surface.

Section 7.1.1: Simulation Results for Monomers on Graphene

We begin by running a battery of simulations to explore the salient kinetic behaviors of this system of monomers adsorbing on a graphene sheet. We then use our analytical means to better explain and understand these behaviors.

In Figure 7.01 (below), we see the number of adsorbed monomers as a function of time for a representative sample of systems. As can be seen, the characteristic time is longest for the lowest coverage and decreases as the number of adsorbed particles goes up. The waiting time approaches zero as the system approaches monolayer coverage. This is the same behavior that we observed for monomers adsorbing on a 1-D, homogeneous lattice, which is not surprising, since in both non-interacting cases, each lattice site can be considered to be independent of all the rest, and thus lattice size and geometry do not play a role.

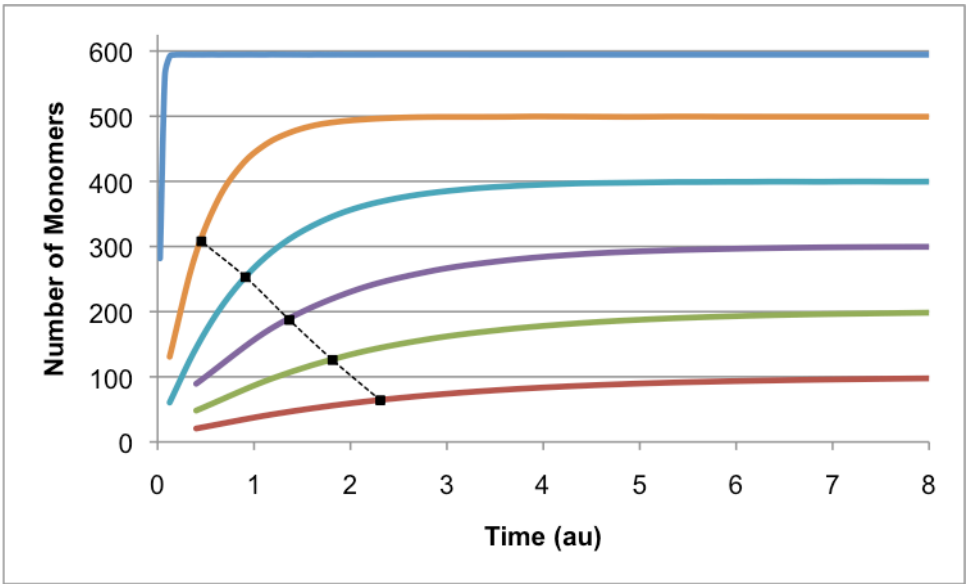

Figure 7.01
The number of particles as a function of time for non-interacting dimers adsorbing on graphene. The characteristic time decreases steadily as the equilibrium coverage goes up.

Figure 7.01 also shows the characteristic time of each curve as a black point, with a dotted line connecting these points to show the trend. We found the characteristic time of each curve by plotting $\ln(1-N/N_{eq})$ versus time and measuring the slope of the linear regression line, as discussed in Chapter 4. This is a common method used to measure the approximate rate of increase of pseudo-exponential functions like those seen in Figure 7.01. The rate-plots are seen below in Figure 7.02. Notice that the lines are almost perfectly linear, meaning that the source curves in Figure 7.01 are true exponential decay functions with a constant rate of change throughout their evolution.

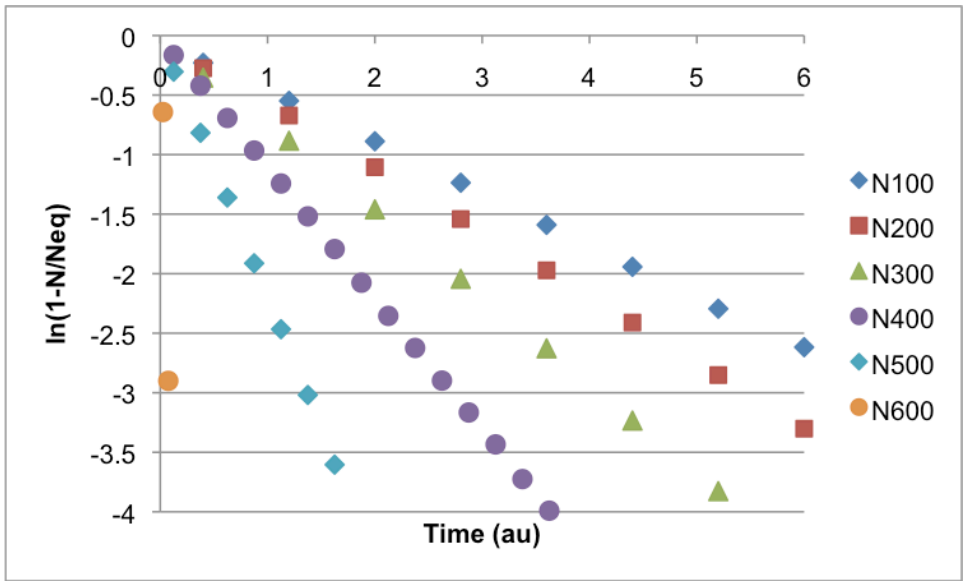

Figure 7.02
The rate curves for a system of neutral monomers adsorbing on graphene. The curve are perfectly linear, meaning that the processes of adsorption is driven at a single rate.

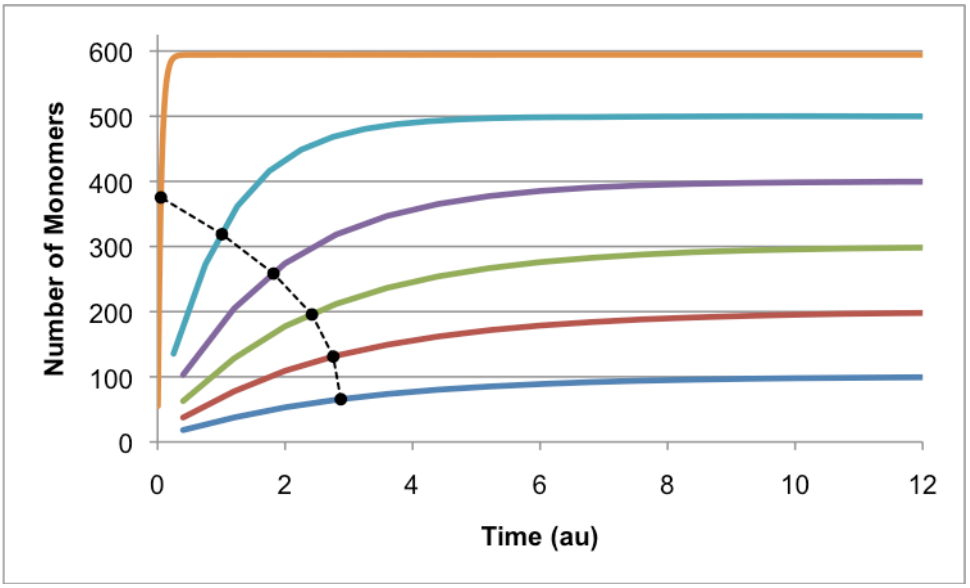

Figure 7.03
Number of particles versus time for a system of interacting monomers on a 2-D, homogeneous lattice. The inclusion of interactions causes the characteristic times to tend upward, meaning the waiting time is slightly longer to reach the same coverage.

We see a change in kinetic behavior, however, as we increase the magnitude of particle-particle interactions. Above (in Figure 7.03) we can see the kinetic curves with a system with

particle-particle interactions equivalent to the true interaction energy for methane, which is about 14% of the adsorption energy. Although we see a lengthening in the equilibration times around 50% coverage, the characteristic times still decrease as the number of particles goes up. This monotonic decrease, however, bends upward, much like we saw for monomers on a 1-D, heterogeneous lattice.

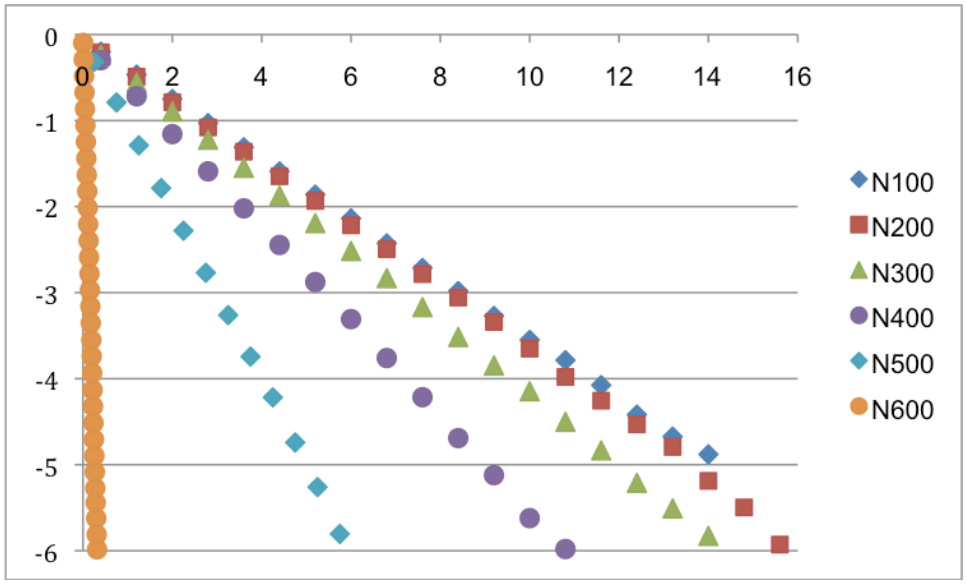

Figure 7.04
Rate curves for interacting monomers adsorbing on a 2-D, homogeneous lattice. Again they are perfectly linear.

When we look at the rate-plots for 1xR (one times the “real” interaction energy for methane) monomers, shown above in Figure 7.04, we again see that the curves are linear, meaning that a single process is driving the evolution of the system. This process is likely a net flux of particles onto the surface that is dependent on an “effective energy” that includes the adsorption and interaction energies.

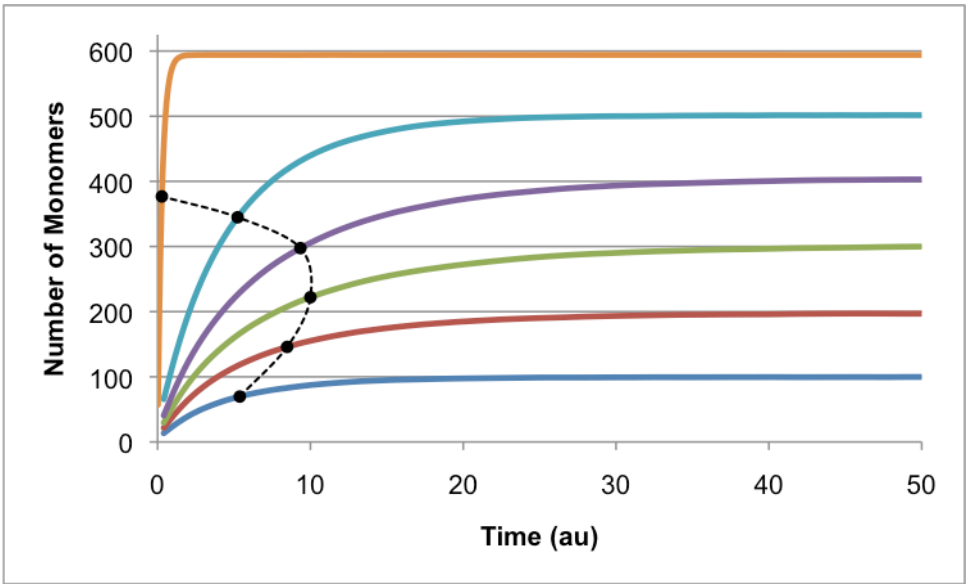

Figure 7.05
Number of admolecules as a function of time for a system for a system of monomers adsorbing on a 2-D, homogeneous lattice. The monomer have three times the normal interaction energy for methane (3xR).

In the next set of simulations, we set the particle-particle interaction energy to be three times the real value for methane, so that the interaction energy is about 40% of the adsorption energy. Already we see the equilibration time increase as the number of particles goes from 100 to 300 (that is, up to around 50% fractional coverage). The waiting time decreases as the number of particles continues to increase, and again we see essentially zero waiting time at monolayer coverage. We see here, then, that an increase in equilibration time with coverage is possible even for monomers, but only when the particle-particle interaction energy is extremely high.

We also see a change in the rate-plots to accompany this change in kinetic behavior. In Figure 7.06 (below), we see that the rate-plots for the very low (dark blue) and very high (light blue and orange) coverages are mostly linear, but that there is a marked curvature in the rate-plots for the coverages around 50%. This curvature means that the rate of uptake changes even as adsorption continues to take place. Because of the direction of the curve (concave-up), we know that adsorption is slowing down as time goes on, perhaps due to increased diffusion on the lattice.

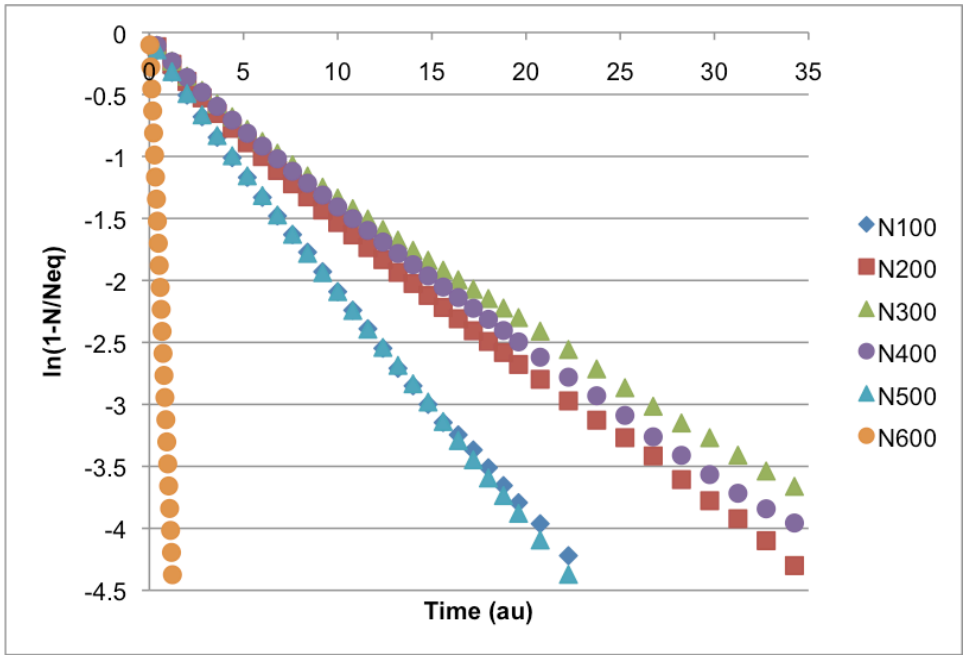

Figure 7.06
Rate curves for monomers adsorbing on a 2-D, homogeneous lattice. The rate curves for very low (dark blue) and very high (light blue and orange) coverages are mostly linear, while we see a marked curvature for rate curves for the moderate to high coverages (red, green, and purple).

We have discussed the characteristic times as a function of coverage for several systems of adsorbing monomers with different magnitudes of particle-particle interactions. All of these curves are plotted together in Figure 7.07 (below). We notice that the characteristic time decreases linearly as the equilibrium coverage goes up for non-interacting monomers (dark blue points) on this surface, just as it was for a one-dimensional, homogeneous lattice. As we increase the strength of the interaction energies (in integer multiples of the accepted value for methane), we see the characteristic time begin to actually increase with the final coverage. The peak in this characteristic time rises and moves to the right as the strength of the nearest-neighbor interactions increases. This is different behavior from what we saw for monomers on a one-dimensional, homogeneous lattice; however, this triangular lattice allows for six nearest neighbors instead of only two, so the total interaction energy is much larger here than in our previous results. We describe in more detail in the following sections our efforts to explain this kinetic behavior.

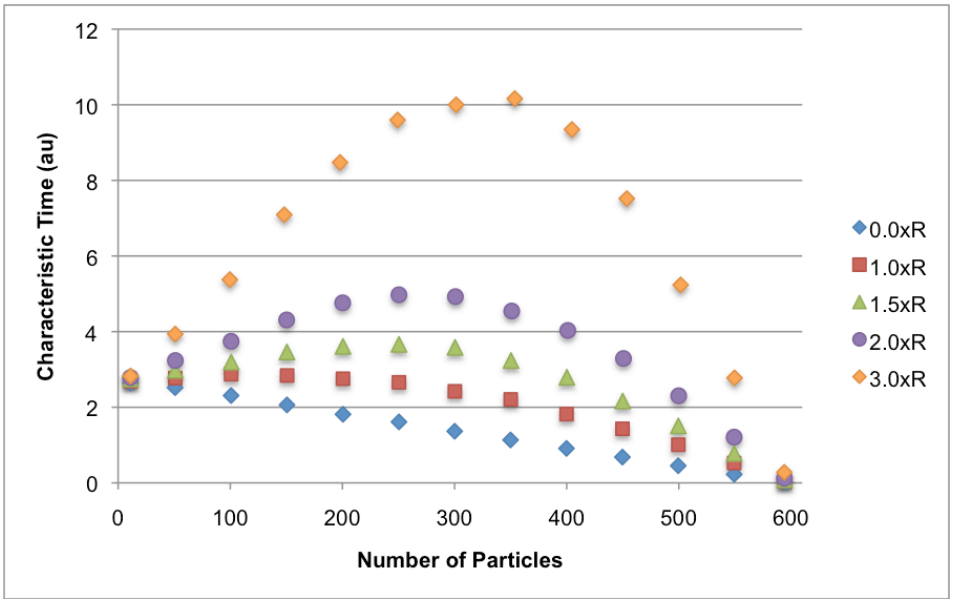

Figure 7.07
Characteristic time versus equilibrium coverage for systems of monomers adsorbing on a two-dimensional, homogeneous lattice. The waiting time decreases linearly with final coverage for the case of neutral monomers (blue points), but the characteristic time begins to increase as the equilibrium coverage when particle-particle interactions are introduced.

Section 7.1.2: Calculations for Monomers

We use calculations when possible to verify and explain our simulation results. The calculations were similar to those we performed for monomers on a 1-D, homogeneous lattice. However, because the lattice was more complicated, and because we included particle-particle interactions, these calculations were more involved. We provide an overview of our calculations, both equilibrium- and kinetic-based, in the sections below, with a more thorough discussion found in Appendix F.

Section 7.1.2.1: Equilibrium Calculations for Monomers

As mentioned above, and as detailed in Appendix F, we were able to develop a statistical mechanical treatment of the system of monomers adsorbing on a graphene sheet. We used a unit cell of seven sites, arranged in a honeycomb pattern, to match the triangular lattice used in our simulations. Using such a large unit cell was necessary to account for all the different microstates available; each microstate had not only a different number of particles but also a different total energy due to the inclusion of particle-particle interactions. Once we had identified

the number of particles and total energy of each microstate, we were able to find the partition function and then determine the equilibrium coverage for a given temperature and chemical potential.

Figure 7.08 (below) shows the number of particles versus the chemical potential of the system. The points (sim) are from simulations, while the lines (calc) show the values predicted by our calculations. As can be seen, we found very good agreement between the theoretical and simulated values across the spectrum of chemical potentials. Furthermore, this agreement was maintained even as we changed the interaction energy from zero to three times the real value for methane (which is about 50% of the adsorption energy). This is a strong confirmation of our simulation techniques; because we are finding the same equilibrium values through the Kinetic Monte Carlo algorithm as we expected from our statistical mechanical treatment of the system, we can trust that our simulations are providing us with a real representation of how the system should behave. The statistical mechanical calculations used here can be found in their entirety in Appendix D.

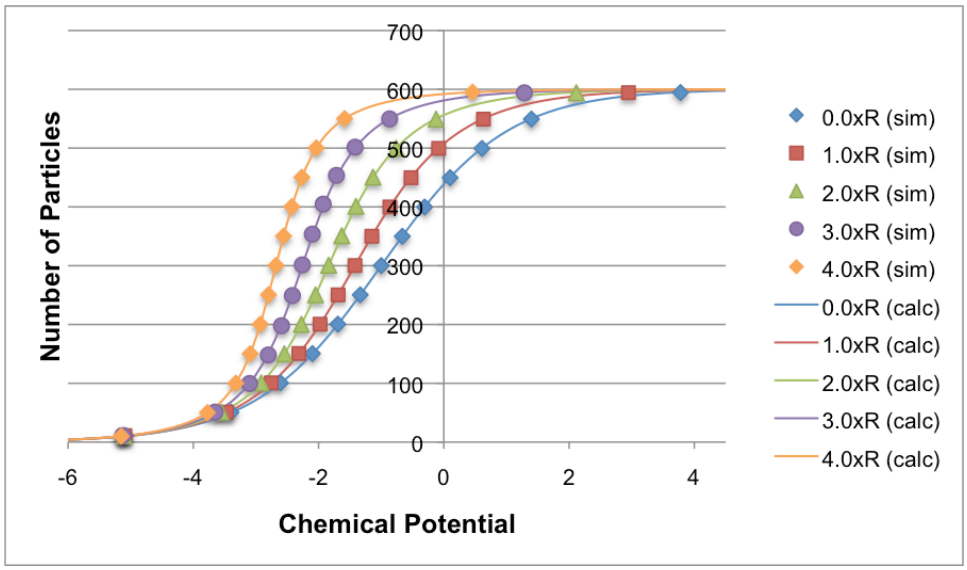

Figure 7.08
Number of adsorbed particles at equilibrium versus chemical potential for systems with increasing particle-particle interactions adsorbing on a 2-D, homogeneous lattice. We see good agreement between our statistical mechanical calculations (curves) and our simulation results (points) across the range of chemical potentials and interaction energies.

Section 7.1.2.2: Kinetic Calculations for Monomers

We saw from our treatment of monomers on a 1-D, homogeneous lattice, that we could expect a quasi-linear relationship between fractional coverage and equilibration time. We saw a linear relationship for non-interacting monomers, although the curve bent upward as the magnitude of the particle-particle interactions increased. For monomers on a 1-D, homogeneous lattice and a 2-D, heterogeneous square lattice, we never succeeded in causing an actual increase in equilibration time with coverage.

When we consider monomers on a 2-D, homogeneous triangular lattice, we see the same bending upward that we observed before, but a relatively small increase in interaction energy results in an increase in waiting time with equilibrium coverage. This reversal in kinetics is the behavior that we are trying to explain. Because this behavior develops with increased particle-particle interaction energy, we can surmise that energy has a strong influence on this behavior. This is in accord with our previous results for monomers. Furthermore, the triangular lattice means more nearest-neighbors for each particle on the lattice, so the total energy of each particle will be much larger than what we had seen for the other lattices. With our triangular lattice, each particle can have six nearest-neighbor particles, whereas the 1-D lattice only allows for two nearest-neighbors and the square lattice, four.

To try to explain this behavior, we returned to the kinetic equation that we had worked with before, shown below (also Equation 3.07).

$$\frac{dn}{dt} = e^{\beta\mu}(1-n) - e^{\beta\varepsilon(n)}n \tag{7.01}$$

The issue here is that the binding energy is no longer a constant, but rather depends on the fractional coverage of the lattice. Hence, the kinetic equation can no longer be solved as a simple differential equation. We tried to assume an alternative total binding energy that incorporated both the adsorption and interaction energies, but this treatment was unsucessful. The issue is with the fact that the total energy changes with coverage; regardless of the particle-particle interaction energy, at low coverages each molecule only sees the surface, while to reach the highest

coverages, an overwhelming chemical potential is required in either case. As the number of particles on the surface increases, so too does the energy per particle, up to the equilibrium value. Further treatment of this system necessitated a better understanding of the energy per particle.

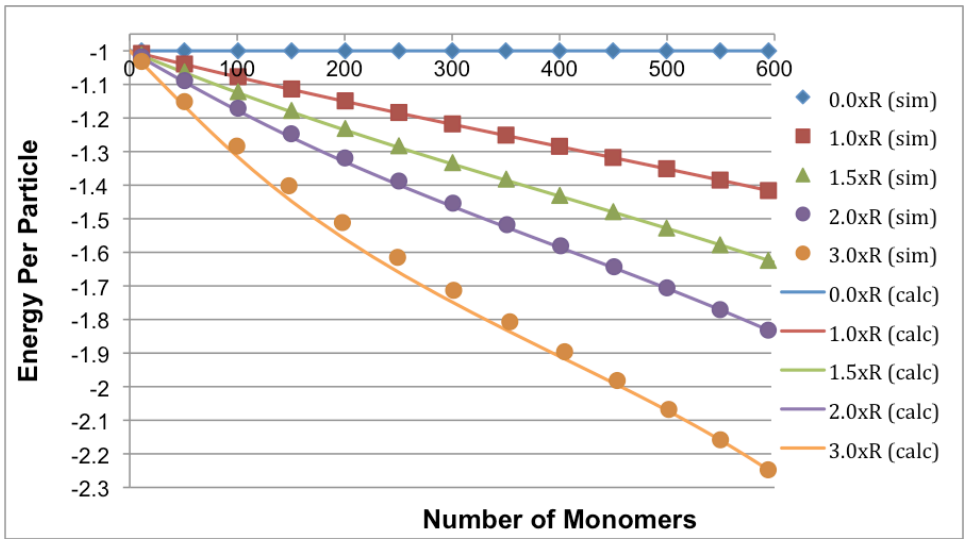

Figure 7.09
Average binding energy per particle as a function of the number of adsorbed particles for systems of monomers with increasing particle-particle interactions adsorbing on a 2-D, homogeneous lattice. Notice the pseudo-linear relationship between the number of particles on the lattice and the average binding energy per particle; this relation only breaks down when the interaction energies reach three or four times the typical values for methane.

We see above in Figure 7.09 the total binding energy as a function of the number of particles on the lattice. In each case (except, of course, of that of neutral monomers), the total energy increases as the number of particles on the lattice increases, due to the fact that a fuller lattice means a greater likelihood that a given particle will have nearest-neighbors with which to bond. The magnitude of this increase in total binding energy depends on the strength of the particle-particle interaction energy. The points (sim) shown in Figure 7.09 are the energies per particle from our simulation results, while the lines (calc) are the predicted values based on our equilibrium calculations. Again we see good agreement across all possible fractional coverages, as well as at different interaction energies. There are only a few small deviations, which we have consistently shown to be artifacts due to the finite nature of our simulation lattices as compared to

the assumed infinite lattices of the calculations. The statistical mechanical calculations used here can be found in their entirety in Appendix D.

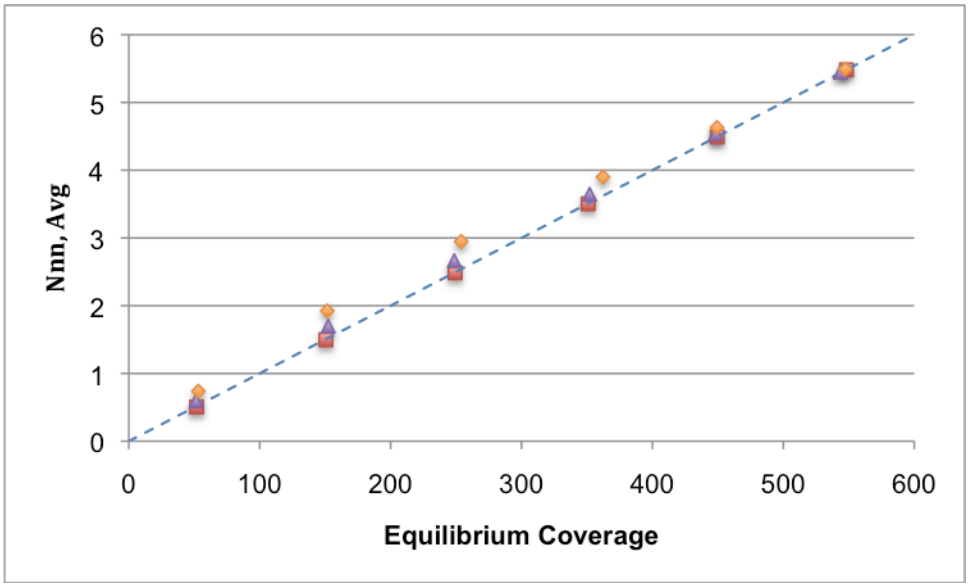

Figure 7.10
Average number of nearest neighbors versus total number of particles at equilibrium. The blue line represents the ideal case; the non-interacting case is in perfect agreement (red), while the 1.5xR (purple) and the 3xR (orange) cases show a slight clumping.

We can see from the curves in Figure 7.09 that the relationship between the total energy per particle and the number of particles is almost linear. It is a very good approximation for low interaction energies, and while the approximation breaks down somewhat for the higher interaction energies, it is still quite close. Still, we need to confirm that the reason the average energy increases linearly is because the adsorbed particles have proportionally more nearest-neighbors with whom to interact. In order to determine this, we tracked the average number of nearest neighbors as a function of final coverage for a system of neutral monomers and two systems of interacting monomers, one with 1.5 times the typical interactions for methane (1.5xR) and another with three times as much (3xR). Our results from this set of simulations can be seen above in Figure 7.10. The dotted blue line shows the ideal case, for which the average number of nearest neighbors at equilibrium increases proportionally to the total number of adsorbed particles at equilibrium. The non-interacting case (red) matches this result, showing an even distribution of particles on the lattice. For the case of the monomers with moderate interactions

(purple), we see a very slight shift upwards from the ideal case, meaning that there is a slightly higher number of nearest neighbors, on average, which implies that there is a small degree of clumping of particles on the surface. The strongly-interacting monomers (orange) show this same clumping effect to a slightly larger degree, although we would still consider it to be negligible. The peak deviation from the ideal value for 3xR monomers is only about 16%. We already know that these strongly-interacting dimers push the limit of our approximation of average energy per particle as a linear function, as we pointed out in our discussion of Figure 7.09. But what we have shown is that there is little clumping going on in the lattice, and that the particles are fairly evenly spaced, and so using the average energy per particle is a reasonable guess for the energy of a typical particle on the lattice.

Having convinced ourselves of the validity of using a linear approximation for the energy per particle, we can now proceed with our analytical treatment. We assume the total binding energy of a particle to be in the form: $\varepsilon(n) = \varepsilon_0 + n*\varepsilon'$. Here, $\varepsilon' = 6*\varepsilon_{int}$ since each particle can have up to six nearest neighbors. Then, Equation 7.01 becomes:

$$\frac{dn}{dt} = e^{\beta\mu}(1-n) - e^{\beta\varepsilon_0}e^{\beta n\varepsilon'}n \tag{7.02}$$

Now, if we assume that $\beta n\varepsilon'$ is quite small, we can expand that term as a Taylor Series so that:

$$\frac{dn}{dt} = e^{\beta\mu}(1-n) - e^{\beta\varepsilon_0}\left(1 + n\beta\varepsilon' + \frac{1}{2}(n\beta\varepsilon')^2 + \ldots\right)n \tag{7.03}$$

We can solve the simplest case (the 2nd order approximation) directly, giving us an expression in the form of:

$$\tau = \left(\sqrt{\left(\exp(\beta\mu) + \exp(\beta\varepsilon)\right)^2 - 4\varepsilon'\exp(\beta\mu)\exp(\beta\varepsilon)}\right)^{-1} \tag{7.04}$$

Using Equation 7.04 above, we plotted the characteristic time τ as a function of equilibrium coverage, comparing the results of these analytical calculations based on the kinetic equation developed in our previous work to the waiting times measured in our simulations. Both sets of results are shown below in Figure 7.11.

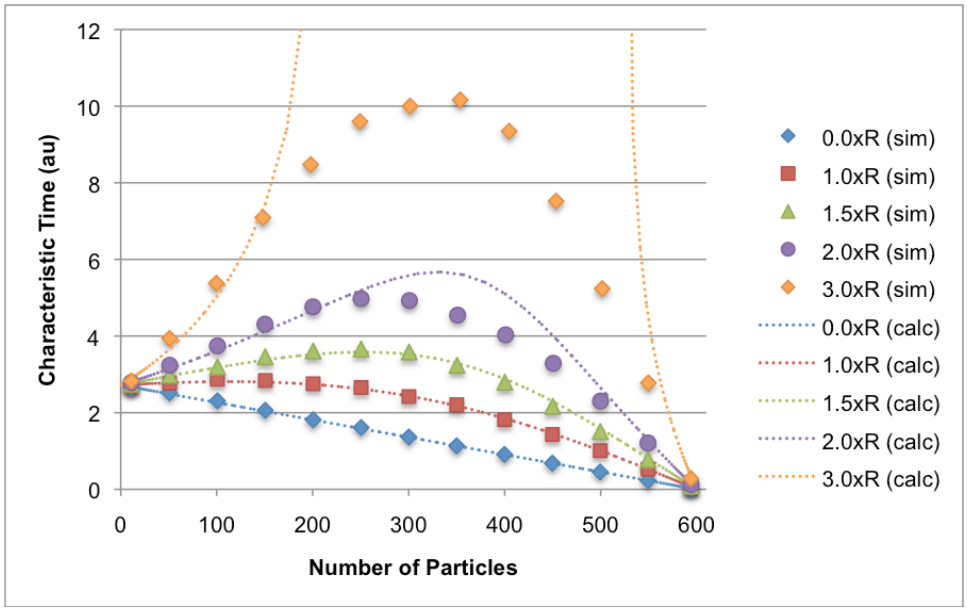

Figure 7.11
Characteristic Time as a function of number of particles at equilibrium for several systems with different particle-particle interaction energies. We see that our calculated characteristic time τ (from Eq. 7.04) shows good agreement with our simulation results for systems with weak and moderate interaction energies, although our model breaks down for systems with strong interaction energies.

We see very good agreement between our simulated waiting times and the values produced by our treatment of the kinetic equation. We see almost perfect agreement up to 1.5xR, which is around 20% of the adsorption energy. Even up to 2xR, where the interaction energy is almost 30% of the binding energy, there is fairly good agreement between theoretical and simulated values. By 3xR, or an interaction energy of almost 40% of the adsorption energy, the model has broken down. This is in spite of the fact that we used rather liberal approximations when performing the calculations.

Section 7.1.3: Conclusions for Monomers

Thus we have shown that the increase in equilibration time with coverage comes directly from the same kinetic equation that we used for the simplest models. We had to treat the equation in a more complicated way and include the detail of the expanded system. We were

able to derive a closed-form solution that predicted the characteristic time of the evolution of a system of interacting monomers based on temperature, adsorption and interaction energies, and chemical potential. We showed how our kinetic equation explained the behavior of the system in all situations.

Our understanding is the increase in equilibration time with coverage occurs when the increase in total energy increases faster than the requisite increase in chemical potential. At very low coverages, there is little interaction between particles on the lattice and so the interaction energy plays a negligible role; therefore the characteristic times are all about the same. Similarly, near monolayer, a very strong chemical potential is needed to force the particles onto the crowded lattice, and so the energy, binding and interaction, are less important. However, in the middle coverages, particularly around 50-75%, a smaller incremental change in chemical potential is needed to add the "next" particle, since the particle will gain energy from interactions with its neighbors. Because approximately the same chemical potential is needed for more particles, it will take around the same amount of time *per particle* to fill the lattice, but since there are more particles, the evolution will take more time. Thus, we can see *why* the equilibration time increases with interaction energy. Another factor is the increased diffusion on the surface as particles try to settle into the most energetically favorable configurations, while in the non-interacting case, all configurations are interchangeable, so there is no preference.

Section 7.2: Adsorption of Dimers on Graphene

The next part of our study was to consider the adsorption of dimers on a homogeneous, 2-D lattice. Our motivation here was to understand the adsorption of ethane on graphene, with the ability to extend this model to other dimers.

The main difference in this model is the ability of the admolecules to reorient themselves with respect to the surface. This reorientation introduces an inherent heterogeneity to the system, as the binding energy of a dimer changes depending on whether it lays flat along the surface or stands perpendicularly to it. This further complicates the inclusion of particle-particle interactions, as the interaction between two particles depends on the orientation of each particle relative to the other.

Section 7.2.1: Non-Interacting Dimers on Graphene

We begin by examining our main simulation results for dimers on graphene. We see that the number of particles increases monotonically as time elapses, in a pseudo-exponential decay, as shown below in Figure 7.12. Like before, we have plotted the characteristic times of each curve (the black dotted line serves only to guide the eye). We see that the characteristic time also decreases as the number of adsorbed particles at equilibrium increases, although there seems to be two different regions of this behavior, a low-coverage tendency and a high-coverage tendency. We also notice that while the curves in general seem to be exponential decays, in fact there are noticeable bends in the upper coverages, meaning there seems to be two separate processes taking place for each of these systems.

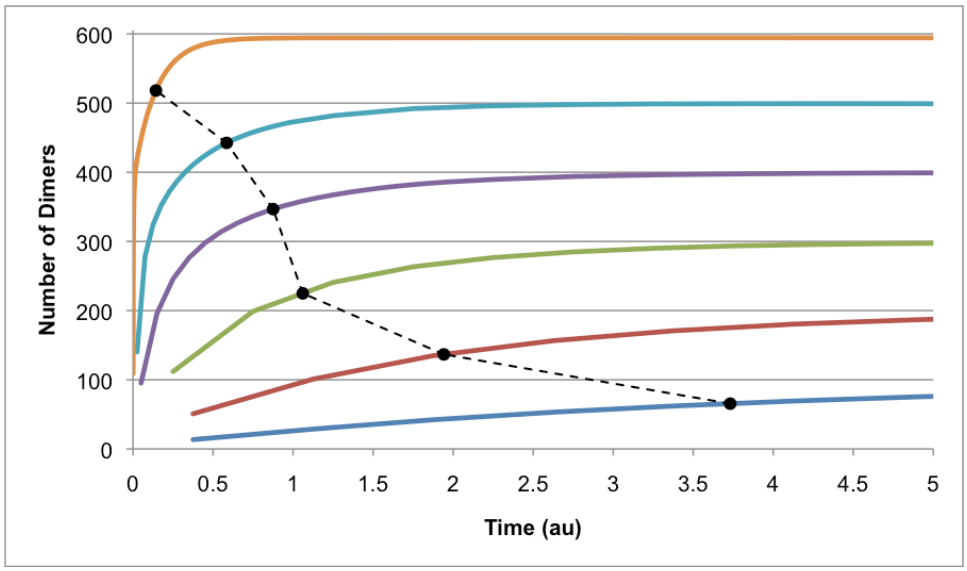

Figure 7.12
Number of adsorbed dimers as a function of time for a system of neutral dimers adsorbing on a 2-D, homogeneous lattice. We see that the characteristic time decreases as the equilibrium coverage goes up, with two regions with distinct kinetic behaviors, one for equilibrium coverages of less than 300 adsorbed dimers, and another for systems with more dimers than that at equilibrium.

Section 7.2.1.1: Kinetic Behavior of Adsorbing Dimers (Low Coverage)

We have begun by looking at the total number of particles as a function of time, because that is what is seen in isotherm experiments. We have the added advantage, however, of seeing the details in our models and simulations that cannot be seen in experiments. In fact, while we

count the total number of particles on the lattice, some of those particles are laying flat on the surface and others are standing upright on it. We now look at the number of flat dimers and the number of upright dimers as a function of time to see how the orientation changes through the equilibration process. Figure 7.13 below shows the number of particles in each orientation as a function of time.

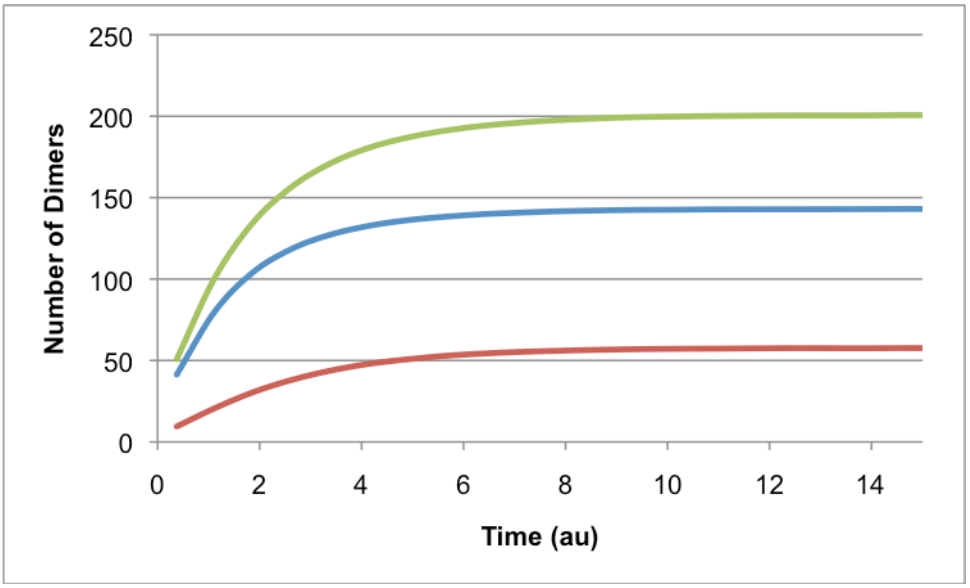

Figure 7.13
Number of dimers as a function of time for a system of neutral dimers adsorbing on a 2-D, homogeneous lattice. Flat dimers (blue) make the greatest contribution to the total coverage (green), while upright dimers play a much smaller role (red).

When we plot the number of dimers as function of time, as we have in Figure 7.13 (above), we see that all the curves increase monotonically. We also notice that the number of flat dimers (blue) increases much more quickly than the number of upright dimers (red). From our previous work with a 1-D, homogeneous lattice, we know that the increased flux of flat dimers is due to a net transition of upright dimers to flat dimers, which is to say, the filling effect. With about 200 dimers adsorbed, the lattice is still only about 58% filled, so space is not an issue, and flat dimers are energetically preferred.

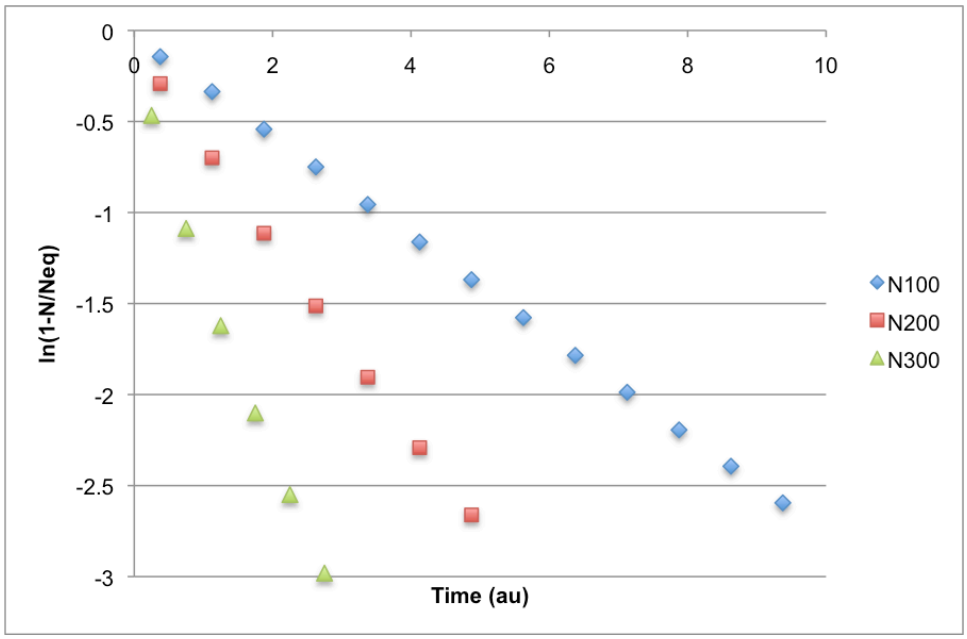

Figure 7.14
The rate curves for systems of neutral dimers adsorbing on a 2-D, homogeneous lattice. For these systems, which have low coverages at equilibrium, we see that the rate curves are pseudo-linear, meaning the evolution of the system is driven by a single process with a single rate associated with it.

Figure 7.14 (above) shows the rates for some of the lowest lattice coverages. We see in each case that there is a linear relationship between time and the logarithm of the coverage, meaning there is a single rate to the process. With 300 particles on the lattice, the lattice is about 78% covered, but only has half of the possible number of particles adsorbed, due to the possibility of reorientation. Even with most of the lattice covered, we see that equilibration is governed by a single rate. As we discussed in Chapter 6, this single process is in fact adsorption of flat and upright dimers, with the latter having a net transition to the flat orientation.

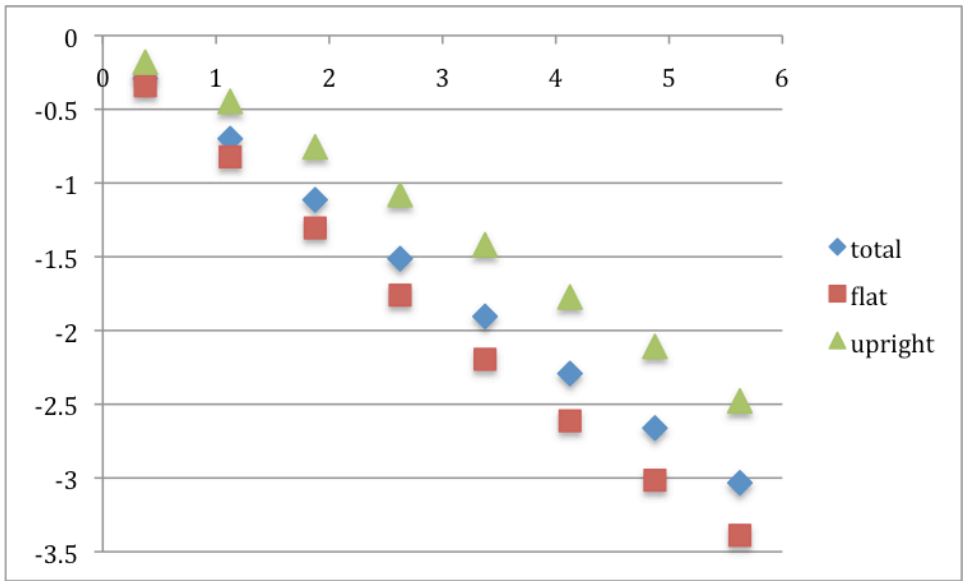

Figure 7.15
The rate curves for a low-coverage system of dimers adsorbing on a 2-D, homogeneous lattice, broken out to show the contribution of dimers in each orientation. The flat dimers progress slightly faster and the upright dimers are slightly slower, but all the rate-curves are linear, and the total rate curve is a combination of the component parts.

Above, in Figure 7.15, we have broken out one of the rate curves we considered in Figure 7.14 (for the system equilibrating to 200 dimers). This system has no overshoot, as was shown in Figure 7.13. We see that the rates are linear, and that the total rate lies between the rate for flat dimers and for upright dimers. Furthermore, we notice that the uptake of flat dimers (red) is greater than that of upright dimers (green), which means that the number of flat dimers is going up slightly faster than average (the overall curve, blue) and the number of upright dimers is going up slightly slower than average. This is further evidence of the filling effect, that the flat dimers are proceeding faster because of help from the reorientation of upright dimers.

Section 7.2.1.2: Kinetic Behavior of Adsorbing Dimers (High Coverage)

We look now at the kinetics of adsorption for systems reaching high coverages. While we are looking at systems with between 300 and 600 particles (half of the possible number of particles up to a true monolayer), we are seeing only about a 20% change in the coverage of the lattice. That means that reorientation of particles to make space available on the lattice is a key part of this evolution.

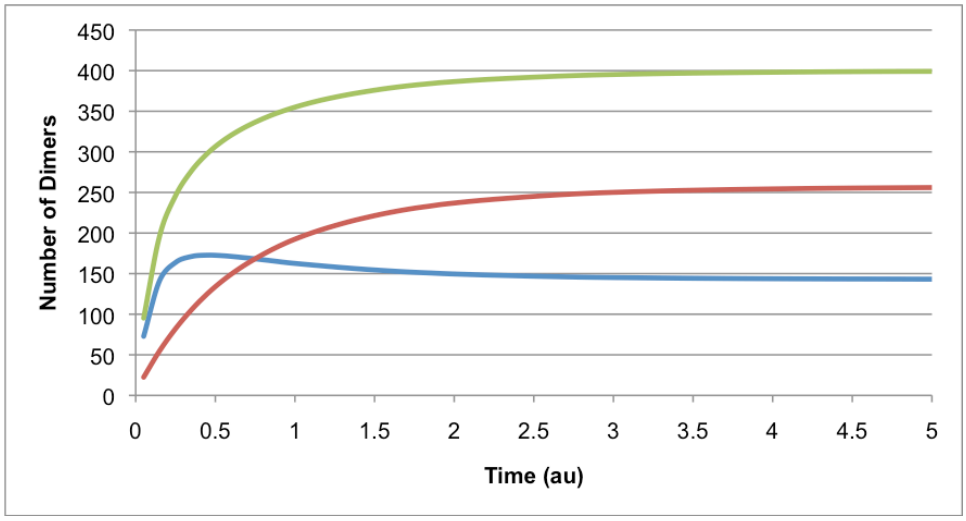

Figure 7.16
Number of particles as a function of time for a high-coverage system of dimers adsorbing on a 2-D, homogeneous lattice. We see a small overshoot in the number of flat dimers (blue), and near equilibrium the total number of particles (green) goes as the number of upright dimers (red).

Above, in Figure 7.16, we see the the number of particles as a function of time for an equilibrium of 400 particles. Here, we see that, for time less than 0.5, the system behaves similarly to what we have seen for lower coverages, where the number of flat dimers increases more quickly due to a net transition from upright to flat orientations. However, at about 0.5, we see a peak in the number of flat dimers, after which time the number of dimers begins to fall. This is because, very early in the evolution, the lattice is mostly empty and so the flat orientation is energetically preferred, like in the cases of the low coverages. The difference here is in the strength of the chemical potential, which drives a large flux of particles onto the surface. That is why, firstly, the coverage here reaches some 300 admolecules so quickly. However, the chemical potential is so strong that more particles will adsorb on the lattice. Since the lattice is mostly covered, flat dimers must soon begin giving up their space, whether by desorbing or reorienting themselves, to allow more particles to join the lattice. When looking at the overshoot, we see that about 83% of the lattice is covered, mostly by flat dimers. At equilibrium, almost 92% of the lattice is covered. Thus, the remainder of the equilibration time is spent reshuffling the particles so that another 100 particles (17% of the total number at monolayer) can be fit onto the lattice and covering only another 9% of it.

Looking now at the number of particles versus time for a system that reaches monolayer, shown below in Figure 7.17, we see a very pronounced bend in the curve. We see that the number of particles reaches 400 almost immediately, and most of the rest of the equilibration time is spent going from 400 to 600 particles. Furthermore, the distribution of the particles is such that the 400 particles fully cover the lattice. Thus, the occupation of the lattice is approximately 100% for almost the entire equilibration, despite the fact that there is a constant flux of particles onto the surface. Thus, reorientation is the driving force during the equilibration of this system as it reaches monolayer at equilibrium.

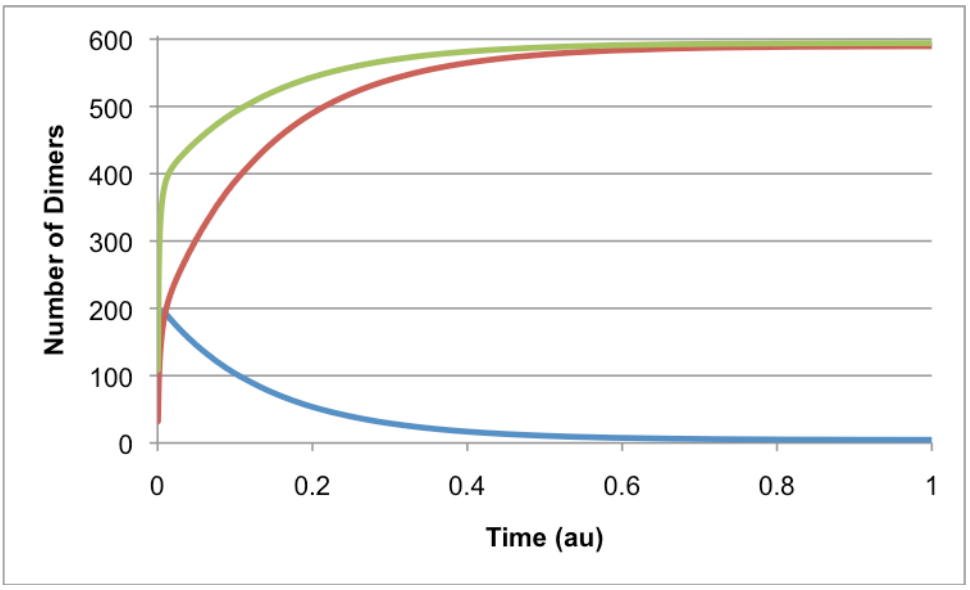

Figure 7.17
Number of particles as a function of time for a monolayer system of dimers adsorbing on a 2-D, homogeneous lattice. We see the number of flat dimers (blue) rise very quickly and the fall away, while at equilibrium the total number of particles (green) is comprised almost entirely of upright dimers (red).

When we zoom in on Figure 7.17, as we have below in Figure 7.18, we see that the the overshoot occurs around 0.005. We have noted the times at which the overshoot occurs for comparison to the rates, seen below in Figure 7.19.

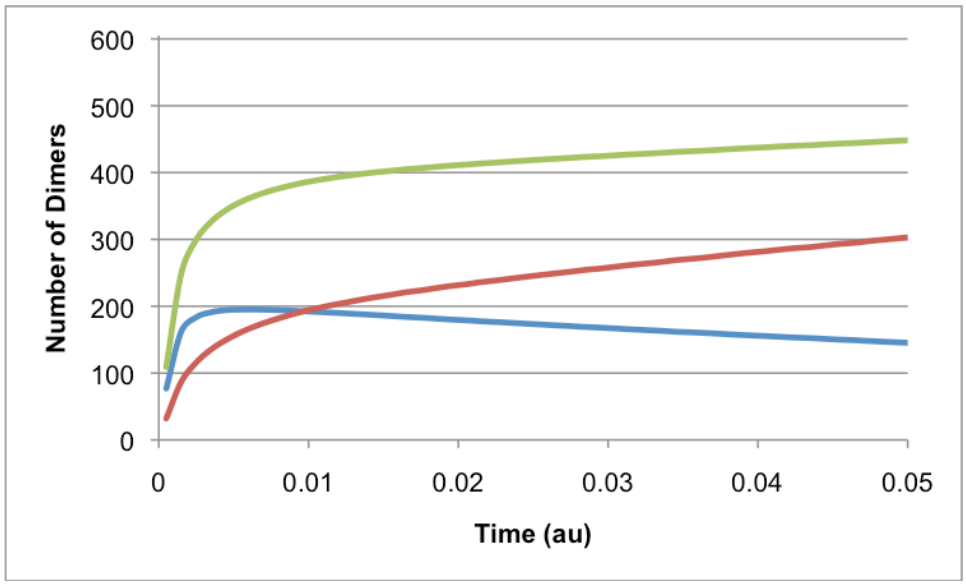

Figure 7.18
Number of particles as a function of time for a monolayer system of dimers adsorbing on a 2-D, homogeneous lattice (zoomed in). We can now see that the overshoot (of almost 200 dimers, which is not an insignificant amount) occurs after very little time has passed, around 0.007 time units.

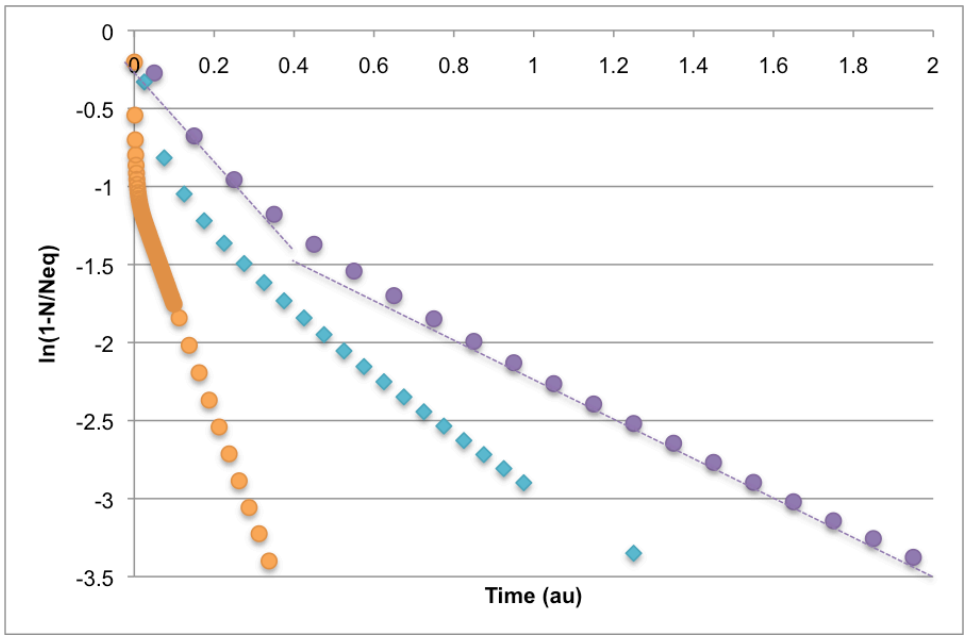

Figure 7.19
Rate curves for high-coverage systems of dimers adsorbing on a 2-D, homogeneous lattice. The dotted lines (purple) guide the eye to show the two regions of kinetic behavior: the initial filling and the reorientation, as described for the system in Fig. 7.16. For the monolayer system (orange), the two distinct kinetic regions are easy to see.

We see in these curves for the higher coverages that there are two distinct rates corresponding to the two distinct equilibration processes, first the initial filling of the lattice and then the reorientation of particles to make space for increased uptake. Dotted lines have been added for the case of 400 particles (purple) to guide the eye and show that the change in rate occurs around 0.45, which is to say, when the overshoot of the flat dimers occurs. Similar changes in rate can be seen for 500 dimers (light blue), and 600 dimers (orange). As we saw in Figure 7.18, the change in rate for monolayer occurs almost instantaneously (~0.007 time units), which is supported above in Figure 7.19.

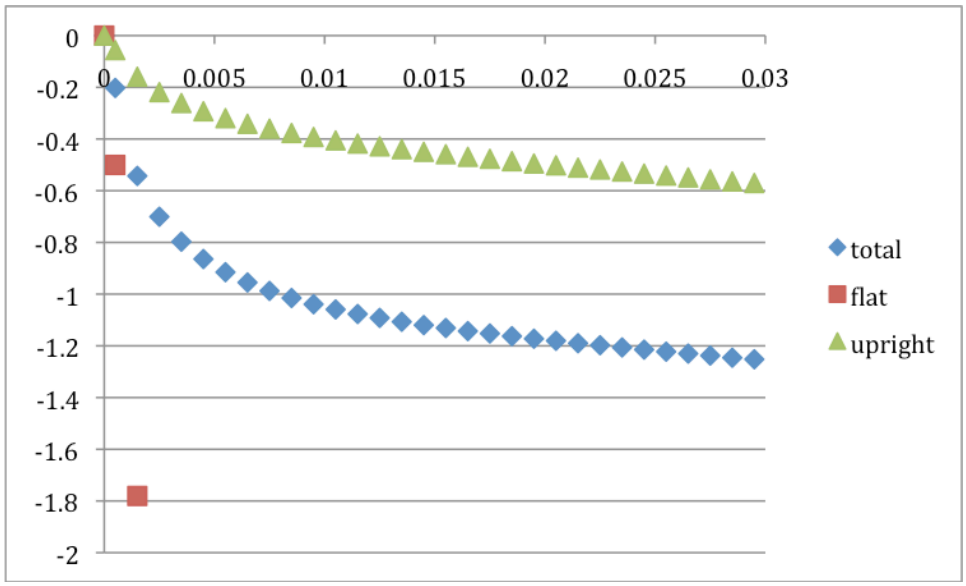

Figure 7.20
Rate curves for the monolayer system of dimers adsorbing on a 2-D, homogeneous lattice. The total rate curve (blue) follow the curve for flat dimers (red) at first, and then begins to follow the upright dimers at equilibrium.

We then broke out the rate curve for the monolayer system (orange curve, Fig. 7.19) in order to better understand how the rates of the component parts of the system contribute to the overall kinetics of adsorption. The total rate curve (blue) follows the curve for flat dimers (red) for the first few time steps, until the overshoot is reached (at about 0.007 time units). Then the total rate curve bends to follow the rate curve for the upright dimers (green), which drives the evolution of the system after the overshoot has been reached. This shows that the total rate of the system

is the equilibration first of one part of the system (the flat dimers plus the filling effect) and then the equilibration of the other part of the system (the upright dimers plus the reorientation).

Section 7.2.1.3: The Overshoot for Dimers on a 2-D, Homogeneous Lattice

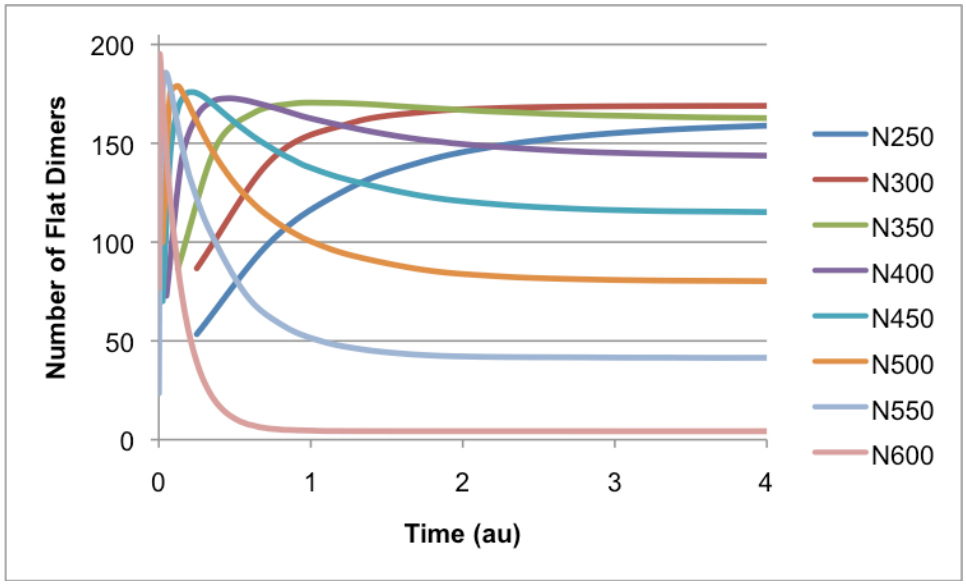

Figure 7.21
The overshoots for dimers adsorbing on a 2-D, homogeneous lattice. As the equilibrium coverage rises, the overshoot occurs sooner and falls away faster, but the peak is always very close to the peak number of dimers predicted in the isotherm: 168.

We will briefly comment on the overshoots that develop in systems that equilibrate with more that 300 adsorbed dimers (out of 600 possible). The behavior we observe is very similar to what we saw for dimers adsorbing in on a one-dimensional, homogeneous lattice. As the equilibrium coverage increases, the overshoot occurs at an earlier point in the evolution of the system, with a more rapid descent afterward. However, the peak heights of the overshoots change very little. In Figure 7.21 (above), we see the overshoots go from a peak value of 170.4 for the shortest one to 195 for the system that reaches monolayer. In comparison, the peak number of flat dimers at equilibrium, as predicted by our isotherm, is 168. This means that the overshoots here follow the isotherm for this system in much the same way as they did for the 1-D case. It seems that here the overshoots peak at slightly more than the indicated value, which may be related to the increased size of the lattice allowing for greater coverage before falling away.

Section 7.2.1.3: Calculations for Non-Interacting Dimers on Graphene

In addition to the work discussed above focused on simulations of dimers adsorbing a graphene, we also continued to use analytical calculations in an attempt to better understand this behavior.

It unfortunately proved impossible to develop kinetic equations to fully explain the adsorption behavior of dimers in the same way that we could for monomers. The increased complexity of the system proved to be too much. However, we were still able to implement a statistical mechanical treatment of the system in order to confirm that our simulations were in fact giving us good data. The statistical mechanical calculations used here can be found in their entirety in Appendix E.

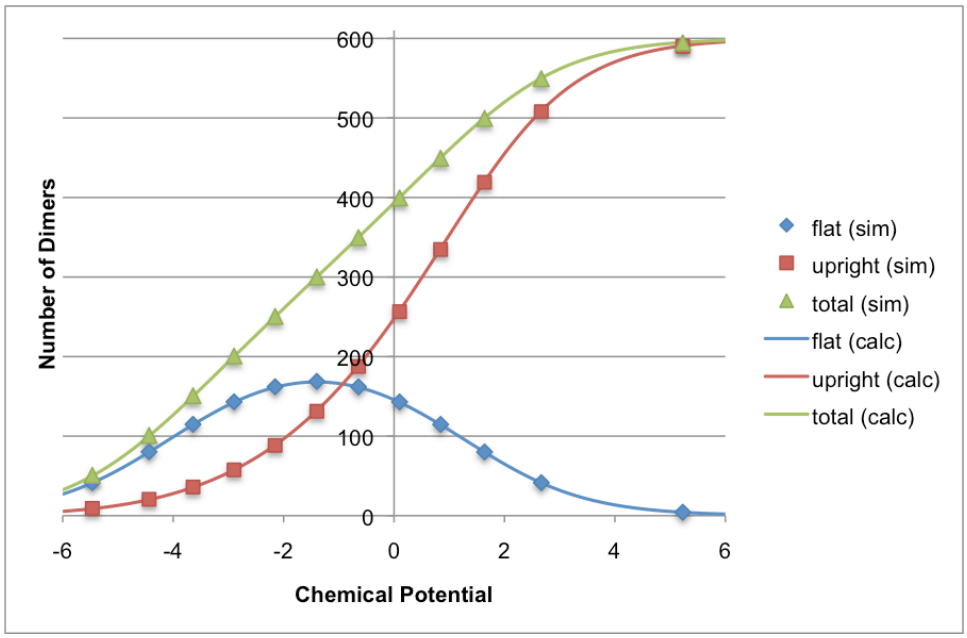

Figure 7.22
Number of particles as a function of chemical potential for a system of dimers adsorbing on a 2-D, homogeneous lattice. Flat dimers (blue) dominate the lattice as low coverages, while upright dimers (red) make the greater contribution to the total coverage (green) as the system approaches monolayer.

In Figure 7.22 (above), we see that the number of particles increases monotonically with chemical potential. For low chemical potentials (and correspondingly, low coverages) the

coverage is dominated by flat dimers. At high coverages, the number of flat dimers falls as upright dimers fill the lattice.

We can also gain further insight about the kinetic behavior based on these graphs. It can be seen that the number of flat dimers peaks when the total number of particles is at 300. For coverages lower than this, flat dimers dominate, while at coverages above this, upright dimers take over. This supports our observations of the kinetic behavior of the system, that we see a certain behavior up to about 300 particles, and a different kind of rate from this midway point up until monolayer is achieved.

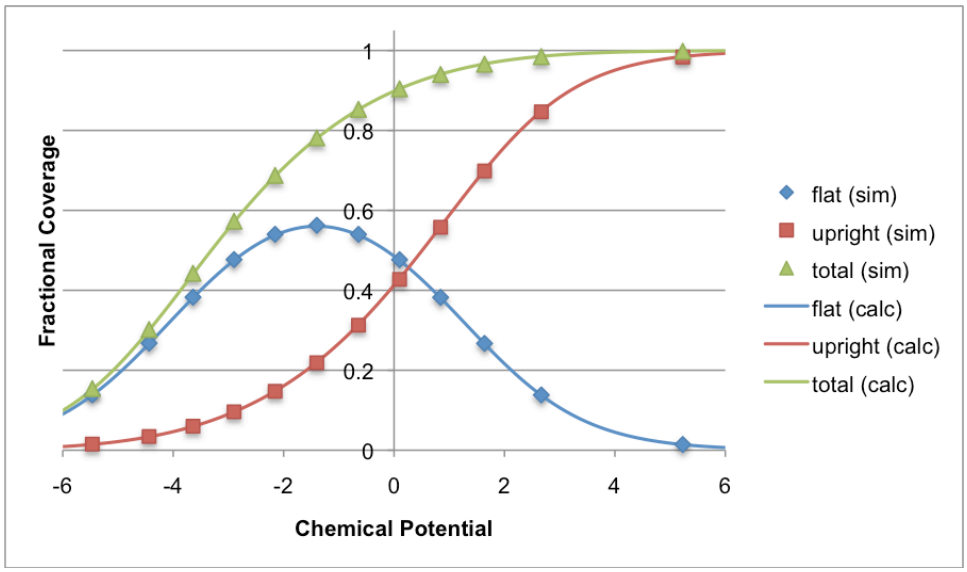

Figure 7.23
Fractional coverage versus chemical potential for a system on neutral dimers adsorbing on a 2-D, homogeneous lattice. This graph demonstrates the fact that, while there are fewer flat dimers, they play an important role in filling the lattice.

We see similar behavior when we plot the fractional coverage versus chemical potential, as we have above in Figure 7.23. We prefer to consider number of particles instead of fractional coverage because that is what is observed in isotherm experiments, they see the molecules leave the gas, so it makes more sense for us to consider particles entering the lattice rather than the coverage of the lattice.

In both cases, we have good agreement between the simulation data (shown as data points) and the calculated values (shown in the lines). Notice again that the peak in the fractional

coverage of flat dimers occurs when there are 300 particles on the lattice at equilibrium. Though there are only half as many particles as there will be at monolayer, we see that about 80% of the lattice is covered. That is to say, that half of the particles are needed to reach 80% coverage, and the other half are needed to go from 80% to 100% coverage, hence the change in kinetic behavior at this end of the spectrum.

Section 7.2.2: Adsorption of Interacting Dimers on Graphene

We have seen that dimers exhibit fundamentally different kinetic behavior compared to monomers because of the inherent heterogeneity of the available binding energies. In the section above we considered only non-interacting dimers, so the kinetic behavior was driven by the orientation of the particle (flat or upright) and the resulting binding energies. However, we want to know how the inclusion of particle-particle interactions will change the kinetic behavior that we observe in the system.

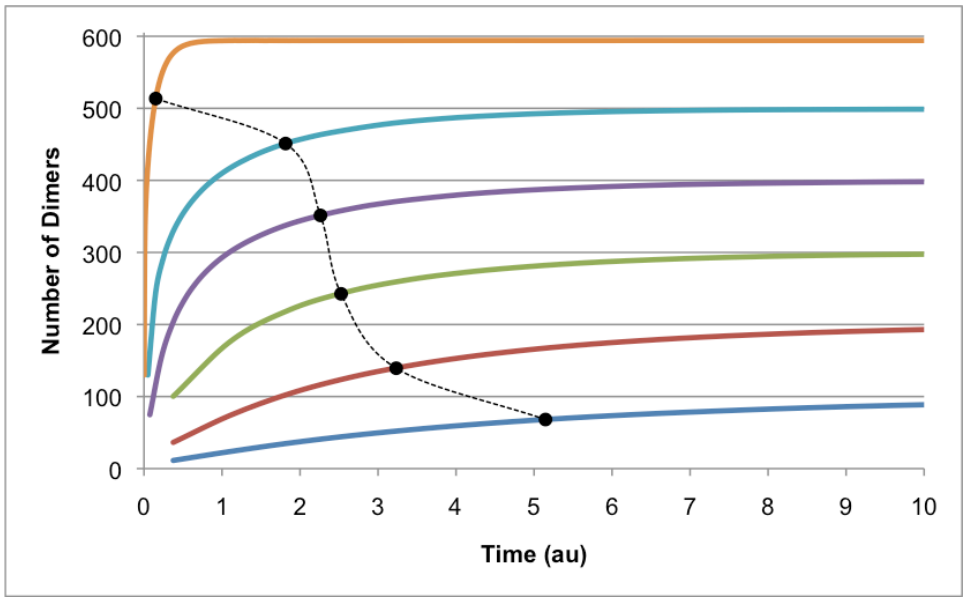

Figure 7.24
Number of particles as a function of time for interacting dimers adsorbing on a 2-D, homogeneous lattice (0.5xR). Although the characteristic time (black) decreases as the fractional coverage goes up, we see the waiting time already beginning to rise for systems with moderate and high coverages at equilibrium.

We see above in Figure 7.24 the number of particles as a function of time for a range of equilibrium coverages when we include half of the typical interaction energy for ethane (0.5xR).

We see similar behavior to what we have seen for the non-interacting case, which is not altogether unexpected as the interaction energy is only 7% of the binding energy of the admolecules. Notice in particular that the characteristic times for the lowest coverages (up to 300 particles) are very close to what we say for the non-interacting case, which again is not surprising as the low coverage means that the particle-particle interactions play less of a role. Looking at the higher coverages (400 and 500 particles, in particular), we see the characteristic times are slightly longer than we saw for the non-interacting case. We believe that this results from the fact that interactions play a much greater role in this region of coverage, when the particles are beginning to rearrange and reorient themselves to make the best use of binding energies (adsorption and interaction energies) and chemical potential.

We will not include the number of particles as a function of time graphs here because of their great similarity to what was shown for non-interacting dimers (see Figures 7.13, 7.16, and 7.17). We see the same preference for flat dimers at lower coverages with a transition to upright dimers at higher coverages, with the development of an overshoot in the number of flat dimers when the number of admolecules reaches about 300.

In Figure 7.25, shown below, we see that simulations continue to agree with our statistical mechanical treatment of the equilibrium state of the system. As before, we see very good agreement between the equilibrium values provided by our simulations and those predicted by our calculations. We also notice that the main curve (green) shifts to the left, as does the peak in the number of flat dimers, since the increased total energy due to the inclusion of particle-particle interactions means that a lower chemical potential can result in the same coverage. Otherwise these curves are very similar to what we saw for the non-interacting case.

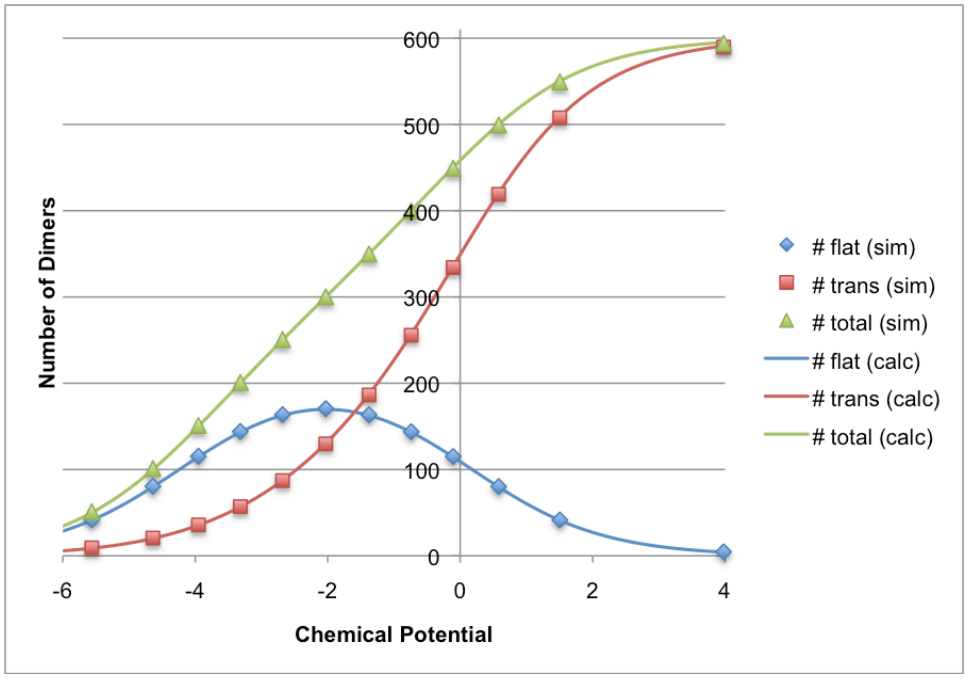

Figure 7.25
The number of particles versus chemical potential (isotherm) for a system of weakly-interacting dimers adsorbing of a 2-D, homogeneous lattice. There is good agreement between our calculations and our simulation results for all values of the chemical potential.

Next we increased the interaction energies up to the full value for ethane (1.0xR) in order to see what effect even higher particle-particle interactions would have on the kinetics of the system. We show the total number of particles as a function of time for a range of equilibrium values in Figure 7.26 below.

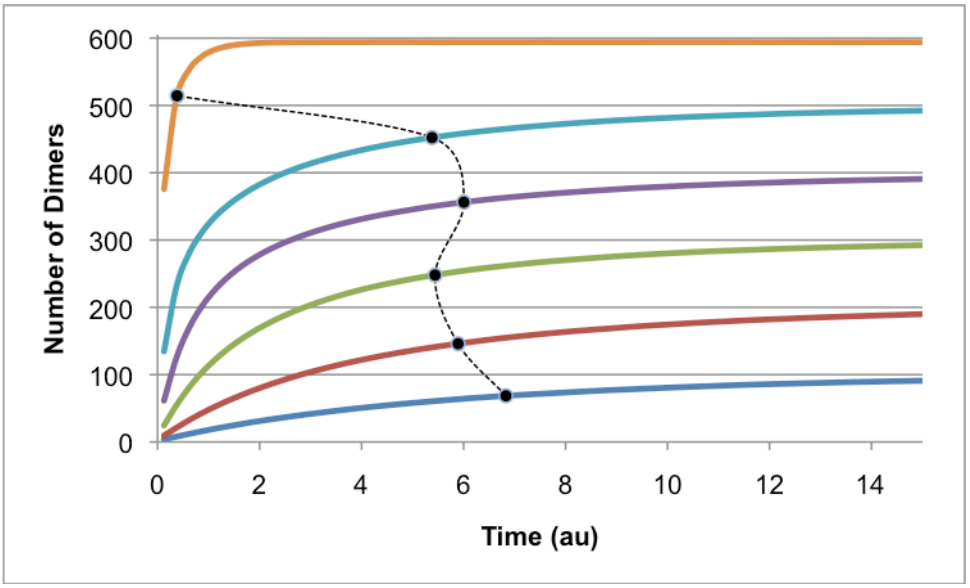

Figure 7.26
Number of particles as a function of time for a system of interacting dimers on a 2-D, homogeneous lattice (1.0xR). Even for this small value of the interaction energy, we are already predicting a small increase in the characteristic time (black) with coverage.

We see again, for the lower numbers of particles (100 to 300), a general increase in the characteristic time as the equilibrium coverage goes down. For the intermediate values (300 to 500), we see the characteristic time actually increase by a small amount. Again, this intermediate phase is where we see the biggest change in kinetic behavior, as we have an overshoot for the flat dimers and a general transition from flat to upright dimers. This dynamic is exaggerated in the presence of particle-particle interactions because the increased energy means that a smaller increase in chemical potential is required to adsorb another particle, and thus the flux per particle is approximately the same and thus it takes longer to reach a higher coverage.

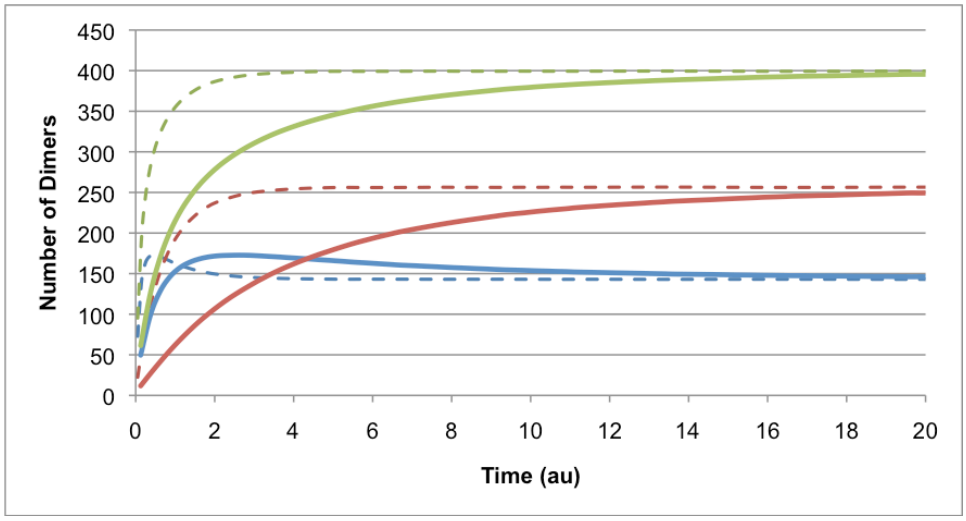

Figure 7.27
Number of particles for a system of of neutral dimers (dotted lines) and a system of interacting dimers (1xR) (solid lines). Notice that both systems equilibrate to the same coverage and the have the same contributions of each state. The increased energy of the interacting dimers means that a lower chemical potential is required, and so its kinetics are slower.

This is looking at the number of particles (flat – blue, upright – red, total – green) for a system equilibrating to 400 particles with no interactions (dotted lines) and 2xR interactions (solid line). The inclusion of interactions slows down equilibration because a lower chemical potential is required to reach the same coverage.

The rate curves for non-interacting dimers (dotted lines) and for dimers with 1.0xR interactions (points) are shown below in Figure 7.28. The curves are roughly the same shape and are in the same alignments with respect to each another; the main difference is that the curves for the interacting system are rotated about 30° counterclockwise. This counterclockwise shift corresponds to the decrease in the kinetic of adsorption we observed in Figure 7.27.

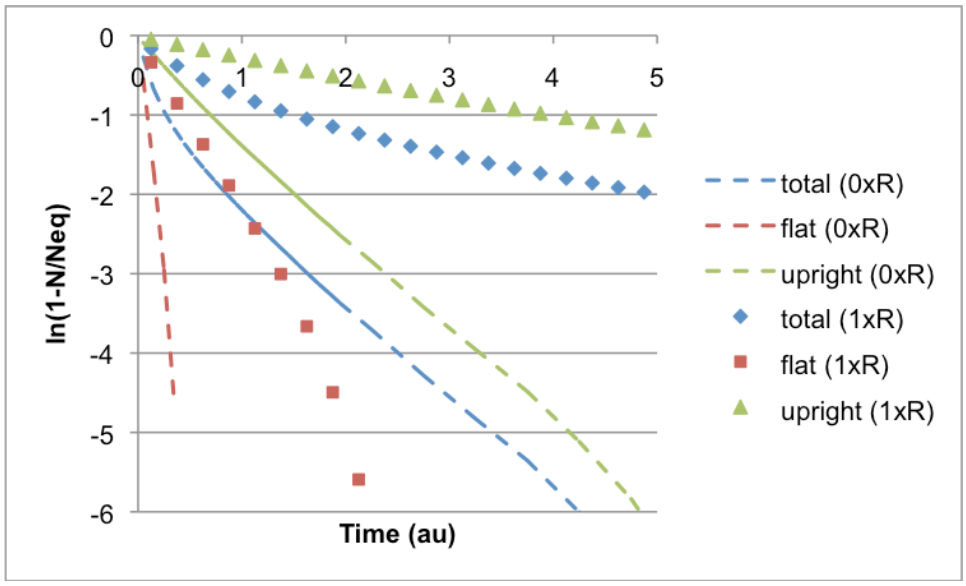

Figure 7.28
Rate curves broken out into component contributions for a system of neutral dimers (dotted lines) and a system of interacting dimers (1xR) (points). The curves are approximately the same shape and in the same positions relative to one another; the difference is that the curves for the interacting system are rotated about 30° counterclockwise.

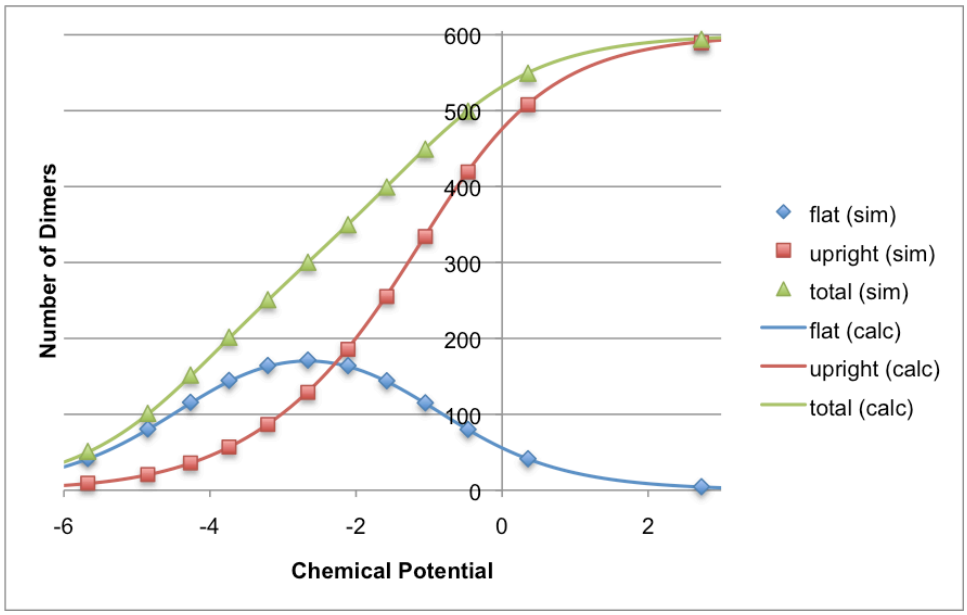

Figure 7.29
Number of particles as a function of chemical potential (isotherm) for a system of interacting dimers on a 2-D, homogeneous lattice (1xR). Despite the inclusion of particle-particle interactions, we continue to see good agreements between our calculations and our simulations results.

We see above in Figure 7.29 that even as we continue to increase the particle-particle interaction energies, our simulations continue to provide us with equilibrium data (points) that agree well with the expected values from our calculations (lines). Since we are unable to develop kinetic equations to model the system directly, it is an important validation to know that our simulations are correctly representing the behavior of the system.

Section 7.2.3: Overall Kinetic Behavior of Dimers Adsorbing on Graphene

We see the characteristic time as a function of number of particles for all three interaction energies below in Figure 7.30. In each case, we see a linear decrease in characteristic time as the number of particles increases up to about 300. We see the greatest change in kinetics when the equilibrium number of particles is between 300 and 500. For the non-interacting and weakly-interacting cases, the characteristic time flattens out in this region, meaning it takes approximately the same amount of time to equilibrate despite the large increase in number of particles. It should be kept in mind, at the same time, that the actual fractional coverage is also almost constant across this range of number of particles, due to reorientation.

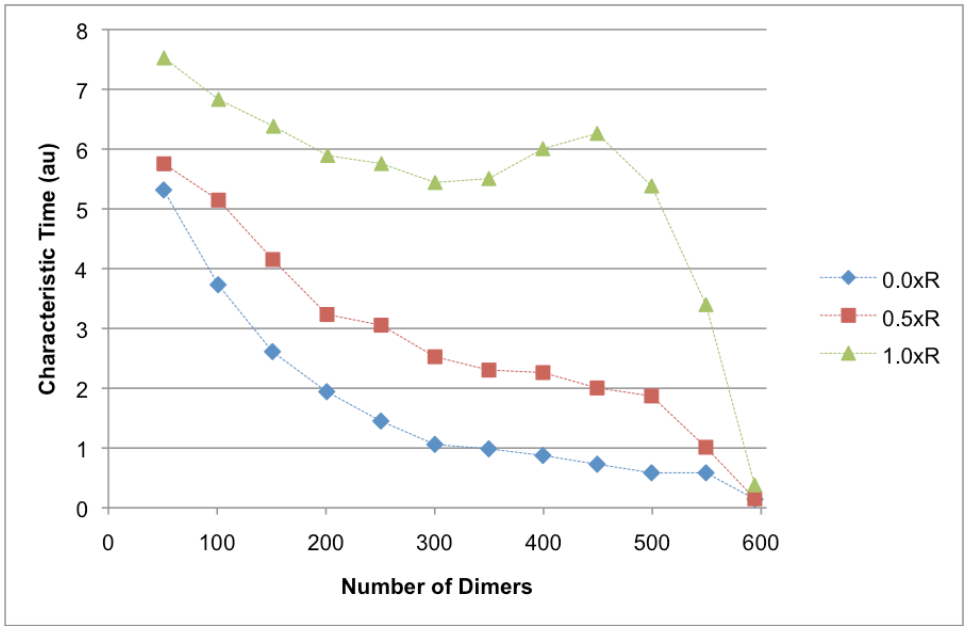

Figure 7.30
Characteristic time versus number of adsorbed particles at equilibrium. The waiting time decreases with coverage except for high values of the interaction energy. The increase in characteristic time with coverage occurs in the region of 400 to 500 particles, where the system is reorienting itself from being mostly-flat to mostly-transverse.

Section 7.3: Adsorption of Trimers on Graphene

The final phase of this study was to consider the adsorption kinetics of trimers on graphite. These are the longest molecular chains that can reasonably be modeled with our simulation scheme. Furthermore, it is the trimer hydrocarbon, propane, that begins to exhibit the change in kinetic behavior that we wish to observe and explain.

Section 7.3.1: Non-Interacting Trimers on Graphene

We consider first the case on non-interacting trimers as a baseline for comparison. This will allow us to determine what effect the inclusion of particle-particle interactions will have. As before, we perform simulations that provide us with the number of particles as a function of time, from which we can extract the quantities of interest.

In this system of trimers, we allow them to lay completely flat on the surface, stand perfectly perpendicular to the surface, or be in an intermediate state between these two, where two of the “links” can bond to the surface and the third unit stands upward, forming a sort of “L” shape. The flat trimers have the strongest adsorption energy, but require the most lattice space. Conversely, the upright trimers had the least binding energy *per particle*, but have the greatest binding per site. The “ells” fall in the middle with regard to both lattice space required and binding energy.

The number of particles as a function of time for neutral trimers can be seen below in Figure 7.31. We observe behavior similar to what we observed for dimers, where there were two regions of kinetic behavior, one for low coverages and another for moderate to high coverages. This is the behavior we see for trimers as well. Despite the change in kinetic behavior, the waiting time decreases monotonically as the equilibrium coverage goes up.

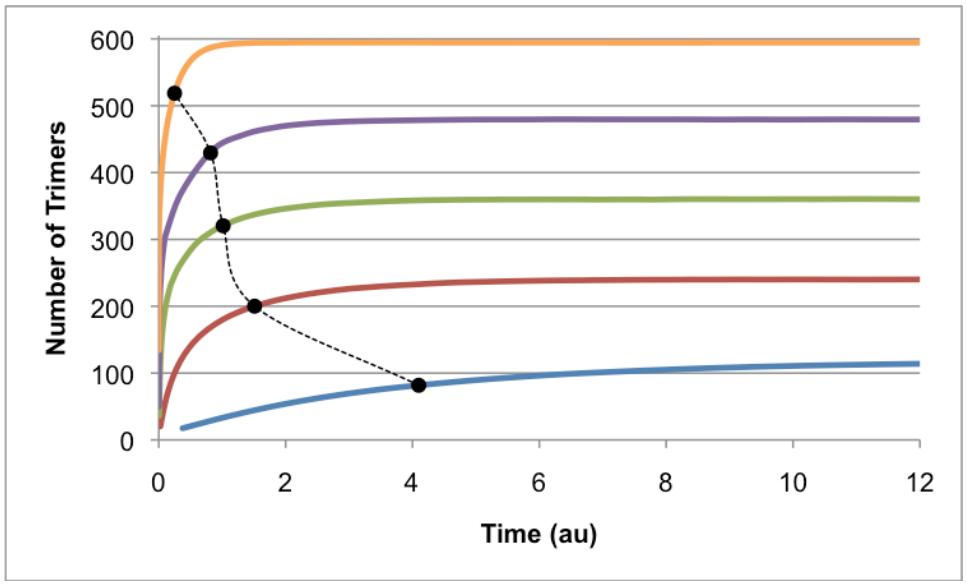

Figure 7.31
Number of particles versus time for a system of non-interacting trimers adsorbing on a 2-D, homogeneous lattice. The characteristic time (black points) decreases as the equilibrium coverage goes up.

Section 7.3.1.1: Kinetic Behavior of Adsorbing Trimers (Low Coverage)

We consider first systems with relatively low coverages. A typical example of one of these simulation results is seen below in Figure 7.32. In this simulation, the system adsorbs about 120 particles (out of 600 possible). Despite the relatively small number of adsorbed particles, at equilibrium about 50% of the lattice is covered. We see that most of the particles are in the flat or ell orientation (blue and red). In fact, there is very little representation of upright trimers (green). It should also be noted that all of the curves are increasing monotonically, meaning that the particles can adsorb and find their preferred orientation without having a system-wide reorientation mid-evolution.

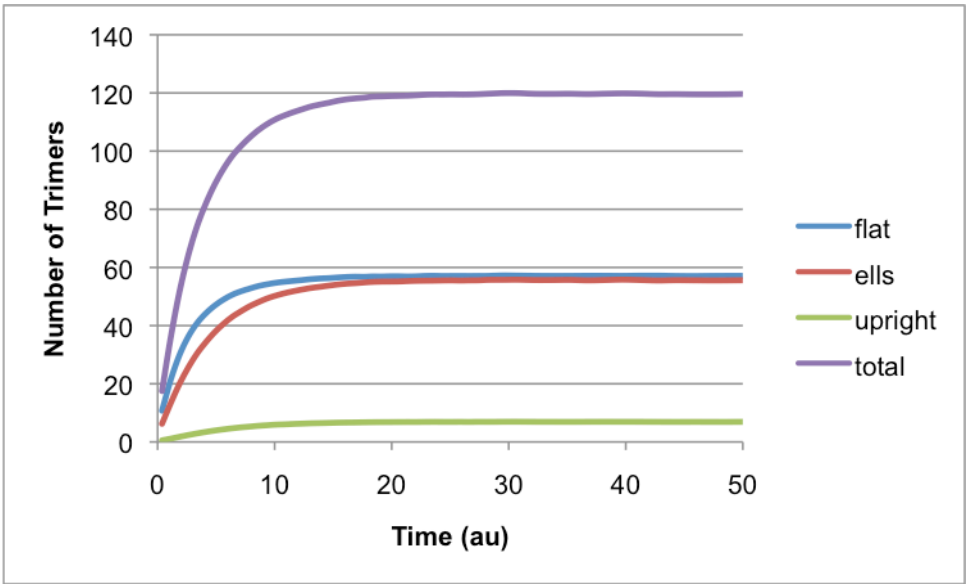

Figure 7.32
Number of particles as a function of time for a low-coverage system of trimers adsorbing on a 2-D, homogeneous lattice. The flat (blue) and ell (red) states contribute the most to the total number of particles (purple), while the upright trimers (green) contribute the least.

Looking below at Figure 7.33, we see the rate curves for the lowest three coverages of dimers (60, 120, and 180). Although our maximum number of particles is only 30% of the number of particles at monolayer, we are considering a system in which 67% of the lattice is covered at equilibrium. We see in all three cases that the rate curve is linear, meaning there is a single rate that governs the kinetics of this system. In all three cases the number of upright trimers is negligible, so these three rates represent a sort of combination between flat and ell trimers. All of that said, there is likely a filling effect, wherein particles adsorb in any configuration but will tend to reorient themselves into the flat or ell positions, so it is not surprising that we have been unable to develop a mathematical description of the characteristic time of this system.

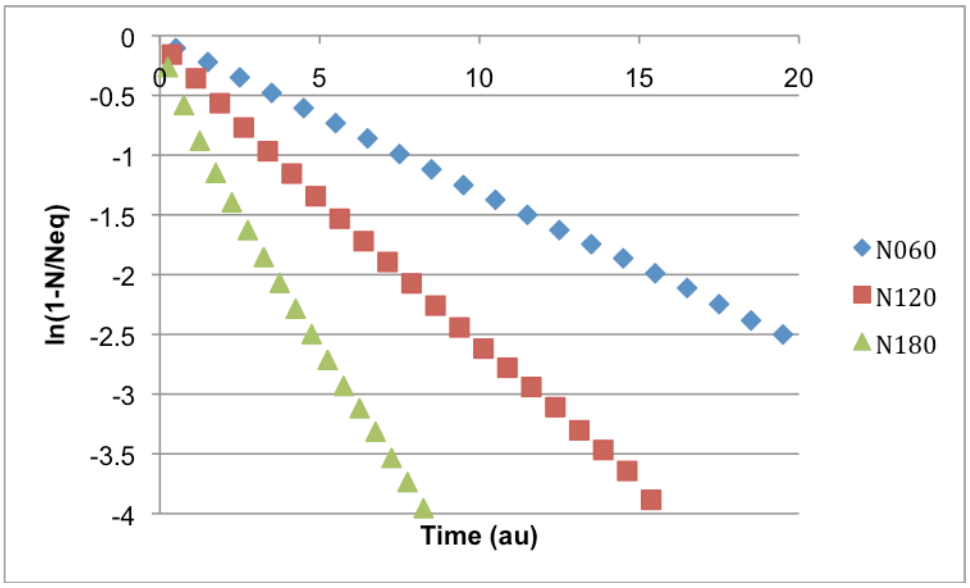

Figure 7.33
Rate curves for systems of trimers adsorbing on a 2-D, homogeneous lattice. For these low-coverage systems, there are no overshoots, and so each system proceeds apace towards its equilibrium, hence the pseudo-linear rate curves.

Section 7.3.1.2: Kinetic Behavior of Adsorbing Trimers (Medium Coverage)

When we look at the number of particles as a function of time for a system that will reach an intermediate coverage at equilibrium, we see an overshoot develop for the flat trimers. An example of this can be seen below in Figure 7.34, in which the system is equilibrating to 300 admolecules (~90% of the lattice covered). It should be noted that this overshoot first appears for a system of 240 particles (~80% lattice coverage), but is more pronounced in the system shown here. This behavior is expected and is consistent with what we observed for dimers; as particles begin to fill an empty lattice, the strong-binding flat admolecules are still preferred, but as the lattice fills up, these flat trimers must give up their space in preference for ell and upright trimers.

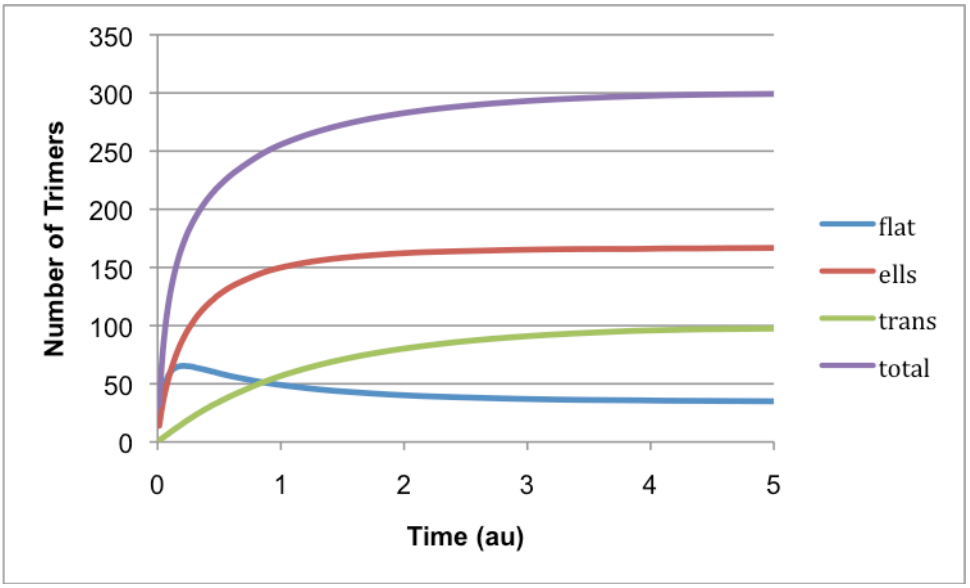

Figure 7.34
Number of particles versus time for a system of neutral trimers adsorbing on a 2-D, homogeneous lattice (moderate coverage). An overshoot has formed for flat dimers (blue), although the ell (red) and upright (green) trimers are still increasing functions.

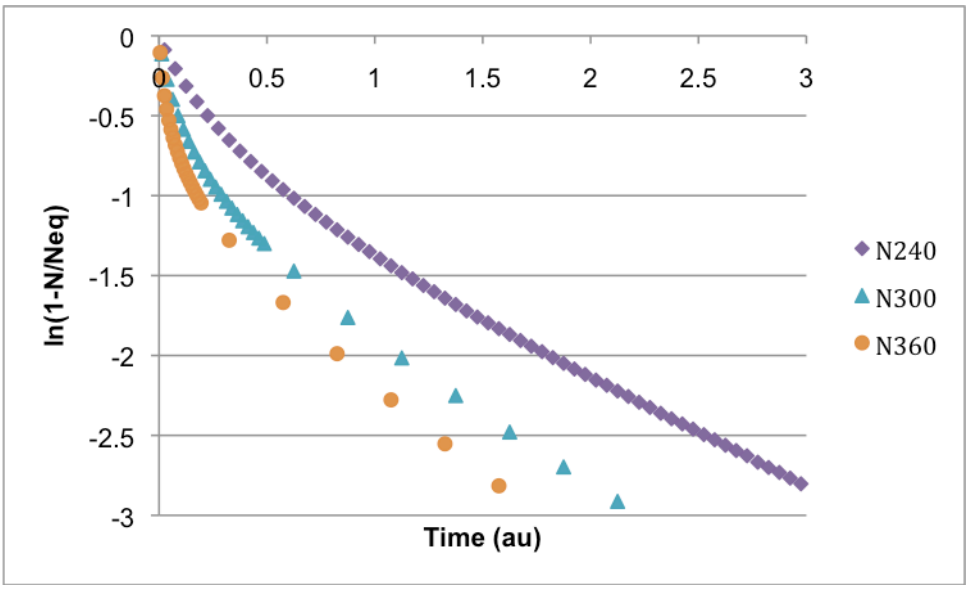

Figure 7.35
Rate curves for non-interacting trimers adsorbing on a 2-D, homogeneous lattice (moderate coverage). A small bend early in the evolution corresponds to the overshoot in the flat trimers, after which each system continues its evolution at a constant rate.

Looking at the rates for the intermediate coverages (240, 300, and 360 particles), as shown above in Figure 7.35, we see a marked curvature in the rate curves, meaning that there are multiple rates in the evolution of the system. These two rates correspond with the two processes at work: the initial filling of the lattice with flat trimers, and the transition of flat trimers to ell and transverse orientations.

Section 7.3.1.3: Kinetic Behavior of Adsorbing Dimers (High Coverage)

For systems that will equilibrate to the highest numbers of particles (420 to 595 admolecules), we see an overshoot in both the number of flat trimers and ell trimers. A typical example of this behavior is seen below in Figure 7.36, in this case a system that equilibrates with 540 adsorbed particles. The overshoot of the flat trimers occurs after a very short amount of time. At this time, the lattice is about 80% covered. As the number of flat trimers decreases, a transition to the "L" orientation takes place. By the time the number of ell trimers peaks, the fractional coverage of the lattice is around 95%. Most of the time needed for the evolution of this system is used for the transition of ell trimers to upright and the uptake of additional upright trimers, so that the final fractional coverage is about 99%.

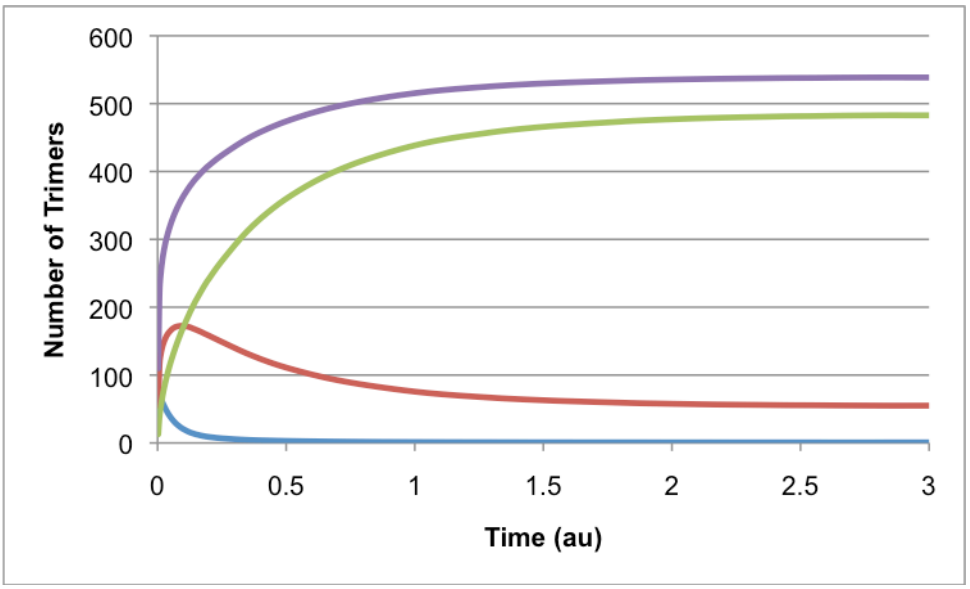

Figure 7.36
Number of particles as a function of time for a system of neutral trimers adsorbing on a 2-D, homogeneous lattice (high coverage). Now both the flat (blue) and ell (red) trimers undergo an overshoot, while the upright trimers (green) contribute the most to the total coverage (purple).

When we look at the rate curves for the highest-adsorbing systems, systems of 540 (red) and 595 (green) adsorbed particles, shown below in Figure 7.37, we see that there are now three distinct rates represented. We believe that these represent the three processes at work: the initial filling of flat trimers, the transition from flat to ell, and the final transition to upright and the final filling of the lattice. We have included trend lines to show the rates for the first and last processes, with the third rate occurring between these two. We also point out that the deviations of the rate curve from these trend lines coincide with the overshoots of the flat and ell trimers discussed above.

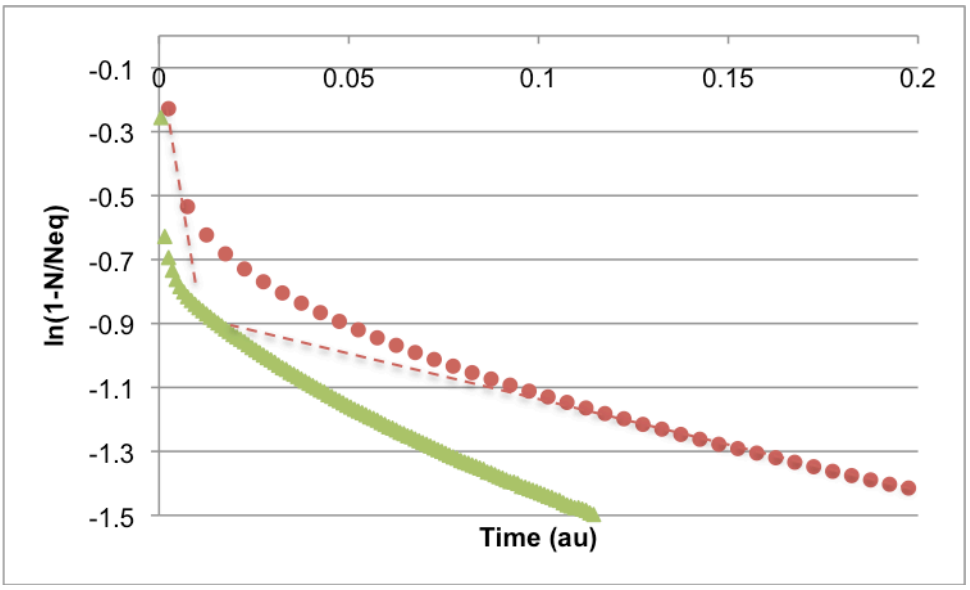

Figure 7.37
Rate curves for systems of non-interacting trimers adsorbing on a 2-D, homogeneous lattice. The dotted lines guide the eye, showing the three regions of kinetic behavior (one for each line, and then the region in between them).

Section 7.3.1.4: Equilibrium Calculations for Neutral Trimers on Graphene

As was the case with dimers, we were unable to develop kinetic equations to directly describe the adsorption behavior of these trimers. However, we were still able to use a statistical mechanical treatment to calculate the equilibrium state of the system for a given set of parameters. The statistical mechanical calculations used here can be found in their entirety in Appendix F.

The isotherm for trimers on graphene is shown below in Figure 7.38. For all values of chemical potential we see good agreement between the simulation results (points) and our calculated values (curves). We see that for low values of the chemical potential, there are approximately equal numbers of flat and ell trimers with very few upright trimers. For equilibrium coverages of more than 300 particles, there is a change in the number of particles versus chemical potential curve. The number of flat and ell trimers falls off quickly, and upright trimers quickly take over the lattice. It should be noted that 300 particles cover approximately 80% of the lattice, so the remainder of the change in chemical potential and the addition of the other 300 particles (to reach monolayer) only accounts for a 20% increase in coverage due to reorientation.

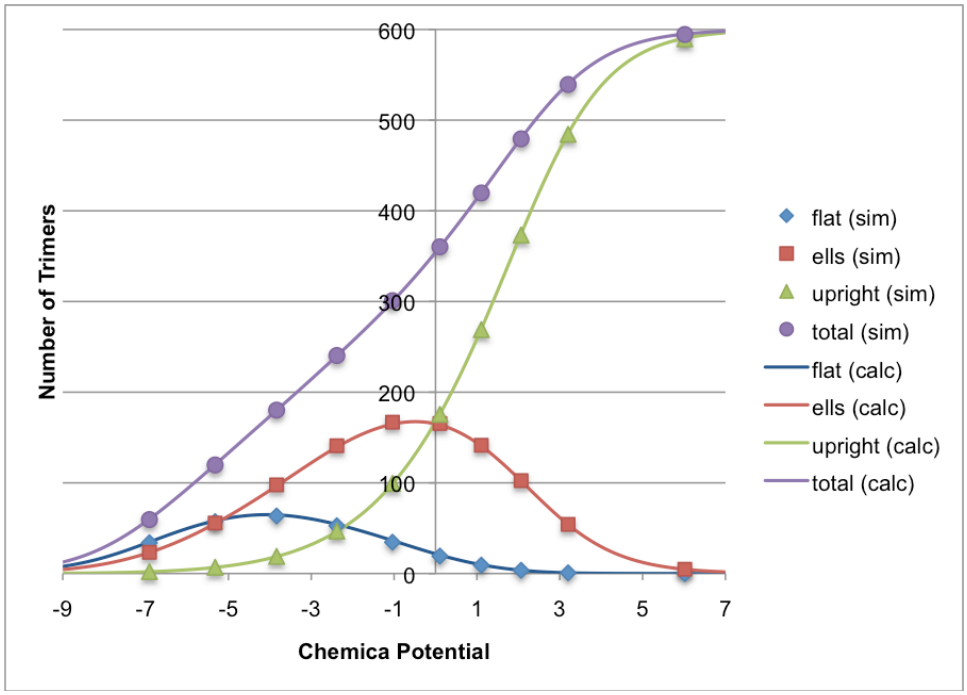

Figure 7.38
Number of particles as a function of chemical potential (isotherm) for non-interaction trimers adsorbing on a 2-D, homogeneous lattice. We see good agreement between our analytical calculations (curves) and our simulation results (points).

Section 7.3.2: Adsorption of Interacting Trimers on Graphene

After we have a baseline of kinetic behavior from studying non-interacting trimers, we included particle-particle interactions in order to gain a better understanding of how a more realistic system would behave.

Section 7.3.2.1: Weakly-Interacting Trimers (0.5xR)

Weakly-interacting trimers show us similar behavior to what we saw for the non-interacting case. When we plot the number of particles as a function of time, as we have below in Figure 7.39, we see again that the characteristic time begins to increase when the system has 300 to 500 particles (and when the fractional coverage is 80% to 90%). Except for a small increase in characteristic time with coverage, the evolutions of the individual systems were not significantly different from what we saw for the non-interacting case.

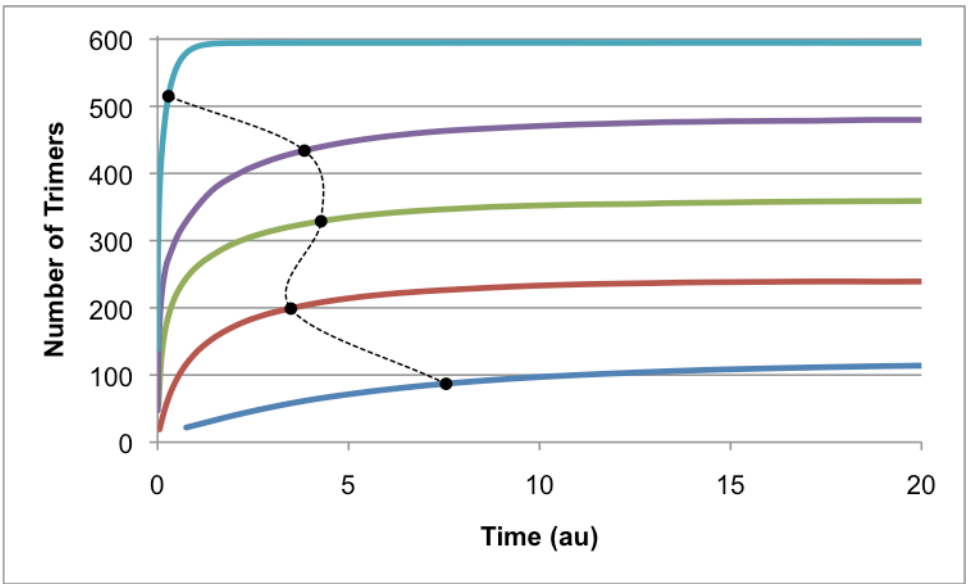

Figure 7.39
Number of particles versus time for a system of trimers adsorbing on a 2-D, homogeneous lattice (weak interactions). Already there is an increase in the characteristic time (black) with coverage in the range of 400 to 500 trimers, wherein the system is experiencing a transition from flat to upright trimers.

We also looked at the number of particles as a function of chemical potential. Again, we see qualitative similarity with what we saw for the non-interacting case. The bend in the total number of particles is slightly more pronounced at 300 particles, when the number of flat trimers begins to fall and upright trimers begin to cover the lattice. The peak in the number of ell trimers is slightly higher and shifted to a lower value of the chemical potential, as is the peak of the flat trimers. This makes sense, as these particles have more nearest neighbors and thus enjoy a greater particle-particle binding energy when the lattice is diffuse. Conversely, the number of ell

trimers falls off more quickly when the upright trimers begin to dominate, as these have a greater particle-particle interaction energy in tightly-packed lattices. Most importantly, we notice that the equilibrium values extracted from our simulations (points), continue to agree well with our statistical mechanical treatment of the system, even in the case of this complex system and even including particle-particle interaction energies. The statistical mechanical calculations used here can be found in their entirety in Appendix F.

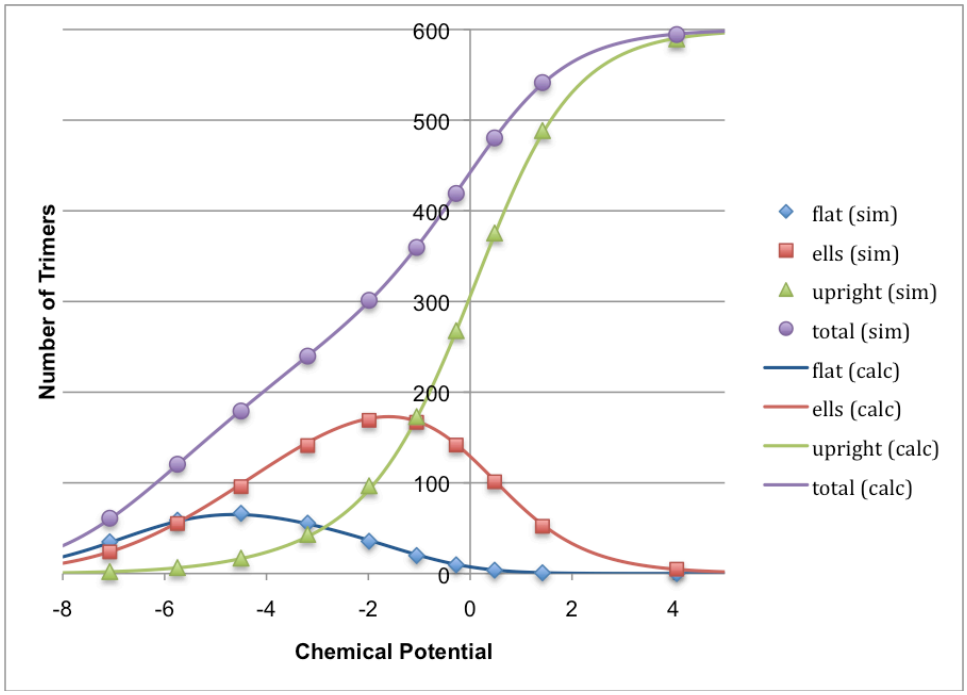

Figure 7.40
Number of particles versus chemical potential for a system of weakly-interacting trimers adsorbing on a 2-D, homogeneous lattice. Even with the inclusion of particle-particle interactions, our simulation results agree well with our calculations.

Section 7.3.2.2: Interacting Trimers (Real Values for Propane)

We then considered the adsorption of trimers using the actual particle-particle interaction energies for propane. We see that the trend of increasing characteristic time for intermediate coverages continues. The characteristic times for sytems of 300 to 500 adsorbed particles are significantly longer than the smallest value (for about 200 particles). Again, it should be noticed that the minimum characteristic time shown below in Figure 7.41 (240 admolecules) represents an 80% coverage of the lattice. The increase in characteristic from 240 to 480 particles

corresponds to an increase in fractional coverage from 80% to 98%. This mass reorientation is likely the driver of the increased equilibration time.

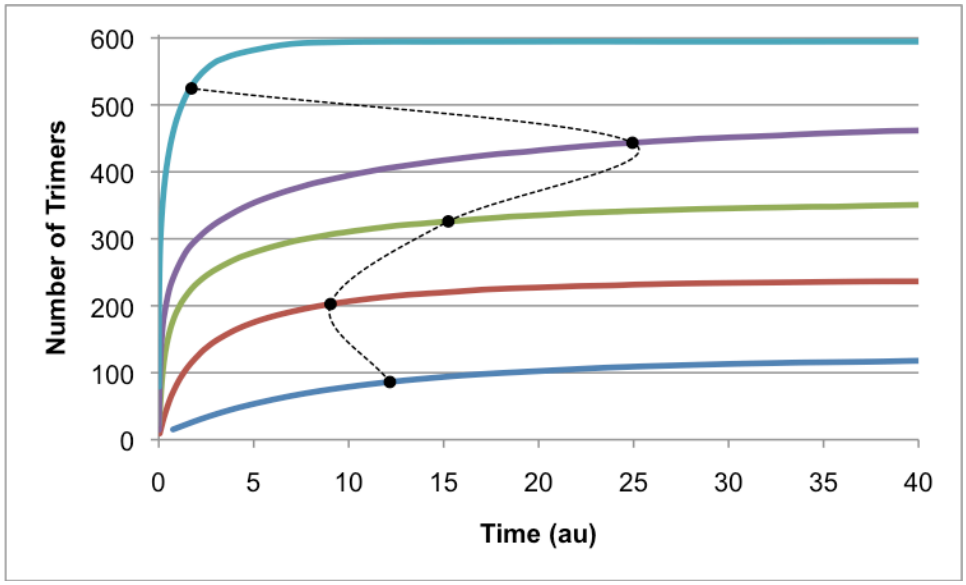

Figure 7.41
Number of particles as a function of time for a system of interacting trimers adsorbing on a 2-D, homogeneous lattice (moderate interactions). Even using just the typical adsorption energies for propane, we see that the increase in characteristic time (black) with respect to coverage is a natural consequence of the system.

When we look at the simulated isotherm for strongly-interacting trimers on graphene, as show below in Figure 7.42, we see a continuation of the trends we observed in the previous cases. We again see a bend in the total coverage (purple) when the system passes 300 adsorbed molecules (at which point the fractional coverage is about 90%). This corresponds to a general shift in the coverage of the lattice. With fewer than 300 particles adsorbed, flat and ell trimers cover most of the lattice. Conversely, once the equilibrium coverage passes 300 particles, the system quickly moves to a state in which upright trimers dominate. This correlates approximately with a change in kinetic behavior of the system, with this reorientation requiring an increased characteristic time.

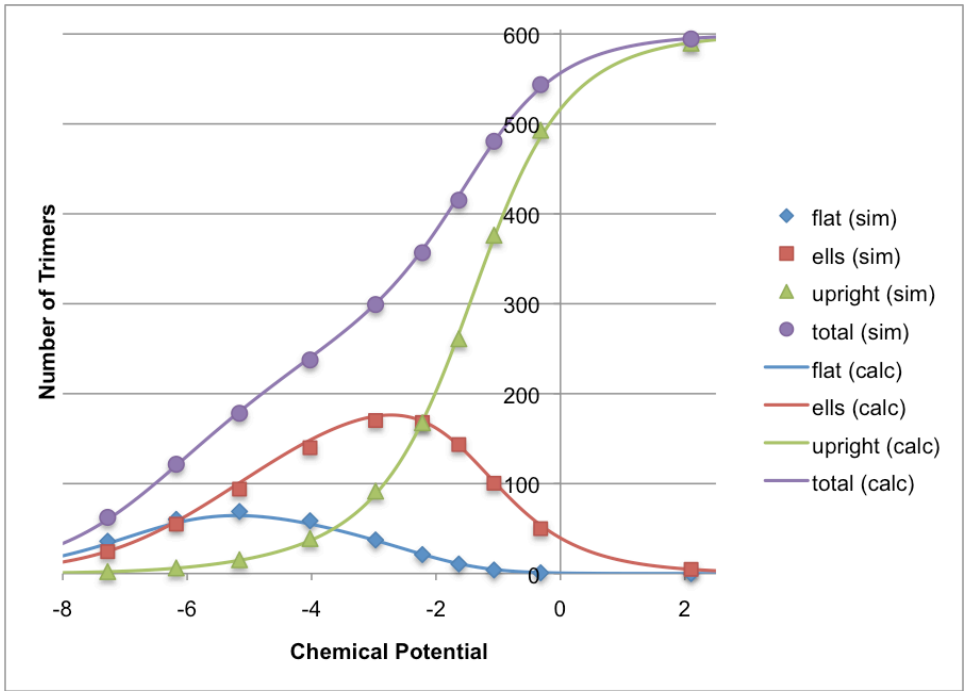

Figure 7.42
Number of particles as a function of chemical potential (isotherm) for a system of interacting trimers adsorbing on a 2-D, homogeneous lattice (moderate interactions). Our simulation results continue to match their predicted values.

Section 7.3.3: Overall Kinetic Behavior of Trimers on Graphene

The trends we have discussed in the preceding sections can be seen when the kinetic behavior of all three systems considered are combined. We see below in Figure 7.43 the characteristic time as a function of number of particles at equilibrium. We see in all cases that the characteristic time decreases as the number of particles approaches 240 particles, which represents a fractional coverage of about 80%. In the non-interacting case, the characteristic time continues to trend downward with a very small rate of change. Once we include interactions, we see the characteristic time begin to increase in this region from 300 to 540 particles, where the total coverage goes from 80% to 98% fractional coverage. This increase in characteristic time is due to the time needed for the particles to reorient themselves on a lattice that is already mostly full. Furthermore, the characteristic time increases in the region in which the system begins to transition to a state dominated by upright trimers. Interactions disproportionately affect transverse trimers (which are most prevalent when there are more than 300 particles on the lattice), so when

the strength of the interaction energy is increased, a smaller chemical potential is required to reach a given coverage, and thus the waiting time increases further.

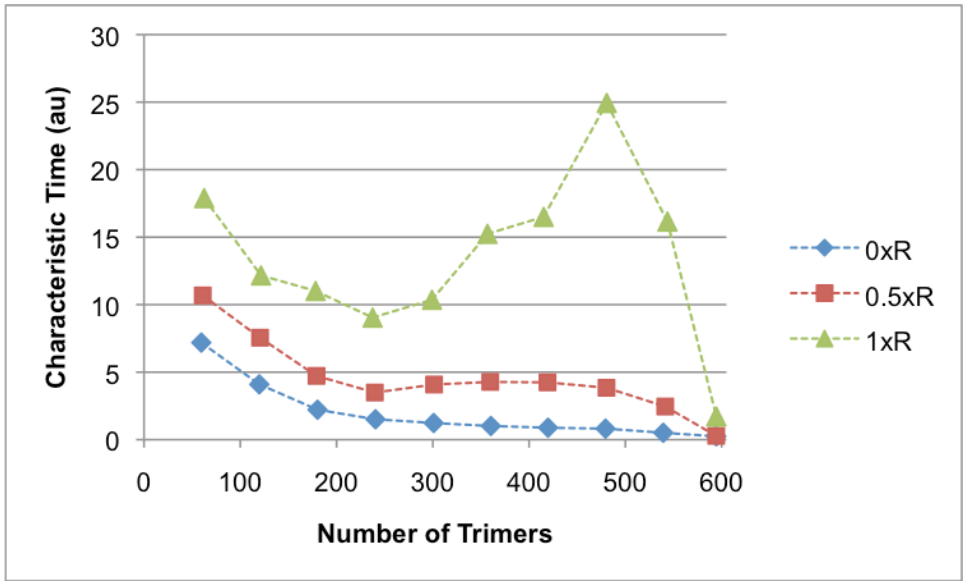

Figure 7.43
Characteristic time as a function of the number of trimers at equilibrium. While the waiting time still decreases with coverage for the non-interacting case, we see that an increase in characteristic time with respect to coverage is a natural consequence of this system, even for very small interaction energies. This increase in waiting time occurs in the region of 400 to 500 trimers, where the system is undergoing a transition from mostly-flat to mostly-transverse admolecules.

CHAPTER EIGHT
CONCLUSION

The purpose of this study was to elucidate the kinetics of adsorption of chain molecules on carbon surfaces. In general, we sought to understand the process of adsorption of polyatomic molecules, identifying the parameters that played the greatest role in the characteristic time of the system. More specifically, we wanted to understand the interplay of parameters that could lead to a reversal of the natural trend of the characteristic time, causing it to increase with coverage instead of decrease. In both of these aims we were successful.

Though much of our work with monomers was done before this current study, we built on our previous findings to make several key discoveries. When we considered the adsorption of monomers on a two-dimensional, homogeneous triangular lattice, we found that the characteristic time could either decrease or increase as the equilibrium coverage goes up. This finding confirmed an earlier hypothesis, that the increase in characteristic time with coverage could be found in any system, and that the parameter controlling this behavior is the strength of the particle-particle interaction energy. Indeed, while we were able to see the characteristic time curve bend upward, with a curvature increasing with the magnitude of the interaction energy, it was not until this set of simulations that we were able to observe the waiting time actually increasing with coverage for a system of monomers. Our understanding of this behavior is that interactions make adsorbed particles more likely to remain on the lattice, and so a smaller chemical potential is needed for the system to reach equilibrium, resulting in a longer characteristic time for the system.

When we considered this system of monomers, we included particle-particle interactions of increasing magnitude, which caused the characteristic time curve (linear in the neutral case) to bend upward; when taken to an extreme, we observed a dramatic increase in waiting time with

coverage. Thus, as we increased the magnitude of the interaction energy of the system, we saw a radical change in the kinetics of the system, including a complete reversal of the kinetic behavior we saw for the non-interacting case. Because of this change, we expected that our previous calculations analyzing the behavior of this system would no longer be valid. However, we were able to expand our calculations to include interaction energies, and we able to correctly predict the characteristic time as a function of equilibrium coverage, showing good agreement with our simulated results. Although our calculations break down when the interaction energies involved become overly large, we were able to develop a closed-form analytical solution that would predict the characteristic time for monomers, using a range of values of the interaction energy that is sufficient to cover a majority of known adsorbates.

In another part of the study, we considered the adsorption of dimers on carbon surfaces. We used two different models of the external surface of a carbon nanotube bundle, and another representing a planar sheet of graphene, and observed the adsorption of dimers on these lattices. At every step of our study, we saw very good agreement between our simulation results and our equilibrium calculations. These simulation results also gave us several important insights into the adsorption behaviors of these systems of dimers, especially the source of the overshoot and the role of the filling effect in the equilibration process. Finally, we gained further understanding of the effect of particle-particle interactions on the kinetics of adsorption.

The formation of an overshoot has been observed in several of the systems that we have studied, but until now we were not able to explain its cause. These overshoots interest us because they are a phenomenon that cannot be directly observed in experiments and are only found during the evolution of the system, not at equilibrium, making them uniquely “kinetic” in their transience. Previously, we had determined them to be based on differences in the relative rates of adsorption found in the system. Now we realize that they arise from the fact that the system is in pseudo-equilibrium throughout its evolution (with the exception of the systems that approach monolayer coverage); as the system evolves, it is in fact following the isotherm from left to right, and as the number of flat dimers at equilibrium rises and falls, so does the number of flat dimers within an evolving system, creating an overshoot.

We mentioned above that the overshoot stems from inherent differences in adsorption rates in the system, and that is indeed the case. The difference in the kinetics of adsorption of a system of dimers is driven by the filling effect. In this process, we find that it is generally easier for upright dimers to adsorb than flat ones, simply due to the space limitations on the lattice. However, for low coverages, when lattice space is not limited, flat dimers are energetically preferable. The result of this imbalance is the filling effect, through which dimers adsorb in the upright state and then reorient themselves into the flat configuration. This process is faster than direct adsorption from the gas phase, meaning the characteristic time is less than it otherwise would be.

It is the relationship between the filling effect and the overshoot that drives much of the kinetic behavior we observe in dimers adsorbing on carbon surfaces. The filling effect is always present; the overshoot only develops when the chemical potential of the system (and thus the final coverage) is greater than the chemical potential at which the number of flat dimers at equilibrium (as seen on the isotherm graph) is at a maximum. This threshold value is usually about half of the total number of particles adsorbed at monolayer completion, or half of the number of adsorption sites in the lattice, corresponding to a fractional coverage of 75-90%.

The most important consequence of the interplay between the filling effect and the overshoot is the distinction of kinetic behaviors of low- and high-coverage systems. When we look at the characteristic time as a function of number of particles at equilibrium, we see one set of behaviors for systems with less than the threshold coverage discussed above, and a different set of behaviors for systems that will equilibrate to greater than the threshold value. In the former case, the filling effect drives the system to reach a higher coverage of flat dimers than upright dimers, and the evolution of the system stops. For the latter case, however, the filling effect causes the lattice to become oversaturated with flat dimers, after which time there is a general reorientation of admolecules from the flat to the upright state. Thus, we see a difference in the process of equilibration that parallels the difference in kinetics.

When we include particle-particle interactions in our simulations with dimers, we see a general upward trend in the characteristic time, much as we did for the case of monomers.

However, interactions disproportionately affect upright dimers, and so the characteristic times were influenced far more for systems equilibrating above the threshold coverage. It was in this region, where the lattice is almost completely covered and the admolecules are undergoing a general shift from flat to upright, that we see the peak in the characteristic time of the system. Again, when this reorientation is taking place, the total binding energy of the system is increasing because of the shift to upright dimers, and so a smaller increase in chemical potential is required, which eventually leads to a longer waiting time. Finally, we mention that we saw similar behavior for dimers across the three lattices considered, meaning that particle-particle interaction energies play a greater role in adsorption kinetics that adsorption energies. While the difference in adsorption energy between the flat and upright states may also play a role, that consideration is beyond the scope of this study.

The final part of our investigation considered the adsorption of trimers on a two-dimensional, homogeneous lattice. We again found good agreement between our calculated equilibrium values and our simulated results, meaning we correctly implemented our model for the system. The most important finding here was that the increase in waiting time with coverage appeared when we used the system parameters for alkanes (in agreement with results from adsorption experiments for propane). On the other hand, in our simulations of monomers and dimers, the waiting time decreased with coverage for the systems representing alkanes (which agrees with experimental results for methane and ethane). This means that the behavior that we sought to explain arose organically from our models. For the case of trimers, this behavior came forth again from the role played by interaction energies between upright trimers.

In this investigation we have studied the adsorption kinetics of polyatomic molecules on carbon surfaces. We have developed models to represent the adsorption of monomers, dimers, and trimers on nanostructures with different surface geometries. Our simulation results have shown good agreement both with our analytical calculations and with experimental results. The common thread through the course of our study has been the importance of partice-particle interactions on the kinetics of adsorption. It seems that any system can show an increase in characteristic time with coverage, given sufficiently strong particle-particle interactions. However,

when we used the interaction energies that are typical for alkanes, we were able to reproduce experimental results for alkanes on carbon nanotubes.

BIBLIOGRAPHY

1) *Physical Adsorption: Forces and Phenomena*; Bruch, LW; Cole, MW; and Zaremba, E; Dover Publications, in press, 2007.

2) Iijima, S. “Helical Microtubules of Graphitic Carbon”. *Nature* **1991**, *354*, 56-58.

3) Burde, JT and Calbi, MM. “Physisorption Kinetics in Carbon Nanotube Bundles”. *J. Phys. Chem. C* **2007**, *111*, 5057-5063.

4) Burde, JT; Zúñiga-Hansen, N; Park, CL; and Calbi, MM. “Kinetics of External Adsorption on Nanotube Bundles: Surface Heterogeneity Effects”. *J. Phys. Chem. C* **2009**, *113*, 16945-16950.

5) Jakubek, ZJ and Simard, B. “Endohedral Condensation and Higher Exohedral Coverage of Kr on Open Single-Walled Carbon Nanotubes at 77 K”. *Langmuir* **2005**, *21*, 10730-10734.

6) Jakubek, ZJ and Simard, B. “Two Confined Phases of Argon Adsorbed Inside Open Single Walled Carbon Nanotubes”. *Langmuir* **2004**, *20*, 5940-5945.

7) Calbi, MM and Riccardo, JL. “Energy Barriers at the Ends of Carbon Nanotube Bundles: Effects on Interstitial Adsorption Kinetics”. *Phys. Rev. Lett.* **2005**, *94*, 246103.

8) Thess, A; Lee, R; Nikolaev, P; Dai, H; Petit, P; Robert, J; Xu, C; Lee, YL; Kim, SG; Rinzler, AG; Colbert,DT; Scuseria, GE; Tománek, D; Fischer, JE; and Smalley, RE. “Crystalline Ropes of Metallic Carbon Nanotubes”. *Science* **1996**, *273*, 483-487.

9) Rols, S; Johnson, MR; Zeppenfeld, P; Bienfait, M; Vilches, OE; and Schneble, J. “Argon adsorption in open-ended single-wall carbon nanotubes”. *Phys. Rev. B* **2005**, *71*, 155411.

10) Burde, JT and Calbi, MM. “Early Removal of Weak-Binding Adsorbates by Kinetic Separation”. *J. Phys. Chem. Lett.* **2010**, *1*, 808-812.

11) Calbi, MM; Cole, MW; Gatica, SM; Bojan, MJ; and Stan, G. “Colloquium: Condensed phases of gases inside nanotube bundles”. *Rev. Mod. Phys.* **2001**, *73*, 857-865.

12) Gatica, SM; Bojan, MJ; Stan, G; and Cole, MW. “Quasi-one- and two-dimensional transitions of gases adsorbed on nanotube bundles”. *J. Chem. Phys.* **2001**, *114*, 3765-3769.

13) Calbi, MM; Gatica, SM; Bojan, MJ; and Cole, MW. “Phases of neon, xenon, and methane adsorbed on nanotube bundles”. *J. Chem. Phys.* **2001**, *115*, 9975-9981.

14) Calbi, MM and Cole MW. “Dimensional crossover and quantum effects of gases adsorbed on nanotube bundles”. *Phys. Rev. B* **2002**, *62*, 115413.

15) Ancilotto, F; Gatica, SM; and Cole, MW. “From one to infinity: effective dimensionalities of fluids in nanoporous materials”. *J. Low Temp. Phys.* **2005**, *138*, 201-210.

16) Heroux, L; Krungleviciute, V; Calbi, MM; and Migone, AD. “CF_4 on Carbon Nanotubes: Physisorption on Grooves and External Surfaces”. *J. Phys. Chem. B* **2006**, *110*, 12597-12602.

17) Kostov, MK; Calbi, MM; and Cole, MW. “Phonons and specific heat of neon and methane on the surface of a nanotube bundle”. *Phys. Rev. B* **2003**, *68*, 245403.

18) Gatica, SM; Calbi, MM; Diehl, RD; and Cole, MW. “Review: Novel Physics of Gases Near Carbon Nanotubes and Buckyballs”. *J. Low Temp. Phys.* **2008**, *152*, 89-107.

19) Muris, M; Dufau, N; Bienfait, M; Dupont-Pavlovsky, N; Grillet, Y; and Palmari, JP. “Methane and Krypton Adsorption on Single-Walled Carbon Nanotubes”. *Langmuir* **2000**, *16*, 7019-7022.

20) Talapatra, S and Migone, A. “Existence of Novel Quasi-One-Dimensional Phases of Atoms Adsorbed on the Exterior Surface of Close-Ended Single Wall Nanotube Bundles”. *Phys. Rev. Lett*. **2001**, *87*, 206106.

21) Wilson, T and Vilches, O. “Adsorption of ^{4}He on carbon nanotube bundles”. *Physica B* **2003**, *329-333*, 278-279.

22) Pearce, JV; Adams, MA; Vilches, OE; Johnson, MR; and Glyde, HR. “One-Dimensional and Two-Dimensional Quantum Systems on Carbon Nanotube Bundles”. *Phys. Rev. Lett.* **2005**, *95*, 185302.

23) Talapatra, S; Zambano, AZ; Weber, SE; and Migone, AD. “Gases Do Not Adsorb on the Interstitial Channels of Closed-Ended Single-Walled Carbon Nanotube Bundles”. *Phys. Rev. Lett.* **2000**, *85*, 138-141.

24) Krungleviciute, V; Heroux, L; Talapatra, S; and Migone, AD. “Gas Adsorption on HiPco Nanotubes: Surface Area Determinations, and Neon Second Layer Data”. *Nano Lett.* **2004**, *4*, 1133-1137.

25) Teizer, W; Hallock, RB; Dujardin, E; and Ebbesen, TW. “^{4}He Desorption from Single Wall Carbon Nanotube Bundles: A One Dimensional Adsorbate”. *Phys. Rev. Lett.* **1999**, *82*, 5305-5308.

26) Shi, W and Johnson, JK. “Gas Adsorption on Heterogeneous Single-Walled Carbon Nanotube Bundles”. *Phys. Rev. Lett.* **2003**, *91*, 015504.

27) Bienfait, M; Zeppenfeld,P; Dupont-Pavlovsky, N; Muris, M; Johnson, MR; Wilson, T; DePies, M; and Vilches OE. “Thermodynamics and structure of hydrogen, methane, argon, oxygen, and carbon dioxide adsorbed on single-wall carbon nanotube bundles”. *Phys. Rev. B* **2004**,*70*, 035410.

28) Kuznetsova, A; Yates, JT, Jr.; Liu, J; and Smalley, RE. “Physical adsorption of xenon in open single walled carbon nanotubes: Observation of a quasi-one-dimensional confined Xe phase”. *J. of Chem. Phys.* **2000**, *112*, 9590-9598.

29) Talapatra, S; Krungleviciute, V; and Migone, AD. “Higher Coverage Gas Adsorption on the Surface of Carbon Nanotubes: Evidence for a Possible New Phase in the Second Layer”. *Phys. Rev. Lett.* **2002**, *89*, 246106.

30) Stan, G; Bojan, MJ; Curtarolo, S; Gatica, SM; and Cole MW. “Uptake of gases in bundles of carbon nanotubes”. *Phys. Rev. B* **2000**, *62*, 2173-2180.

31) Ancilotto, F; Calbi, MM; Gatica, SM; Cole, MW. “Bose-Einstein condensation of helium and hydrogen inside bundles of carbon nanotubes”. *Phys. Rev. B* **2004**, *70*, 165422.

32) Trasca, R; Calbi, MM; and Cole, MW. “Lattice model of gas condensation within nanopores”. *Phys. Rev. E* **2002**, *65*, 061607.

33) Gatica, SM; Stan, G; Calbi, MM; Johnson, JK; and Cole, MW. “Axial Phase of Quantum Fluids in Nanotubes”. *J. Low Temp. Phys.* **2000**, *120*, 337-359.

34) Stan, G and Cole MW. “Low coverage adsorption in cylindrical pores”. *Surf. Sci.* **1998**, *395*, 280-291.

35) Bulnes, FM; Pereyra, VD; and Riccardo, JL. “Collective surface diffusion: n-fold way kinetic Monte Carlo simulation”. *Phys. Rev. E* **1998**, *58*, 86-92.

36) Gatica, SM and Cole, MW. “Capillary condensation in cylindrical nanopores”. *Phys. Rev. E* **2005**, *72*, 041602.

37) Maddox, MW and Gubbins, KE. “Molecular Simulation of Fluid Adsorption in Buckytubes”. *Langmuir* **1995**, *11*, 3988-3996.

38) Reid, CR; O’Koye, IP; and Thomas, KM. “Adsorption of Gases on Carbon Molecular Sieves Used for Air Separation. Spherical Adsorptives as Probes for Kinetic Selectivity”. *Langmuir* **1998**, *14*, 2415-2425.

39) Calbi, MM; Toigo, F; and Cole, MW. “Dilation-Induced Phases of Gases Absorbed within a Bundle of Carbon Nanotubes”. *Phys. Rev. Lett.* **2001**, *86*, 5062-6065.

40) Calbi, MM; Toigo, F; and Cole, MW. “Dilation and intercalation of gases within carbon nanostructures”. *J. Low Temp. Phys.* **2002**, *126*, 179-186.

41) Rawat, DS; Calbi, MM; and Migone, AD. “Equilibration Time: Kinetics of Gas Adsorption on Closed- and Open-Ended Single-Walled Carbon Nanotubes”. *J. Phys. Chem. C* **2007**, *111*, 12980-12986.

42) Rawat, DS; Krungleviciute, V; Heroux, L; Bulut, M; Calbi, MM; and Migone, AD. “Dependence of Single-Walled Carbon Nanotube Adsorption Kinetics on Temperature and Binding Energy”. *Langmuir* **2008**, *24*, 13465-13469.

43) Dillon, AC and Heben, MJ. “Hydrogen Storage Using Carbon Adsorbents: Past, Present and Future”. *Appl. Phys. A* **2001**, *72*, 133-142.

44) Reid, CE and Thomas, KM. “Adsorption of Gases in a Carbon Molecular Sieve: Linear Adsorptives as Probes for Kinetic Selectivity”. *Langmuir* **1999**, *15*, 3206-3218.

45) Steele, WA. “Monolayers of Linear Molecules Adsorbed on the Graphite Basal Plane: Structures and Intermolecular Interactions”. *Langmuir* **1996**, *12*, 145-153.

46) Newton, JC and Taub, H. “Neutron Diffraction Study of the S2 Monolayer Phase of Ethane Physisorbed on Graphite”. *Surf. Sci.* **1996**, *364*, 273-278.

47) Zhang, S and Migone, A. “Melting Transition from the S1 and S2 Phases of Ethane Adsorbed on Graphite”. *Surf. Sci.* **1989**, *222*, 31.

48) Zhang, S and Migone, A. “Heat Capacity Study of Bilayer Ethane Films Adsorbed on Graphite”, *Phys. Rev. B* **1990**, *42*, 8674.

49) Eden, VL and Fain, SC. “Ethylene on Graphite; a Low-Energy Electron Diffraction Study”. *Phys. Rev. B* **1990**, *43*, 10697-10705.

50) Satija, SK; Passell, L; Eckart, J; and Ellenson, W. “Neutron Diffraction from Ethylene Adsorbed on Graphite”. *Phys. Rev. Lett.* **1983**, *51*, 411-414.

51) Lee, M; Alkhafaji, MT; and Migone, AD. “Heat Capacity Study of Monolayer Propane on Graphite”. *Langmuir* **1997**, *13*, 2791-2794.

52) Herwig, KW; Newton, JC; and Taub, H. “Structure and Growth of Butane Films Adsorbed on Graphite”. *Phys. Rev. B* **1994**, *50*, 15287-15297.

53) Alkhafji, MT and Migone, AD. “Heat Capacity Study of the Melting of Submonolayer Butane Films Adsorbed on Graphite”. *Phys. Rev. B* **1993**, *48*, 1761-1764.

54) Alkhafaji, MT and Migone, AD. “Heat Capacity Study of Butane on Graphite”. *Phys. Rev. B*, **1996**, *53*, 11152-11158.

55) Hansen, FY and Taub, H. “Melting Mechanism in Monolayers of Flexible Rod-Shaped Molecules”. *Phys. Rev. Lett.* **1992**, *69*, 652-656.

56) Hansen, FY; Newton, JC; and Taub, H. “Molecular Dynamics Studies of the Melting of Butane and Hexane Monolayers Adsorbed on the Basal Plane Surface of Graphite”. *J. Chem. Phys.* **1993**, *98*, 4128-4141.

57) Hansen, FY; Criswell, L; Fuhrmann, D; Herwig, KW; Diama, A; Dimeo, RM; Neumann, DA; Volkmann, UG; and Taub, H. “Intramolecular Diffusive Motion in Alkane Monolayers Studied by High Resolution Quasi-Elastic Neutron Scattering and Molecular Dynamics Simulations”, *Phys. Rev. Lett.* **2004**, *92*, 046103 1-4.

58) Hansen, FY; Herwig, KW; Matthies, B; and Taub, H. “Intramolecular and Lattice Melting in n-Alkane Monolayers: an Analog of Melting in Lipid Bilayers”. *Phys. Rev. Lett.* **1999**, *83*, 2362-2365.

59) Lennard-Jones, JE. “On the Determination of Molecular Fields”. *Proc. R. Soc. Lond. A* **1924**, *106*, 463-477.

60) Zuniga-Hansen, N and Calbi, MM. “Thermal Desorption from Heterogeneous Surfaces”. *J. Phys. Chem. C* **2012**, *116*, 5025-5032.

61) Burde, JT and Calbi, MM. “Adsorption kinetics of diatomic molecules”. *Phys. Chem. Chem. Phys.* **2014**, *16*, 8070-8077.

62) Rawat, DS and Migone, AD. “Ethylene Films Adsorbed onto Purified HiPco Single Walled Carbon Nanotubes: A Comparison with Ethane and Longer Alkanes”. *Ads. Sci. & Tech.* **2011**, *29*, 723-731.

63) Albesa, AG; Rafti, M; Rawat, DS; Vicente, JL; and Migone, AD. “Ethane/Ethylene Adsorption on Carbon Nanotubes: Temperature and Size Effects on Separation Capacity”. *Langmuir*, **2012**, *28*, 1824-1832.

64) Rawat, DS and Migone, AD. “Phases of Ethane Adsorbed on Purified HiPco Single-Walled Carbon Nanotubes”. *Phys. Rev. B*, **2007**, *75*, 195440.

65) Rawat, DS and Migone, AD. “Non-Monotonic Kinetics of Alkane Adsorption on Single-Walled Carbon Nanotubes”. *J. Phys. Chem. C*, **2012**, *116*, 975-979.

66) Rawat, DS; Furuhashi, T; and Migone, AD. “Adsorption Characteristics of Linear Alkanes Adsorbed on Purified HiPco Single-Walled Carbon Nanotubes”. *J. Phys. Chem. C*, **2010**, *114*, 20173-20177.

67) Rawat, DS; Furuhashi, T; and Migone, AD. “Study of a Butane Monolayer Adsorbed on Single-Walled Carbon Nanotubes”. *Langmuir*, **2009**, *25*, 973-976.

APPENDIX A: THE KINETIC MONTE CARLO ALGORITHM

To derive Equation 3.05, we consider the probability that an event will *not* occur in a site N within a time interval Δt′ that occurs at a time t′ after a reference time t, written as: P(t′+Δt′ | N,t). Then, we can rewrite this probability as:

$$P(t' + \Delta t' \mid N,t) = P(t' \mid N,t)P(\Delta t' \mid N,t) \tag{A.01}$$

Since the probability of nothing happening in the interval t′+Δt′ is the product of the probabilities that nothing will happen in the interval between t′ and t nor in the interval Δt′. However, we can also see that the probability of *nothing* happening in the interval Δt′ can be rewritten in terms of the probability that *something* will happen during that same interval so that:

$$P(\Delta t' \mid N,t) = [1 - W(N,t)\Delta t'] \tag{A.02}$$

Where W(N,t) is the sum of all the probabilities that some event will occur. Then, substituting Equation 3.13 into Equation 3.12, we see:

$$P(t' + \Delta t' \mid N,t) = P(t' \mid N,t)[1 - W(N,t)\Delta t'] \tag{A.03}$$

We now look at the time derivative of the probability of nothing happening using the definition of derivative.

$$\frac{\partial P(t' \mid N,t)}{\partial t'} = \lim_{\Delta t' \to 0} \frac{[P(t' + \Delta t' \mid N,t) - P(t' \mid N,t)]}{\Delta t'} \tag{A.04}$$

We can substitute Equation 17 into the numerator on the right side of the equation, which, once simplified, yields:

$$\frac{\partial P(t' \mid N,t)}{\partial t'} = -W(N,t)P(t' \mid N,t) \tag{A.05}$$

Because W(N,t) is a constant, this differential equation has a simple solution:

$$P(t' \mid N,t) = \exp[-t'W(N,t)] \tag{A.06}$$

However, in keeping with the probabilistic nature of this algorithm, we want to allow a random amount of time to pass between events, so that:

$$P(t' \mid N,t) = \alpha_2 \tag{A.07}$$

Where α_2 is a random number between zero and one. This means that a random amount of time will pass during which *nothing* happens and at the end of which the next event occurs.

Therefore:

$$P(t' \mid N,t) = \alpha_2 = \exp[-t'W(N,t)] \tag{A.08}$$

Solving for t′, we find:

$$t' = \frac{-1}{W(N,t)} \ln(\alpha_2) \tag{A.09}$$

Recall that t′ is defined as the length of time since the last event occurred, which is the time interval increment for our simulation.

APPENDIX B
CALCULATIONS – A STATISTICAL MECHANICAL TREATMENT OF DIMERS ADSORBING ON A 1-D, HOMOGENEOUS LATTICE

In this appendix, we detail the statistical mechanical calculations we performed for a system of interacting dimers adsorbing on a 1-D, homogeneous lattice, representing the groove on the exterior of a carbon nanotube bundle. Table B.01 shows our counting of the possible microstates of the system, followed by the equations we used to find the expectation value of the lattice coverage (Eq. B01). We used a computer code to calculate all of the expectation values as a function of chemical potential.

Table B.01
Microstates for Dimers on a 1-D, Homogeneous Lattice

State	Degeneracy g_i	Particles N_i	Energy E_i
1	1	0	0
2	4	1	ε_F
3	4	1	ε_U
4	2	2	$2\varepsilon_F+2\varepsilon_{11}$
5	4	2	$2\varepsilon_U+\varepsilon_{22}$
6	2	2	$2\varepsilon_U$
7	8	2	$\varepsilon_F+\varepsilon_U+\varepsilon_{12}$
8	4	3	$\varepsilon_F+2\varepsilon_U+2\varepsilon_{12}+\varepsilon_{11}$
9	4	3	$3\varepsilon_U+2\varepsilon_{22}$
10	1	4	$4\varepsilon_U+4\varepsilon_{22}$

$$\langle N(\mu)\rangle = \frac{\sum_{allstates} N_i g_i \exp\left(N_i\mu - E_i\right)}{\sum_{allstates} g_i \exp\left(N_i\mu - E_i\right)} \qquad \text{(B.01)}$$

APPENDIX C
CALCULATIONS – A STATISTICAL MECHANICAL TREATMENT OF DIMERS ADSORBING ON A 2-D, HETEROGENEOUS LATTICE

In this appendix, we detail the statistical mechanical calculations we performed for a system of interacting dimers adsorbing on a 2-D, heterogeneous lattice, representing the exterior of a carbon nanotube bundle. Table C.01 shows our counting of the possible microstates of the system, followed by the equations we used to find the expectation value of the lattice coverage (Eq. C.01). We used a computer code to calculate all of the expectation values as a function of chemical potential.

Table B.01
Microstates for Dimers on a 2-D, Heterogeneous Lattice

State	Degeneracy g_i	Particles N_i	Energy E_i
1	1	0	0
2	2	1	$2\varepsilon_{Fg}+2\varepsilon_{11}$
3	4	1	$\varepsilon_{Fg}+\varepsilon_{Fe}$
4	2	1	$2\varepsilon_{Fe}$
5	4	1	$2\varepsilon_{Fe}+\varepsilon_{11}$
6	8	2	$2\varepsilon_{Fg}+\varepsilon_{Ue}+\varepsilon_{11}+\varepsilon_{12}$
7	8	2	$\varepsilon_{Fg}+\varepsilon_{Fe}+\varepsilon_{Ue}+2\varepsilon_{12}$
8	4	2	$\varepsilon_{Fg}+\varepsilon_{Fe}+\varepsilon_{Ug}+\varepsilon_{12}$
9	4	2	$\varepsilon_{Fg}+\varepsilon_{Fe}+\varepsilon_{Ue}$
10	2	2	$2\varepsilon_{Fe}+\varepsilon_{Ug}+2\varepsilon_{12}$
11	2	2	$2\varepsilon_{Fe}+\varepsilon_{Ug}$
12	4	2	$2\varepsilon_{Fe}+\varepsilon_{Ue}+2\varepsilon_{12}$
13	8	2	$2\varepsilon_{Fe}+\varepsilon_{Ug}+\varepsilon_{11}+\varepsilon_{12}$
14	8	2	$2\varepsilon_{Fe}+\varepsilon_{Ue}+\varepsilon_{11}+\varepsilon_{12}$
15	4	3	$2\varepsilon_{Fg}+2\varepsilon_{Ue}+2\varepsilon_{11}+2\varepsilon_{12}+2\varepsilon_{22}$
16	4	3	$2\varepsilon_{Fg}+2\varepsilon_{Ue}+\varepsilon_{11}+2\varepsilon_{12}+\varepsilon_{22}$
17	4	3	$2\varepsilon_{Fg}+2\varepsilon_{Ue}+\varepsilon_{11}+2\varepsilon_{12}$
18	4	3	$\varepsilon_{Fg}+\varepsilon_{Fe}+\varepsilon_{Ug}+\varepsilon_{Ue}+4\varepsilon_{12}+\varepsilon_{22}$
19	4	3	$\varepsilon_{Fg}+\varepsilon_{Fe}+\varepsilon_{Ug}+\varepsilon_{Ue}+4\varepsilon_{12}$
20	4	3	$\varepsilon_{Fg}+\varepsilon_{Fe}+\varepsilon_{Ug}+\varepsilon_{Ue}+2\varepsilon_{12}+\varepsilon_{22}$
21	4	3	$\varepsilon_{Fg}+\varepsilon_{Fe}+2\varepsilon_{Ue}+2\varepsilon_{12}+2\varepsilon_{22}$
22	4	3	$\varepsilon_{Fg}+\varepsilon_{Fe}+2\varepsilon_{Ue}+4\varepsilon_{12}$

23	4	3	$\varepsilon_{Fg}+\varepsilon_{Fe}+2\varepsilon_{Ue}+2\varepsilon_{12}+\varepsilon_{22}$
24	2	3	$2\varepsilon_{Fe}+2\varepsilon_{Ug}+2\varepsilon_{12}+2\varepsilon_{22}$
25	4	3	$2\varepsilon_{Fe}+\varepsilon_{Ug}+\varepsilon_{Ue}+4\varepsilon_{12}$
26	2	3	$2\varepsilon_{Fe}+2\varepsilon_{Ue}+4\varepsilon_{12}+\varepsilon_{22}$
27	4	3	$2\varepsilon_{Fe}+\varepsilon_{Ug}+\varepsilon_{Ue}+2\varepsilon_{12}+\varepsilon_{22}$
28	4	3	$2\varepsilon_{Fe}+2\varepsilon_{Ug}+\varepsilon_{11}+2\varepsilon_{12}+2\varepsilon_{22}$
29	4	3	$2\varepsilon_{Fe}+2\varepsilon_{Ue}+\varepsilon_{11}+2\varepsilon_{12}+2\varepsilon_{22}$
30	8	3	$2\varepsilon_{Fe}+\varepsilon_{Ug}+\varepsilon_{Ue}+\varepsilon_{11}+2\varepsilon_{12}+\varepsilon_{22}$
31	8	3	$2\varepsilon_{Fe}+\varepsilon_{Ug}+\varepsilon_{Ue}+\varepsilon_{11}+2\varepsilon_{12}+\varepsilon_{22}$
32	8	4	$2\varepsilon_{Fg}+3\varepsilon_{Ue}+\varepsilon_{11}+3\varepsilon_{12}+3\varepsilon_{22}$
33	4	4	$\varepsilon_{Fg}+\varepsilon_{Fe}+\varepsilon_{Ug}+2\varepsilon_{Ue}+4\varepsilon_{12}+3\varepsilon_{22}$
34	4	4	$\varepsilon_{Fg}+\varepsilon_{Fe}+3\varepsilon_{Ue}+4\varepsilon_{12}+3\varepsilon_{22}$
35	4	4	$\varepsilon_{Fg}+\varepsilon_{Fe}+\varepsilon_{Ug}+2\varepsilon_{Ue}+6\varepsilon_{12}+\varepsilon_{22}$
36	4	4	$\varepsilon_{Fg}+\varepsilon_{Fe}+\varepsilon_{Ug}+2\varepsilon_{Ue}+4\varepsilon_{12}+3\varepsilon_{22}$
37	4	4	$2\varepsilon_{Fe}+2\varepsilon_{Ug}+\varepsilon_{Ue}+4\varepsilon_{12}+3\varepsilon_{22}$
38	2	4	$2\varepsilon_{Fe}+\varepsilon_{Ug}+2\varepsilon_{Ue}+4\varepsilon_{12}+\varepsilon_{22}$
39	2	4	$2\varepsilon_{Fe}+\varepsilon_{Ug}+2\varepsilon_{Ue}+4\varepsilon_{12}+3\varepsilon_{22}$
40	8	4	$2\varepsilon_{Fe}+2\varepsilon_{Ug}+\varepsilon_{Ue}+\varepsilon_{11}+3\varepsilon_{12}+3\varepsilon_{22}$
41	8	4	$2\varepsilon_{Fe}+\varepsilon_{Ug}+2\varepsilon_{Ue}+\varepsilon_{11}+3\varepsilon_{12}+3\varepsilon_{22}$
42	2	5	$2\varepsilon_{Fg}+3\varepsilon_{Ue}+\varepsilon_{11}+4\varepsilon_{12}+6\varepsilon_{22}$
43	4	5	$\varepsilon_{Fg}+\varepsilon_{Fe}+\varepsilon_{Ug}+3\varepsilon_{Ue}+6\varepsilon_{12}+5\varepsilon_{22}$
44	2	5	$2\varepsilon_{Fe}+2\varepsilon_{Ug}+2\varepsilon_{Ue}+6\varepsilon_{12}+5\varepsilon_{22}$
45	4	5	$2\varepsilon_{Fe}+2\varepsilon_{Ug}+2\varepsilon_{Ue}+\varepsilon_{11}+4\varepsilon_{12}+6\varepsilon_{22}$
46	8	2	$2\varepsilon_{Fg}+2\varepsilon_{Fe}+4\varepsilon_{11}$
47	4	2	$2\varepsilon_{Fg}+2\varepsilon_{Fe}+3\varepsilon_{11}$
48	4	2	$4\varepsilon_{Fe}+4\varepsilon_{11}$
49	2	2	$2\varepsilon_{Fg}+2\varepsilon_{Fe}+4\varepsilon_{11}$
50	2	2	$2\varepsilon_{Fg}+2\varepsilon_{Fe}+2\varepsilon_{11}$
51	1	2	$4\varepsilon_{Fe}+4\varepsilon_{11}$
52	4	2	$\varepsilon_{Fg}+3\varepsilon_{Fe}+2\varepsilon_{11}$
53	8	2	$\varepsilon_{Fg}+3\varepsilon_{Fe}+3\varepsilon_{11}$
54	16	3	$2\varepsilon_{Fg}+2\varepsilon_{Fe}+\varepsilon_{Ue}+4\varepsilon_{11}+2\varepsilon_{12}$
55	8	3	$2\varepsilon_{Fg}+2\varepsilon_{Fe}+\varepsilon_{Ue}+3\varepsilon_{11}+3\varepsilon_{12}$
56	8	3	$4\varepsilon_{Fe}+\varepsilon_{Ug}+4\varepsilon_{11}+2\varepsilon_{12}$
57	4	3	$2\varepsilon_{Fg}+2\varepsilon_{Fe}+\varepsilon_{Ue}+4\varepsilon_{11}+2\varepsilon_{12}$
58	4	3	$2\varepsilon_{Fg}+2\varepsilon_{Fe}+\varepsilon_{Ue}+2\varepsilon_{11}+3\varepsilon_{12}$
59	2	3	$4\varepsilon_{Fe}+\varepsilon_{Ug}+4\varepsilon_{11}+2\varepsilon_{12}$
60	4	3	$\varepsilon_{Fg}+3\varepsilon_{Fe}+\varepsilon_{Ug}+2\varepsilon_{11}+4\varepsilon_{12}$
61	4	3	$\varepsilon_{Fg}+3\varepsilon_{Fe}+\varepsilon_{Ue}+2\varepsilon_{11}+4\varepsilon_{12}$
62	8	3	$\varepsilon_{Fg}+3\varepsilon_{Fe}+\varepsilon_{Ue}+3\varepsilon_{11}+3\varepsilon_{12}$
63	8	3	$\varepsilon_{Fg}+3\varepsilon_{Fe}+\varepsilon_{Ug}+3\varepsilon_{11}+3\varepsilon_{12}$
64	8	4	$2\varepsilon_{Fg}+2\varepsilon_{Fe}+2\varepsilon_{Ue}+4\varepsilon_{11}+4\varepsilon_{12}+2\varepsilon_{22}$
65	4	4	$2\varepsilon_{Fg}+2\varepsilon_{Fe}+2\varepsilon_{Ue}+3\varepsilon_{11}+6\varepsilon_{12}+\varepsilon_{22}$
66	4	4	$4\varepsilon_{Fe}+2\varepsilon_{Ug}+4\varepsilon_{11}+4\varepsilon_{12}+2\varepsilon_{22}$

67	2	4	$2\varepsilon_{Fg}+2\varepsilon_{Fe}+2\varepsilon_{Ue}+2\varepsilon_{11}+4\varepsilon_{12}+2\varepsilon_{22}$
68	2	4	$2\varepsilon_{Fg}+2\varepsilon_{Fe}+2\varepsilon_{Ue}+2\varepsilon_{11}+8\varepsilon_{12}$
69	1	4	$4\varepsilon_{Fe}+2\varepsilon_{Ug}+4\varepsilon_{11}+4\varepsilon_{12}+2\varepsilon_{22}$
70	4	4	$\varepsilon_{Fg}+3\varepsilon_{Fe}+\varepsilon_{Ug}+\varepsilon_{Ue}+2\varepsilon_{11}+8\varepsilon_{12}$
71	8	4	$\varepsilon_{Fg}+3\varepsilon_{Fe}+\varepsilon_{Ug}+\varepsilon_{Ue}+3\varepsilon_{11}+6\varepsilon_{12}+\varepsilon_{22}$
72	8	3	$2\varepsilon_{Fg}+4\varepsilon_{Fe}+9\varepsilon_{11}$
73	4	3	$2\varepsilon_{Fg}+4\varepsilon_{Fe}+9\varepsilon_{11}$
74	2	3	$2\varepsilon_{Fg}+4\varepsilon_{Fe}+9\varepsilon_{11}$
75	2	1	ε_{Ug}
76	4	1	ε_{Ue}
77	1	2	$2\varepsilon_{Ug}+2\varepsilon_{22}$
78	4	2	$\varepsilon_{Ug}+\varepsilon_{Ue}+\varepsilon_{22}$
79	4	2	$\varepsilon_{Ug}+\varepsilon_{Ue}$
80	4	2	$2\varepsilon_{Ue}+2\varepsilon_{22}$
81	2	2	$2\varepsilon_{Ue}$
82	4	3	$2\varepsilon_{Ug}+\varepsilon_{Ue}+3\varepsilon_{22}$
83	2	3	$\varepsilon_{Ug}+2\varepsilon_{Ue}+3\varepsilon_{22}$
84	4	3	$\varepsilon_{Ug}+2\varepsilon_{Ue}+\varepsilon_{22}$
85	2	3	$\varepsilon_{Ug}+2\varepsilon_{Ue}$
86	4	3	$3\varepsilon_{Ue}+3\varepsilon_{22}$
87	4	3	$\varepsilon_{Ug}+2\varepsilon_{Ue}+3\varepsilon_{22}$
88	2	4	$2\varepsilon_{Ug}+2\varepsilon_{Ue}+5\varepsilon_{22}$
89	2	4	$2\varepsilon_{Ug}+2\varepsilon_{Ue}+4\varepsilon_{22}$
90	2	4	$2\varepsilon_{Ug}+2\varepsilon_{Ue}+6\varepsilon_{22}$
91	4	4	$\varepsilon_{Ug}+3\varepsilon_{Ue}+5\varepsilon_{22}$
92	4	4	$\varepsilon_{Ug}+3\varepsilon_{Ue}+4\varepsilon_{22}$
93	1	4	$4\varepsilon_{Ue}+6\varepsilon_{22}$
94	4	5	$2\varepsilon_{Ug}+3\varepsilon_{Ue}$
95	2	5	$\varepsilon_{Ug}+4\varepsilon_{Ue}+7\varepsilon_{22}$
96	1	6	$2\varepsilon_{Ug}+4\varepsilon_{Ue}+12\varepsilon_{22}$

$$\left\langle N(\mu)\right\rangle = \frac{\sum_{allstates} N_i g_i \exp\left(N_i\mu - E_i\right)}{\sum_{allstates} g_i \exp\left(N_i\mu - E_i\right)} \qquad \text{(C.01)}$$

APPENDIX D
CALCULATIONS – A STATISTICAL MECHANICAL TREATMENT OF MONOMERS ADSORBING ON A 2-D, HOMOGENEOUS LATTICE

In this appendix, we detail the statistical mechanical calculations we performed for a system of interacting monomers adsorbing on a 2-D, homogeneous lattice, representing the graphite. Table D.01 shows our counting of the possible microstates of the system, followed by the equations we used to find the expectation value of the lattice coverage (Eq. D.01). We used a computer code to calculate all of the expectation values as a function of chemical potential.

Table D.01
Microstates for Monomers on a 2-D, Homogeneous Lattice

State	Degeneracy g_i	Particles N_i	Energy E_i
1	1	0	0
2	7	1	ε_0
3	21	2	$2\varepsilon_0+\varepsilon_{int}$
4	35	3	$3\varepsilon_0+3\varepsilon_{int}$
5	35	4	$4\varepsilon_0+6\varepsilon_{int}$
6	21	5	$5\varepsilon_0+10\varepsilon_{int}$
7	7	6	$6\varepsilon_0+15\varepsilon_{int}$
8	1	7	$7\varepsilon_0+21\varepsilon_{int}$

$$\langle N(\mu)\rangle = \frac{\sum_{allstates} N_i g_i \exp\left(N_i\mu - E_i\right)}{\sum_{allstates} g_i \exp\left(N_i\mu - E_i\right)} \qquad \text{(D.01)}$$

APPENDIX E
CALCULATIONS – A STATISTICAL MECHANICAL TREATMENT OF DIMERS ADSORBING ON A 2-D, HOMOGENEOUS LATTICE

In this appendix, we detail the statistical mechanical calculations we performed for a system of interacting dimers adsorbing on a 2-D, homogeneous lattice, representing the graphite. Table E.01 shows our counting of the possible microstates of the system, followed by the equations we used to find the expectation value of the lattice coverage (Eq. E.01). We used a computer code to calculate all of the expectation values as a function of chemical potential.

Table E.01
Microstates for Dimers on a 2-D, Homogeneous Lattice

State	Degeneracy g_i	Particles N_i	Energy E_i
1	1	0	0
2	21	1	ε_F
3	7	1	ε_U
4	21	2	$2\varepsilon_U+\varepsilon_{22}$
5	105	2	$\varepsilon_F+\varepsilon_U+2\varepsilon_{12}$
6	105	2	$2\varepsilon_F+4\varepsilon_{11}$
7	35	3	$3\varepsilon_U+3\varepsilon_{22}$
8	210	3	$\varepsilon_F+2\varepsilon_U+4\varepsilon_{12}+\varepsilon_{22}$
9	315	3	$2\varepsilon_F+\varepsilon_U+4\varepsilon_{11}+4\varepsilon_{12}$
10	105	3	$3\varepsilon_F+12\varepsilon_{11}$
11	35	4	$4\varepsilon_U+6\varepsilon_{22}$
12	210	4	$\varepsilon_F+3\varepsilon_U+6\varepsilon_{12}+3\varepsilon_{22}$
13	315	4	$2\varepsilon_F+2\varepsilon_U+4\varepsilon_{11}+8\varepsilon_{12}+\varepsilon_{22}$
14	105	4	$3\varepsilon_F+\varepsilon_U+12\varepsilon_{11}+6\varepsilon_{12}$
15	21	5	$5\varepsilon_T+10\varepsilon_{22}$
16	105	5	$\varepsilon_F+4\varepsilon_U+8\varepsilon_{12}+6\varepsilon_{22}$
17	105	5	$2\varepsilon_F+3\varepsilon_U+4\varepsilon_{11}+12\varepsilon_{12}+3\varepsilon_{22}$
18	7	6	$6\varepsilon_U+15\varepsilon_{22}$
19	21	6	$\varepsilon_F+5\varepsilon_U+10\varepsilon_{12}+10\varepsilon_{22}$
20	1	7	$7\varepsilon_U+21\varepsilon_{22}$

Equation E.01 is the equation used to calculate the expectation value of the lattice at equilibrium as a function of the chemical potential of the system.

$$\langle N(\mu) \rangle = \frac{\sum_{allstates} N_i g_i \exp\left(N_i \mu - E_i\right)}{\sum_{allstates} g_i \exp\left(N_i \mu - E_i\right)} \tag{E.01}$$

APPENDIX F
CALCULATIONS – A STATISTICAL MECHANICAL TREATMENT OF TRIMERS ADSORBING ON A 2-D, HOMOGENEOUS LATTICE

In this appendix, we detail the statistical mechanical calculations we performed for a system of interacting trimers adsorbing on a 2-D, homogeneous lattice, representing the graphite. Table F.01 shows our counting of the possible microstates of the system, followed by the equations we used to find the expectation value of the lattice coverage (Eq. F.01). We used a computer code to calculate all of the expectation values as a function of chemical potential.

Table F.01
Microstates for Trimers on a 2-D, Homogeneous Lattice

State	Degeneracy g_i	Particles N_i	Energy E_i
1	1	0	0
2	42	1	ε_F
3	504	2	$\varepsilon_F+\varepsilon_L+3\varepsilon_{12}$
4	168	2	$\varepsilon_F+\varepsilon_U+3\varepsilon_{13}$
5	504	3	$\varepsilon_F+2\varepsilon_L+7\varepsilon_{11}+8\varepsilon_{12}+\varepsilon_{22}$
6	1008	3	$\varepsilon_F+\varepsilon_L+\varepsilon_U+3\varepsilon_{11}+3\varepsilon_{12}+4\varepsilon_{13}+\varepsilon_{23}$
7	252	3	$\varepsilon_F+2\varepsilon_U+6\varepsilon_{13}+\varepsilon_{33}$
8	504	4	$\varepsilon_F+\varepsilon_L+2\varepsilon_U+3\varepsilon_{11}+3\varepsilon_{12}+8\varepsilon_{13}+2\varepsilon_{23}+\varepsilon_{33}$
9	168	4	$\varepsilon_F+3\varepsilon_U+9\varepsilon_{13}+3\varepsilon_{33}$
10	42	5	$\varepsilon_F+4\varepsilon_U+12\varepsilon_{13}+6\varepsilon_{33}$
11	84	2	$2\varepsilon_F+9\varepsilon_{11}$
12	84	3	$2\varepsilon_F+\varepsilon_U+9\varepsilon_{11}+6\varepsilon_{13}$
13	42	1	ε_L
14	210	2	$\varepsilon_L+\varepsilon_U+\varepsilon_{13}+\varepsilon_{23}$
15	420	3	$\varepsilon_L+2\varepsilon_U+2\varepsilon_{13}+2\varepsilon_{23}+\varepsilon_{33}$
16	420	4	$\varepsilon_L+3\varepsilon_U+3\varepsilon_{13}+3\varepsilon_{23}+3\varepsilon_{33}$
17	210	5	$\varepsilon_L+4\varepsilon_U+4\varepsilon_{13}+4\varepsilon_{23}+6\varepsilon_{33}$
18	42	6	$\varepsilon_L+5\varepsilon_U+5\varepsilon_{13}+5\varepsilon_{23}+10\varepsilon_{33}$
19	42	2	$2\varepsilon_L+2\varepsilon_{12}+\varepsilon_{11}+\varepsilon_{22}$
20	1260	3	$2\varepsilon_L+\varepsilon_U+\varepsilon_{11}+2\varepsilon_{12}+\varepsilon_{22}+2\varepsilon_{13}+2\varepsilon_{23}$
21	1260	4	$2\varepsilon_L+2\varepsilon_U+\varepsilon_{11}+2\varepsilon_{12}+\varepsilon_{22}+4\varepsilon_{13}+4\varepsilon_{12}+\varepsilon_{33}$
22	420	5	$2\varepsilon_L+3\varepsilon_U+\varepsilon_{11}+2\varepsilon_{12}+\varepsilon_{22}+6\varepsilon_{13}+6\varepsilon_{23}+3\varepsilon_{33}$
23	840	3	$3\varepsilon_L+3\varepsilon_{11}+3\varepsilon_{22}+6\varepsilon_{12}$
24	840	4	$3\varepsilon_L+\varepsilon_U+3\varepsilon_{11}+3\varepsilon_{22}+6\varepsilon_{12}+3\varepsilon_{13}+3\varepsilon_{23}$

25	7	1	ε_U
26	21	2	$2\varepsilon_U+\varepsilon_{33}$
27	35	3	$3\varepsilon_U+3\varepsilon_{33}$
28	35	4	$4\varepsilon_U+6\varepsilon_{33}$
29	21	5	$5\varepsilon_U+10\varepsilon_{33}$
30	7	6	$6\varepsilon_U+15\varepsilon_{33}$
31	1	7	$7\varepsilon_U+21\varepsilon_{33}$

$$\langle N(\mu)\rangle = \frac{\sum_{allstates} N_i g_i \exp\left(N_i\mu - E_i\right)}{\sum_{allstates} g_i \exp\left(N_i\mu - E_i\right)} \qquad \text{(F.01)}$$